Juho Posio

Interlaminar shear strength testing of non-unidirectionally reinforced composites

School of Engineering

Thesis submitted for examination for the degree of Master of Science in Technology.

Espoo 10.4.2016

Thesis supervisor:

Professor Jukka Tuhkuri

Thesis advisor:

D.Sc. (Tech.) Mikko Kanerva

Aalto University
School of Engineering

Aalto-yliopisto
Insinööritieteiden
korkeakoulu

Aalto-yliopisto,
PL 11000, 00076 AALTO
www.aalto.fi
Diplomityön tiivistelmä

Tekijä Juho Posio

Työn nimi Kerrosten välisen leikkausjännityksen testaus ei-yhdensuuntaisesti lujitetuissa komposiiteissa

Koulutusohjelma Konetekniikka

Pääaine Lentotekniikka **Koodi** K3004

Työn valvoja Professori Jukka Tuhkuri

Työn ohjaaja Tekniikan tohtori Mikko Kanerva

Päivämäärä 10.04.2016 **Sivumäärä** 70+10 **Kieli** Englanti

Tiivistelmä

Yksi tyypillisimmistä vauriomuodoista komposiittirakenteissa on delaminaatio, murtuma, joka saa alkunsa yksittäisten kuitulujitettujen kerrosten välissä, kun kerrokset irtoavat toisistaan. Delaminaatio voi aiheutua monesta tekijästä, mutta tässä diplomityössä pääpaino on delaminaatiolla, joka saa alkunsa kerrostenvälisestä leikkausvoimasta. Kerrostenvälinen leikkauslujuus (ILSS) on arvo, jota käytetään usein, kun halutaan vertailla erilaisia komposiitteja toisiinsa ja se käytännössä kertoo, kuinka hyvin komposiitti kykenee vastustamaan kerrostenvälistä leikkausvoimaa, ennen kuin se murtuu.

Tämä diplomityö keskittyy ensisijaisesti ILSS-arvojen mittaamiseen sellaisilla laminaateilla, joissa kuitukerrokset eivät ole yhdensuuntaisia. Kokeellinen testaus suoritetaan ILSS:n mittaamiseen kehitetyn standardin, ASTM D2344, perusteella. Koekappaleina käytetään kahdenlaisia laminaatteja, joista ensimmäiset ovat lasikuitulujitettuja, toiset aramidilujitettuja. Testeissä käytetyissä lasikuitulujitetuissa laminaateissa on kahdenlaista laminointia, joita verrataan keskenään, jotta voidaan nähdä miten erilaiset kerrosjärjestykset vaikuttavat käyttäytymiseen ILSS-testeissä. Tarkempaa analyysia varten molemmista laminoinneista luotiin simulaatiomalli. Näin oli mahdollista selvittää, minkä kerrosten väliin leikkausjännityspiikit muodostuvat.

Kokeelliset testit osoittivat, että useimmiten koekappaleet delaminoituivat alemmasta rajapinnasta, jossa lujitekuitujen suunta muuttuu. Tämä pystyttiin osoittamaan myös simulaatioilla, joissa alempaan rajapintaan muodostui suurimmat jännityspiikit. Laminaattien testaaminen kosteana ja korotetussa lämpötilassa heikensi ILSS-arvoja sekä ILSS-käyttäytymistä testeissä. Laminaattien ikäännyttäminen vesi-rikkihappo -upotuksessa ennen testaamista heikensi ILSS-arvoja, mutta ILSS käyttäytyminen pysyi hyvänä, ja laminaatit hajosivat delaminoitumalla. Simuloidut kriittiset leikkausjännitykset olivat 14-24 % matalammat kuin ASTM standardin mukaan lasketut jännitykset. Simuloitu puhtaasti laminoinnista johtuva ero eri laminaattien välillä oli 34-58 % (riippuen reunaefektistä), mikä on suurempi kuin kokeissa havaittu ero (21-26 %).

Avainsanat Komposiitti, ILSS, kerrostenvälinen vaurio, leikkausjännitys, lasikuitu

Aalto University
School of Engineering

Aalto University,
P.O. BOX 11000, 00076 AALTO
www.aalto.fi

Abstract of master's thesis

Author	Juho Posio
Title of thesis	Interlaminar shear strength testing of non-unidirectionally reinforced composites
Degree programme	Mechanical Engineering
Major	Aeronautical Engineering **Code** K3004
Thesis supervisor	Professor Jukka Tuhkuri
Thesis advisor(s)	D.Sc. (tech.) Mikko Kanerva
Date 10.04.2016	**Number of pages** 70+10 **Language** English

Abstract

One of the most detrimental failure types in composite materials is delamination, a fracture that starts to propagate between the individual fibre-reinforced layers of the composite. Delamination can be caused by different forces but in this thesis the focus point is in delamination caused by interlaminar shear. Interlaminar shear strength, ILSS, is a value that is often used for comparing different composite materials to each other and basically tells how well the composite can resist interlaminar shear forces before breaking.

This thesis primarily focuses on experimental testing of non-unidirectionally reinforced laminates in order to find out their interlaminar shear strenght. The testing is done by three point bending according to standard ASTM D2344 that defines the rules for the ILSS testing. Two main types of test specimens are tested: aramid and glass-fibre-reinforced specimens. The glass-fibre-reinforced laminates have two lay-ups, which are being compared to find out how the ILSS behaviour changes with different lay-up. To determine the stresses in different parts of the composite specimen during bending in detail, finite element models of the glass-fibre-reinforced laminates with both lay-ups were created.

Based on the experimental results, the delaminations happened often at the lower interface of the laminates, where the fibre direction changed. This was confirmed with the simulations, which showed peak stresses at the interface. The wet testing conditions and the elevated temperature during testing both had a negative effect on the ILSS values as well as the behaviour of the laminates during ILSS-testing. Ageing in a water-sulphuric-acid immersion decreased the average ILSS values but did not affect the ILSS behaviour and the specimens delaminated in an interlaminar way. Simulated critical shear stresses were 14-24% lower than the values based on the ASTM standard. The simulated pure lay-up-induced decrease in shear stress between the two laminates was 34-58% (depending on the free-edge-effects), which is higher than suggested by the experiments (21-26%).

Keywords Composites, ILSS, interlaminar failure, shear strenght, glass-fibre

Preface

This Master's Thesis was done in the Laboratory of Lightweight Structures at School of Engineering, Aalto University. The thesis was funded by the Finnish Funding Agency for Technology and Innovation (TEKES) through the FIMECC Hybrids project.

Firstly I would like to thank my thesis advisor, D.Sc. Mikko Kanerva for the possibility to write my thesis at the laboratory and for the guidance and comments regarding this work, which have made it possible to finish this thesis project in six months. I would also like to thank M.Sc. Jarno Jokinen for the help with the Abaqus-software and my supervisor, Professor Jukka Tuhkuri for the support.

Special thanks to all coworkers at the laboratory for a nice working atmosphere, which has made the writing process so much easier.

Finally, I would like to express my gratitude to my family and friends who have supported and encouraged me during my studies.

Espoo, April 10, 2016

Juho Posio

Symbols and abbreviations

Symbols

P	Ultimate load
ρ_j	Density of jute fibre
ρ_g	Density of glass fibre
ρ_r	Density of resin
τ	Interlaminar shear stress
t	Thickness
w	Width
V_f	Fibre volume fraction
W_j	Weight of jute fibre
W_g	Weight of glass fibre
W_r	Weight of resin

Abbreviations

FRP	Fibre-reinforced Plastic
ILSS	Interlaminar Shear Strenght
PAN	Polyacrylonitrile
PDMS	Polydimethylsiloxane
UHM	Ultra High Modulus

Contents

1 Introduction

Interlaminar shear strenght, ILSS, is a value that is often used for studying resin-fibre adhesion between different composites. One of the most detrimental failure types in composite materials is a fracture that starts to propagate between the individual fibre-reinforced layers. It is called delamination. Interlaminar shear strenght tells how well the individual fibre-reinforced layers in the composite stick together i.e. how well the composite can resist delamination.

Typically interlaminar shear strength testing is conducted for laminates that are reinforced with unidirectional fibres. The main focus point of this thesis is to find out how non-unidirectionally reinforced composites behave in the ILSS testing and how different lay-up configurations can be compared via ILSS test. This is accomplished through experimental testing of composites with various lay-ups and fibre and resin combinations. To study where the delamination begins in each lay-up, a finite element simulation of the test is also created.

The ILSS value of composites is also greatly affected by environmental factors such as moisture absorption, temperature and mechanical loading. The combined effect is called ageing. Ageing can severely degrade the composite material's stiffness and strength leading to microcracks. Because the ageing process is typically quite slow, accelerated ageing methods have been developed. This can be achieved by conducting the conditioning at a higher temperature. The secondary goal of the thesis is to investigate what kind of effects water and acid immersion and elevated testing temperature have on the ILSS values of the laminates.

The remaining part of this thesis is divided into eight chapters. Chapter 2 is an introduction to composites and the different fibre and resin types that are relevant to this thesis. The ageing effect of the composites is also addressed here. Chapter 3 presents the industry standards that define how interlaminar shear strength testing should be done so that the test results are repeatable and comparable with future test results. It also gives an insight in ILSS testing of multidirectional composites through two example cases that were previously conducted by different research groups. Chapters 4 and 5 cover the experimental testing and the finite element analysis of the test specimens, respectively. The results of the experimental testing and the finite element analysis is presented in chapter 6 and the discussion and conclusions based on the test and simulation results are covered in chapters 7 and 8.

2 Composites

Composites are a type of a material system that has been made from two or more constituent materials that are physically and chemically different and produce a material with better characteristics compared to the individual components. Sometimes the materials in a composite can be equal in carrying the loads. Usually the individual components of a composite system consist of a load carrying material and a matrix material that binds the load carrying material together.

Fibre-reinforced plastics (FRP) are one of the most important subcategories of composite materials. In them the matrix is a plastic that can be made of a single material species or several polymers blended. The load carrying component typically consists of thin fibres that can for example be made of glass, carbon, aramid or basalt. The load carrying fibres can be short or long depending on the properties wanted from the composite. [8]

2.1 Matrix materials

In fibre-reinforced plastics, the matrix material can be either thermoset or thermoplastic. Thermosets are thermosetting polymers, which are materials that cure irreversibly. Thermoplastics on the other hand are plastics that solidify upon cooling but can be reshaped when heated. Due to the sheer number of matrix materials available, only the matrix materials relevant to this thesis are considered in this chapter.

2.1.1 Epoxies

Epoxy resins are polymers that include at least two epoxide groups. Epoxide groups are typically bound to the molecule through a methylene group and are of round shape. There are many different types of epoxy resins because almost all bisphenols, multifunctional phenols, glycols and polyols can be epoxied into epoxy resins. In room temperature they are viscous liquids.

The most common type of epoxy is created when epichlorohydrin reacts with bisphenol-A. The number of bisphenol-A units in the molecule varies from one to ten. The common epoxy, diglycidyl ether of bisphenol-A contains only one bisphenol-A unit.

Epoxy resins are cured using a reactive hardener with which the resin reacts chemically in a stoichiometric reaction. Because the hardener forms a big part of the plastic made of epoxy resin, the mechanical properties of the end product also vary a lot depending on the hardener used to cure the epoxy resin. The amount of hardener needs to be measured carefully before mixing it with the epoxy resin. If the mixture has too much of either component, the surplus will remain in the mixture without curing which weakens the mechanical properties of the resulting plastic.

The different epoxy-hardener-combinations allow for very big variations between the mechanical properties of the cured plastic. For example, the ultimate elongation

before breaking can vary from 1.4% up to 20% and the curing temperatures can vary from room temperature up to 200 °C. Epoxies have a good adhesion to many different surfaces and their mechanical properties are much better than those of polyesters for example. They are good insulators against electricity and heat and can withstand temperatures up to 290 °C. They also have a good resistance to chemicals.

Epoxies are used in many industries such as sports, electric and aerospace industries. They are also used as glues. In sports industry epoxy is usually reinforced with glass fibre and used to make for example skis. In electrical industry epoxies are used in circuit boards and component casings. In aerospace industry, epoxy resins are the most common matrix material. A type of an intermediate product is usually a prepreg consisting of carbon fibre and epoxy. [8]

2.1.2 Vinylesters

Vinylester resins' mechanical properties more or less resemble those of polyester resin but they are different chemically. The most common vinylester is a reaction product of bisphenol-A and epichlorohydrin i.e. epoxy resin but it has been further esterificated with an unsaturated monocarbylic acid. It is then dissolved in styrene to a 40–45 % content by weight.

Because of the chemical structure of the vinylesters, their processing properties resemble those of polyester resins but many of the properties of the end product are similar to epoxies. Vinylesters are cured similarly to polyesters by adding an initiator substance to the resin. The initiator causes a chemical reaction within the vinylester and cures the resin into hard plastic.

The advantages of using vinylesters are their toughness, temperature resistance and good resistance to chemicals, especially acids, compared to polyesters. The adhesion of vinylesters to fibres is good.

Vinylesters are most commonly used in the processing industry in corrosion resistant equipment that are used for example in cellulose, paper, and chemical industries. Typical processing equipment made of vinylesters are pipes, containers, chimneys, reactors, coatings, and waste disposal containers to name a few. [8]

2.2 Fibre types

Fibres are added to a plastic to improve the mechanical properties of the composite. Their primary function is to carry the loads that the composite is subjected to. In commercial use, the most important fibre is glass fibre and 95% of all commercially used fibres are glass fibres. Other significant fibres are carbon and aramid fibres. They are used especially in applications that require light weight and high strength but they are more expensive compared to glass fibres, which is why they are not as common. In addition, other fibre types have been and are currently being developed and for example the use of natural fibres such as jute is increasing. [8]

2.2.1 Glass fibres

Glass fibre is the most used fibre type commercially. The yearly production of glass fibre is growing rapidly. In 2009 it was roughly 5 million tonnes [18] and it had doubled by 2015 [19]. There are many different types of glass fibre, the mechanical properties of whom differ slightly from each other. However the most popular type of glass fibre with a 99% market share is E-glass (electrical glass). It has good electrical and mechanical properties and it is chemically resistant due to the fact that it contains less than 1% of alkalis. The E-glass consists of 55% silicon dioxide SiO_2, 21.5% calcium oxide CaO, 14.5% $Al_2O_3 + Fe_2O_3$, 7.5% boron trioxide B_2O_3 and 1.5% of other alkali metal oxides. The density of E-glass is 2.54 g/cm^3, tensile strength 3.6 GPa and Young's modulus 75 GPa. [8]

Due to its light weight, inherent strength, weather-resistant finish and variety of surface textures, glass fibre is a very versatile material. It is used in many different applications ranging from circuit boards to boats and wind turbine blades. Because of its resistance to a wide range of corrosive materials, it is also often used to make storage tanks for acids. Fibre-glass has proven to be especially useful in the industrial sector, where profit is based upon the least amount of money spent. However, it is not as aesthetically pleasing to the eye as carbon fibre which is why carbon fibre is often preferred in high end consumer products. Fibre-glass has a clean white colour that is illustrated in Figure 1.

2.2.2 Carbon fibres

Carbon fibre is a fibre that is composed mostly of carbon (typically 95–99%) and has a high Young's modulus as well as strength and is therefore suitable for reinforcing plastics. Carbon fibre is black, which is illustrated in Figure 1. There are several ways to produce carbon fibres and the mechanical properties of the fibre are strongly connected to the raw material used to produce the fibre. Rayon and polyacrylonitrile (PAN) as raw materials were the most promising in the beginning. PAN as a raw material has proved to give the fibres with best mechanical properties. Currently almost all carbon fibres with high strength and high Young's modulus that are used for reinforcing plastics are made from PAN. Other suitable raw material for producing carbon fibre is pitch. Using pitch results in carbon fibres that have a very high Young's modulus but lower tensile strength. This makes pitch-based carbon fibres more brittle than PAN-based. Because of this they are mostly used for reinforcing concrete and metals that don't need to carry high tensile loads.

Depending on the raw material, different carbon fibre types can have varying strengths. The most common types, PAN-based fibres, typically have a tensile strength between 4–5 GPa and Young's modulus of 240 GPa. The density of PAN-based carbon fibres is around 1.8 g/cm^3. However, even though the majority of carbon fibres in the market fall under aforementioned mechanical properties, some pitch-based carbon fibres have been developed especially with a very high Young's modulus in mind. The Young's modulus of these special carbon fibres can reach as high values as 760 GPa but their density is also slightly higher (2.15 g/cm^3) and tensile strength lower (3.5 GPa) than those of PAN-based fibres and they are much

more expensive to produce. These Ultra High Modulus (UHM) carbon fibres are mostly used in the aerospace industry where a very high strength but lightweight material is needed.

Carbon fibres are suitable for reinforcing thermoplastics as well as thermosetting polymers. They are mainly used in applications where a high strength but a light weight is required. The annual demand for carbon fibre was 46.5 thousand tonnes in 2013 and is expected to rise up to 89 thousand tonnes by 2020 [17]. About 36% of carbon fibres in the market are used for reinforcing plastics, 12% in aerospace industry, 14% in recreational items such as boats, ice hockey sticks and bicycles etc. The last 38% is divided between many industries among them wind energy, oil industry and pressure vessels. [8]

Figure 1: Aramid, carbon, glass and jute fibre-reinforcements in comparison.

2.2.3 Aramid fibres

Aramid fibres are a class of heat resistant and strong synthetic fibres. They are the third most commonly used fibre type commercially after glass fibre and carbon fibre. The annual demand for aramid fibres was 47 thousand tons in 2012 and is expected to grow 7% yearly [20]. The name aramid is a portmanteau of aromatic polyamide. Compared to other organic fibres they have a much higher tensile strength and Young's modulus and a significantly smaller ultimate elongation. A downside to the use of aramid fibres is their low compressive strength and their difficult adhesion to the matrix material. Aramid fibres are incombustible and can withstand very high temperatures as well as organic solvents. Their strength gets weaker while exposed to light. The main difference between aramid fibres and glass and carbon fibres

is the resiliency of aramid fibres and their hygroscopicity. The colour of aramid fibres is bright yellow and it is very hard to dye the fibres. The most common trade names for aramid fibres are Kevlar and Twaron. The yellow colour of aramid fibres is illustrated in Figure 1.

There are different types of aramid fibres for different purposes. Kevlar, Twaron and Technora are fibres that have excellent tensile strength and Young's modulus in relation to their density. They are often used in fabrics to make bulletproof and shrapnel proof gear. Their usage for reinforcing plastics is not very common, except for bulletproof gear such as combat helmets. The density of Kevlar and Twaron is 1.44 g/cm^3 and tensile strength around 3.5 GPa. Their Young's modulus can vary between 60–124 GPa depending on the fibre type.

Nomex and Teijiconex are trade names for aramid fibres that have inferior mechanical properties compared to Kevlar or Twaron. They are used in applications that take advantage of their resistance to fire and they are often used to make fireproof clothing. Other applications are honeycomb plates that are made from Nomex fibre-paper and that are used as a core material in sandwich-structure composite panels.

Aramid fibres can be used for reinforcing same plastics than carbon or glass fibres. However the adhesion of aramid fibre to the resin is almost always worse than the adhesion of carbon or glass fibre. This is why aramid fibres are often used as a combination with other fibres. When it is combined with glass fibre, the main function of aramid fibres is to reduce weight and improve the stiffness of the material. The glass fibre in turn improves the bending and compression strength and lowers the material costs. When combined with carbon fibres, the main function of the aramid fibre is to reduce weight, absorb vibrations and improve impact strength. In this combination the function of the carbon fibre is to improve the compression and bending strengths of the composite. [8]

2.2.4 Natural fibres

Natural fibres were among the first fibres to be used for reinforcing plastics. When mechanically and physically superior synthetic fibres such as glass and carbon fibres were developed, the use of natural fibres diminished greatly. However, now that the environmental requirements for recyclability and waste disposal have been tightened, the use of natural fibres is seeing a new rise, for example in the automotive industry.

Natural fibres are fibres that naturally grow in the nature such as animal hair and plant fibres. Cellulose based fibres are used widely in construction industry especially in North-America and Japan. Plant based natural fibres are gathered from tree trunks, leaves, seeds, fruit and nuts. Natural fibres that have been found usable in the industry are hemp, jute, kenaf, coir, flax, cotton, ramie, sisal, and soy fibres. Example of woven jute fibre mat is presented in Figure 1.

The advantages of natural fibres are their low price and density and that they are environmentally friendly. Natural fibres are biodegradable and recyclable. They can be recycled several times without a significant decrease in the strength. Another advantage compared to synthetic fibres is that natural fibres do not irritate skin,

which is beneficial in some manufacturing processes. Natural fibre reinforced plastics have good impact strength and stiffness and they have good damping (e.g of sound) qualities. The disadvantages of natural fibres are their sensitivity to temperature and their tendency to absorb a lot of water and moisture. They are also susceptible to insect and fungus attacks. The quality variation of natural fibres is high which complicates the dimensioning of the product and forces the user to apply big safety factors. Their mechanical and physical properties can be improved by surface and post-production treatments of the fibres but that increases the price of the fibres, which decreases the demand for them. [8]

2.3 Fibre preforms

Fibres are very seldom sold as single filaments but as threads (tow) combined of multiple filaments or even as woven fabric. Different fibre preforms in the market include short discontinuous fibres, long continuous fibres, woven fabrics, fibre mats, fibre felts or even three dimensionally woven fabrics.

2.3.1 Short fibres

Short fibres is the most common reinforcement type and it is estimated that they account for over 60% of all the fibre reinforcement in the market. Their typical applications are moulding processes where short fibre pieces are mixed in the resin and then the mixture injected into the mould. This allows composites with many different shapes to be produced fast.

Disadvantages regarding the use of short fibres in fibre-reinforced plastics are that it is quite hard to evenly mix the fibres in the plastic without crushing or breaking the fibres in the process. If the fibres are too short, it is hard to take a full advantage of their strength. In addition, the orientation of individual fibres is difficult to control, so the variation in the resulting composite strength is high. Even in best cases, when the fibres are ideally aligned and the adhesion between fibres and resin excellent, the tensile strength is around 50% and Young's modulus around 10% lower compared to the values achieved by using long continuous fibres.

Short fibres that are used for reinforcing plastics are usually of two different types, chopped fibre or milled fibre. Chopped fibres are fibres of even length that are cut from longer fibres. In theory the fibres can be cut to whatever length desired but in practise the fibre manufacturers are offering only a few selected fibre lengths that have been found to be the most useful in the industry. Typically the chopped fibre lengths vary between 1–100 mm. Milled fibre is fibre that is ground from longer fibres. This process results in very short fibres that are not of even length. The average fibre length of milled fibre varies between 200–300 μm but the length of a single fibre can vary from shorter than 80 μm to longer than 600 μm. [8]

2.3.2 Continuous fibres

Continuous fibres are long fibres that are typically used for reinforcing plastics as yarns or tows that consist of many fibres (filaments). The filament number of yarns

and tows varies from tens to thousands. The thickness of the yarn or tow is given as a tex number. The tex number tells how many grams one kilometre of the fibre weighs. To simplify, the tex number grows as the diameter of the yarn grows.

A bundle of glass fibres is called a roving and a bundle of carbon fibres a carbon fibre tow. A glass fibre roving in the market commonly has a tex number of 1200, 2400 or 4800 but for especially weaving applications there are also rovings with smaller tex numbers such as 320, 480, 600, 740 and 900.

For carbon fibre tows, tex numbers have not become as common, and typically the thickness of the fibre bundle is given as the amount of filaments it is composed of. The most common filament numbers for carbon fibre tows are 1000, 3000, 6000, 12000, 24000 and 48000 but there are also much thicker tows available such as 50000, 160000 or 320000 filaments.

Continuous aramid fibres are similar to textile fibres and they are easy to produce into end products using methods from textile industry, such as weaving. The number of strings is usually given as a tex number and the typical tex numbers for aramid fibres that are used for reinforcing plastics range from 20 to 805 tex. [8]

2.3.3 Woven fabrics

Very often fibres that are used for reinforcing plastics are sold as pre-made woven fabrics. Typically fibre fabrics are two axial structures in one plane that are formed with two strand systems that are perpendicular to each other. The two strand systems go over and under each other and form a structure that keeps the fibres in place. An uniform weave has same amount of fibres in both directions but depending on the purpose, a fibre fabric can also be unidirectional, in which case over 95% of the fibres can be directed to one direction and the remaining perpendicular fibres are there only to keep the directed fibres in place. The most common weave types are plain, twill and satin weaves which are illustrated in Figure 2.

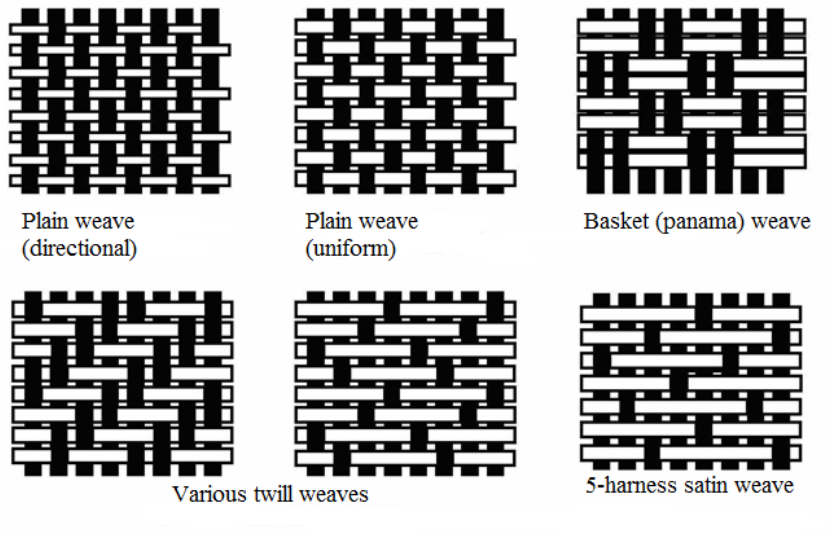

Figure 2: Different weave types. [9]

Plain weave is the simplest weave type. In plain weave every strand goes alternately over and under the strands of the other strand system. Basket weave is a variant of plain weave but in basket weave there are always two or more strands next to each other that are woven together like plain weave. Depending on the thickness of the fibres in each direction a plain weave can be either directional or uniform.

Twill weave is easy to recognize from the diagonal twill stripes that run from side to side of the fabric. The difference between twill weave and plain weave is that in twill weave the strands go over several perpendicular strands in slightly different phase which causes the diagonal pattern.

In satin weave the strands go over even larger amount of perpendicular strands than in twill weave. Satin weave is easy to flex over surfaces of difficult geometries but due to the low amount of bonding points, it is not as stable a structure as plain weave. [8]

2.4 Manufacturing of laminates

The manufacturing of composite laminates is often a time consuming process, especially if the geometry of the desired end product is unconventional. In addition to vacuum bag resin injection, in which the fibre fabrics are placed on the laminating table individually and the resin then injected into them in a vacuum bag, some more efficient methods have been developed. These include for example prepreg-laminating and filament-winding.

Prepreg is a pre-made laminate, in which the fibres or reinforcements are preimpregnated with the resin. The matrix material in prepregs is typically a resin, that cures in two phases. In the prepreg, the resin is in a partially cured state. When the endproduct is laminated, several prepregs are placed on top of each other in a mould. Then the mould is placed in an oven at an elevated temperature, which causes the partially cured resin to melt into a form with a lower viscosity and when the temperature is further raised, the resin solidifies.

When the desired endproduct is of a cylindrical form, filament-winding is one of the most efficient methods to produce it. In filament-winding, continuous fibre rovings are impregnated in a resin bath and then wound on a rotating mandrel in a predetermined pattern providing maximum control over fibre placement and uniformity of the structure. When sufficient layers have been applied on the mandrel, the composite is cured (in an oven) while still on the mandrel. After the curing process, the mandrel is removed. Filament-winding is a widely used process when making pipes, chemical and fuel storage tanks and pressure vessels. [8] Filament-winding process is illustrated in Figure 3.

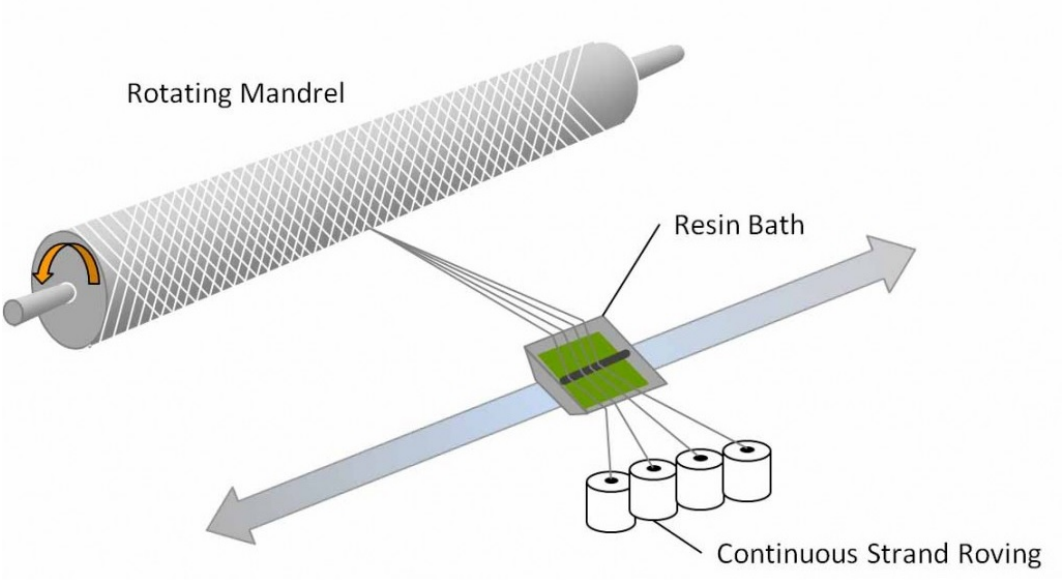

Figure 3: Filament-winding process. [21]

2.5 Ageing effect of composite materials

Due to the chemical structure of the matrix polymer in composite materials, they are susceptible to environmental damage caused by water, temperature or mechanical loading as well as sheer time. The degradation process with moisture absorption is largely reversible but the more serious chemical ageing is not. The ageing can be caused by one single parameter such as temperature but combinations of several individual ageing parameters can greatly degrade the composite material's stiffness and strength leading to cracks and ultimately to a failure of the material.

Environmental ageing of composite materials occurs from the surface or edge inwards and requires time to penetrate into the material's centre. This is somewhat similar to fluid diffusion and it can be dependent on temperature and loading. Because of this, predicting the effects of ageing around areas that experience for example high stress concentrations or temperatures, is very important when designing composite structures. [15]

Because the development of new and better composite materials is fast, it is often not possible to test the structures made out of composites in natural environment for several years' time. This is why accelerated ageing methods have been developed. In polymers, free space exists between molecular chains. Because of this free space, the polymer can absorb fluids, especially when they have similar solubility parameters. This absorption is dependent on temperature, which is why accelerated testing can be performed at elevated temperatures, with results being extrapolatable back to service temperature for life prediction purposes. [14]

2.5.1 Ageing effect on GFRP laminates with different interfacial strengths

S. Pavlidou and C.D. Papaspyrides (2003) researched the effect of hygrothermal history on water sorption and interlaminar shear strength of glass/polyester composites with different interfacial strength. The variations in interfacial strength were achieved through different surface treatments of the fabrics. They studied three kinds of composites. In the first group the glass fibres were treated with a silane coupling agent before laminating. In the second group the fibres were coated with a polydimethylsiloxane (PDMS) elastomer. The third group was a reference group in which the fibres were clean without any treatment.

The test specimens used in experimental ILSS testing were made of polyester and glass fibre. The glass fibre was in the form of a plain-woven E-glass fabric, with 1/1 warp/weft strands. The linear density of glass was 1150 TEX and each strand consisted of filaments of 22 μm. The matrix material was an unsaturated polyester resin, which was cured with methyl ethyl ketone peroxide. The coating material used was polydimethylsiloxane, which was crosslinked by addition of a crosslinking agent, forming an elastomer with a three-dimensional network structure.

In the study, Pavlidou and Papaspyrides used glass fibres with three alternative surface treatments, which included fibres coated with a silane-based size during manufacturing, de-sized fibres and fibres coated with PDMS after removal of the commercial size. The de-sizing was done by heating the fibre fabrics at 600 °C temperature for 2 h. This pyrolysis treatment was sufficient in removing the presizing and organic impurities from the fibre surface. PDMS deposition was performed by dip-coating technique, using toluene as solvent. After de-sizing the fabric, it was attached to a frame, which was then immersed into the elastometric solution at room temperature. Then the fabric was hung until the excess of the solution dripped off and finally it was dried at 120 °C for 10 minutes so that the solvent evaporated.

The composites were fabricated by resin transfer moulding. Each laminate consisted of six fibre cloth layers, which were placed in the mould (diameter: 32 cm, thickness 3 mm). Then the mould was closed and the resin injected under a pressure of 2 bars. After moulding, the materials were cured for 24 h at room temperature and then post-cured at 60 °C for 4 h and 80 °C for 4 h. Test specimens with consistent fabric orientation were then cut from the cured laminates. The dimensions of the test specimens were selected according to standard ASTM D2344, which defines the standard method for short beam shear tests. The length of the specimens was 21 mm and the width 6.35 mm, with fabrics layered parallel to the wide surface of the rectangular specimens. The fibre content of the composites was determined using pyrolysis, during which the matrix material burned off and only the fibres remained. The weight fraction of the fibres was approximately 55%.

Before immersing the specimens in water, the specimens were dried in an oven at 35 °C until their weight remained constant and then cooled in a desiccator. The absorption of water was achieved by soaking pre-weighted specimens in distilled water at 35 °C and measuring the weight periodically with an analytical balance. After being submerged for 30 h, the specimens were dried under vacuum at 35 °C for 18 h. This same procedure was repeated for the second, the third and the fourth

absorption cycle, in order to determine whether the absorption has long term effects that stay in the test specimens even after drying.

An ILSS test was conducted after each absorption and desorption step using an Instron testing machine. The crosshead speed of the machine was 1.3 mm/min. At least five specimens of each composite were tested. The results of the ILSS testing for each composite in each sorption–desorption phase are presented in Figure 4.

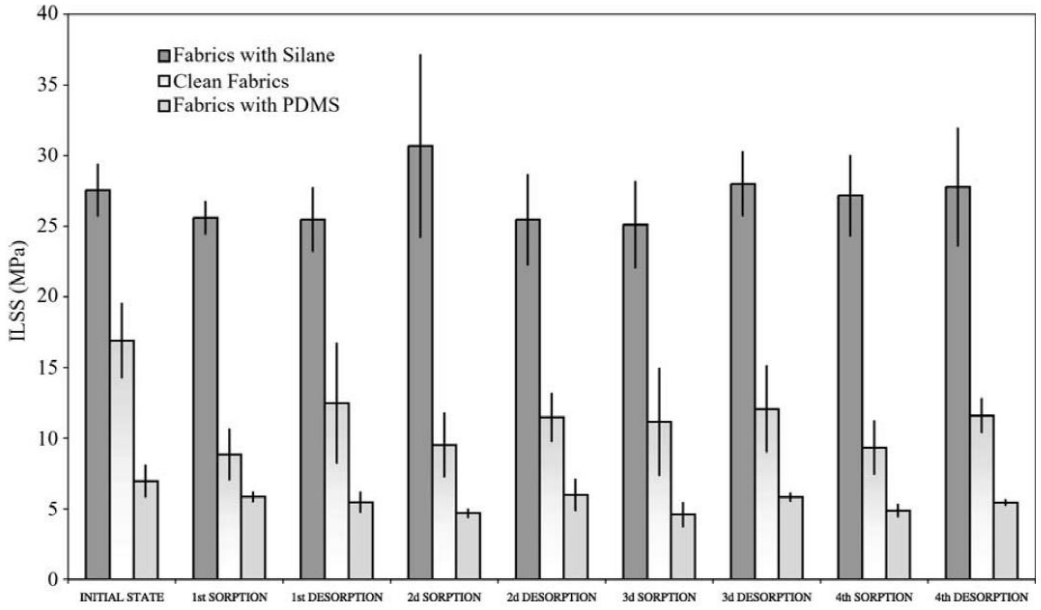

Figure 4: Interlaminar shear strength evolution during the absorption–desorption cycles. [13]

From Figure 4 it can easily be seen that composites containing fabrics treated with silane had much superior ILSS compared to the composites reinforced with clean or PDMS coated fibres. When the factory-made silane coating was cleaned from the fibres, the ILSS values experienced a large decrease. The ILSS further decreased when the fibres were coated with PDMS after cleaning them. The trend was not surprising since silane-coating is known to enhance the chemical bonding at the interface, whereas in the case of clean and PDMS-treated fabrics, the matrix bonds to the reinforcement only through mechanical anchoring.

The ILSS testing revealed two different types of ageing for the composites that had differently treated fibres: matrix and interface dominated absorption. In the case of silane-treated composite, the sorption-desorption cycles did not seem to affect the ILSS much and both dry and wet specimens had around the same ILSS. This was an indication of a 'moisture insensitive' interface. The chemical bonds established through the silane coating prevented moisture penetration at the interface forcing the moisture to penetrate through the matrix material instead. Because of this, the interlaminar shear strength did not change much for wet specimens since delaminations usually happen in the interface of fibre and matrix material. However, the behaviour of clean and PDMS-treated composites was much different. In

their case, the absorption–desorption cycles had a larger impact on ILSS values, mostly because the interface between fibres and matrix material is so weak that the interface offers an easy path for water molecules to penetrate and thus degrade the interface. Upon redrying though, the water diffuses readily out of the composite and the frictional bond reforms. This is seen in Figure 4 as a recovery in ILSS values when the composite is dried. [13]

3 Interlaminar Shear Strength Testing

The failure of a composite structure is often caused by delamination, which is a fracture that starts to propagate between the plies of the composite. Delamination typically starts from a sharp impact or bending forces that cause interlaminar shear stresses between the layers of the composite. Interlaminar shear strength is a value that describes how well a composite can resist shear stresses between the plies of the composite.

3.1 Test standards

Because the ILSS values of different composite systems need to be comparable to each other, there are many different standards that define the how interlaminar shear strength testing should be executed. Different standards vary mostly in the dimensions of the test sample. The most common international standards for ILSS testing are EN ISO 14130 and ASTM D2344/D2344M the latter of which will be used in the ILSS testing of this thesis. The definitions for the test specimens in each standard are further explained below.

3.1.1 ASTM D 2344/D 2344M (2000)

The standard ASTM D 2344/D 2344M, which is followed in this thesis, determines the short-beam strength of high-modulus fibre-reinforced composite materials. The specimen is a short beam prepared from a curved or a flat laminate up to 6.00 mm thick. The beam is loaded in three-point bending.

The test method defined in the standard can be used for continuous or discontinuous-fibre-reinforced polymer matrix composites, for which the elastic properties are balanced an symmetric with respect to the longitudinal axis of the beam.

The standard test method is limited to the use of a loading span length-to-thickness ratio of 4.0 and a minimum specimen thickness of 2.0 mm.

Both unidirectional and multidirectional laminates can be tested, but if the laminate is multidirectional, at least 10 % of the fibres must be oriented in the span direction of the beam. The laminates must also be both balanced and symmetric with respect to the span direction of the beam.

The recommendation for test specimen dimensions is the following: specimen length should be six and width two times the thickness of the specimen.

To get accurate results at least five specimens per test condition should be tested.

Loading nose and supports shall be 6.00 mm and 3.00 mm diameter cylinders, respectively, with a hardness of 60 to 62 HRC. They must have finely ground surfaces without indentation and burrs with all sharp edges relived. The speed of the testing shall be set to 1.0 mm / min.

According to the standard, the ILSS value of the test specimens is calculated based on the dimensions of the specimens and the critical force with which the

failure occurs using equation

$$\tau = \frac{3}{4}\frac{P}{wt} \tag{1}$$

in which τ is the interlaminar shear stress, P the load when the failure occurs, w the width of the specimen and t the thickness of the specimen. [1]

3.1.2 EN ISO 14130 (1998)

In ISO 14130 it is defined that the test specimens shall be flat and free of twist. The surfaces and edges shall be free from defects and the thickness along the whole length shall be within ± 5 % of the mean thickness. The width of each individual specimen shall be constant to within 0.2 mm.

The minimum number of required test specimens is five.

The standard gives specific dimensions for a test sample which should be used whenever possible. The standard test sample should be 2 ± 0.2 mm thick, 20 ± 1 mm long and 10 ± 0.2 mm wide. When it is not possible or desirable to use the standard specimen, the length of should be ten times the thickness of the specimen and the width five times the thickness.

The radius of the loading member shall be 5 mm ± 0.2 mm and that of the supports shall be 2 mm ± 0.2 mm. [2]

3.1.3 EN 2562 (1997)

The standard EN 2562 specifies the method for the determination of the apparent interlaminar shear strength of carbon fibre reinforced plastics in the form of unidirectional laminates by means of a flexural test. It is intended for specimens, in which the length is parallel to the fibre direction but can equally be applied to carbon fibre reinforced plastics in the form of woven fabrics.

The minimum number of test specimens per test condition is five.

The loading nose and supports shall be 3 ± 0.1 mm cylinders in radius. The thickness of the test specimen shall be 2 ± 0.2 mm, the width 10 ± 0.2 mm and the length between the supports 10 ± 0.1 mm. The loading speed should be 1 ± 0.1 mm / min. [4]

3.1.4 BS 2782: Part 3: Method 341A (1977)

Method 341A can be applied to both unidirectionally and multidirectionally reinforced composites but the test specimens must be prepared differently in different cases.

For materials that contain a unidirectional reinforcement the testing should be done in the direction parallel to the axis of the fibres but for materials reinforced with a mat, cloth or woven roving, two groups of test specimens are recommended. The first group should have test specimens with fibres parallel to the testing direction and the second group specimens with fibres perpendicular to the testing direction.

Method 341A defines the dimensions for a test sample as follows: the thickness should be between 2 mm - 5 mm, and the overall length of the test sample six times the mean thickness. The width of the sample should be 10 ± 2 mm. If the thickness of the test piece exceeds 5 mm the thickness should be reduced by machining the face of the test piece which will be subjected to longitudinal compression.

To get accurate test results at least 5 test pieces should be tested in each of the required directions of testing.

According to the standard the loading member of the testing machine must have a radius of 3 mm and width not less than 12.7 mm. Similarly the two parallel supports must have contact edges of 3 mm radius and length not less than 12.7 mm. [3]

3.2 ILSS test methods

There are several different methods to measure interlaminar shear strength. The most common method is short-beam-shear, SBS, but also fracture testing (e.g. double cantilever beam) test is widely used. Short-beam-shear, SBS, test was used in the experimental testing of this thesis. Like the name suggests, the test specimen is a short, rectangular beam. To measure the interlaminar shear strength of the specimen, it is placed on top of two parallel cylinders and a third one will press the specimen at the middle point. As the applied force grows, the specimen starts to bend until a failure occurs. Typically and desirably the failure mode will be a delamination which starts to propagate from a region located about one thickness away from the support cylinder, usually at the axis of symmetry [5].

3.3 Literature survey of ILSS testing of multidirectional composites

Very often the composites that are tested for ILSS are unidirectionally reinforced. Literature of ILSS testing of multidirectional composites is therefore very scarce. In this subchapter two relevant articles considering the effect of lay-up to the ILSS properties of multidirectional composites are surveyed.

3.3.1 Four-point bend ILSS testing of and multidirectional composites

Feraboli P. et al (2003) investigated the possibility of extending the interlaminar shear strength results obtained by four-point bend testing of unidirectional laminates to multidirectional laminates, such as cross-ply and quasi-isotropic, the testing of which is a common practise in the industry but had not been previously validated in the literature. The research was conducted in two parts: experimentally using a four-point bend test and analytically using finite element method.

The tested laminates were carbon fibre reinforced epoxy impregnated tape. Three different lay-ups were used, which were unidirectional $[0°]_s$, cross ply $[0/90°]_s$ and quasi-isotropic $[0/\pm 45/90°]_s$. A diamond coated tip table saw was used to cut a total of 30 test specimens in longitudinal direction from the laminates. The average geometry of the test specimens was 33 mm length, 7.6 mm width and 4.2 mm thickness. The standard deviation in the measured dimensions was negligible. In order to give the same nominal stress in the central region as in three-point bending the s/t ratio was raised to 8.0, which is twice the ratio prescribed by ASTM D2344.

The test specimens were tested to failure on an Instron 1123 electro-mechanical, double-screw test frame under displacement control. The inner span of the support cylinders was 12.7 mm and the outer span 31.7 mm. The crosshead feed rate was 0.5 mm/min and the sampling rate 2 Hz on IBM PC-type computer. In addition to the interlaminar shear strength testing, the flexural strength of the material was also measured using the same general-purpose fixture by adjusting the inner and outer spans of the test system. The test setting is illustrated in Figure 5.

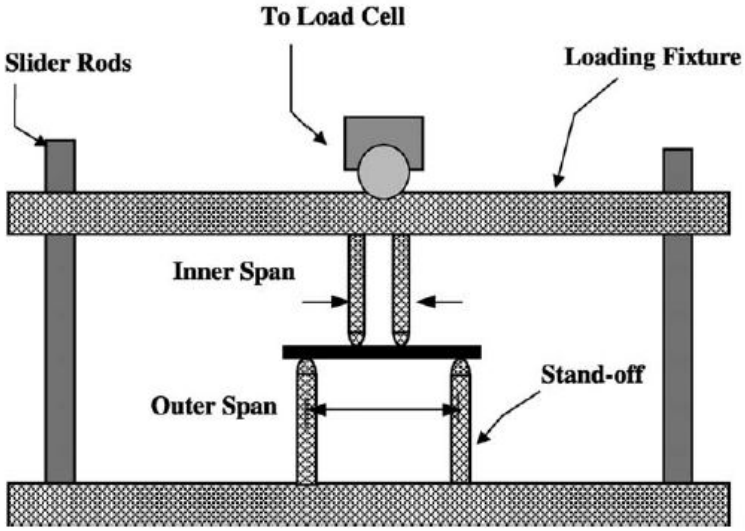

Figure 5: The four-point bending test setting and dimensions. [7]

In interlaminar shear strength testing, the fracture was found to occur suddenly in a macroscopically brittle mode by crack initiation and propagation. A single crack propagates from a region located about one thickness away from the support, usually at the axis of symmetry or within 1/4 of the thickness above. Usually an audible cracking sound was heard at the moment of failure, which lead to a catastrophic delamination. This was also clearly demonstrated in load-displacement curves, where a sharp drop in load was seen. After the first inter-ply failure, the load picked up again and in some cases the peak load reached the original value. In few tests the failure was not visible by plain eye but upon removing the specimen or with slightly higher displacement it manifested visibly.

The test results and specimen dimensions for each test sample are presented in Figures 6–8 below. The first table shows the results of unidirectional laminates, the second quasi-isotropic laminates and the third cross-ply laminates.

Specimen	Thickness in. (m)	Width in. (m)	Length in. (m)	Load lb ft (N)	ILSS psi (MPa)
Uni 1	0.136 (0.0035)	0.254 (0.0065)	1.330 (0.0338)	511 (2273)	11095 (76.5)
Uni 2	0.140 (0.0036)	0.247 (0.0063)	1.347 (0.0342)	495 (2201)	10736 (74.0)
Uni 3	0.139 (0.0035)	0.239 (0.0061)	1.350 (0.0343)	499 (2219)	11265 (77.7)
Uni 4	0.139 (0.0035)	0.230 (0.0058)	1.351 (0.0343)	466 (2073)	10932 (75.4)
Uni 5	0.138 (0.0035)	0.222 (0.0056)	1.348 (0.0342)	472 (2100)	11555 (79.7)
Uni 6	0.139 (0.0035)	0.216 (0.0055)	1.354 (0.0344)	443 (1971)	11066 (76.3)
Uni 7	0.136 (0.0035)	0.237 (0.0060)	1.350 (0.0343)	479 (2131)	11146 (76.8)
Uni 8	0.141 (0.0036)	0.235 (0.0060)	1.348 (0.0342)	495 (2202)	11204 (77.2)
Uni 9	0.140 (0.0036)	0.238 (0.0060)	1.351 (0.0343)	490 (2180)	11029 (76.0)
Uni 10	0.142 (0.0036)	0.239 (0.0061)	1.350 (0.0343)	499 (2220)	11027 (76.0)
Avg.	0.139 (0.0035)	0.236 (0.0060)	1.348 (0.0342)	485 (2157)	11106 (76.6)
Sdev.	0.001 (0.00003)	0.015 (0.0004)	0.009 (0.0002)	20 (89)	216 (1.5)

Figure 6: Test results and specimen dimensions for unidirectional laminates. [7]

Specimen	Thickness in. (m)	Width in. (m)	Length in. (m)	Load lb ft (N)	ILSS psi (MPa)
Quasi 1	0.171 (0.0043)	0.255 (0.0065)	1.297 (0.0329)	652 (2900)	11236 (77.5)
Quasi 2	0.166 (0.0042)	0.271 (0.0069)	1.304 (0.0331)	648 (2882)	10803 (74.5)
Quasi 3	0.157 (0.0040)	0.267 (0.0068)	1.300 (0.0330)	624 (2776)	11164 (77.0)
Quasi 4	0.168 (0.0043)	0.283 (0.0072)	1.302 (0.0331)	744 (3309)	11736 (80.9)
Quasi 5	0.173 (0.0044)	0.298 (0.0076)	1.294 (0.0329)	772 (3434)	11231 (77.4)
Quasi 6	0.167 (0.0042)	0.298 (0.0076)	1.304 (0.0331)	728 (3238)	10971 (75.6)
Quasi 7	0.168 (0.0043)	0.282 (0.0072)	1.300 (0.0330)	692 (3078)	10955 (75.5)
Quasi 8	0.173 (0.0044)	0.271 (0.0069)	1.298 (0.0330)	684 (3043)	10942 (75.4)
Quasi 9	0.166 (0.0042)	0.273 (0.0069)	1.297 (0.0329)	678 (3016)	11221 (77.4)
Quasi 10	0.170 (0.0043)	0.301 (0.0076)	1.297 (0.0329)	772 (3434)	11158 (76.9)
Avg.	0.168 (0.0043)	0.280 (0.0071)	1.299 (0.0330)	699 (3109)	11158 (76.9)
Sdev.	0.005 (0.00013)	0.015 (0.0004)	0.003 (0.0001)	52 (231)	263 (1.8)

Figure 7: Test results and specimen dimensions for quasi-isotropic laminates. [7]

Specimen	Thickness in. (m)	Width in. (m)	Length in. (m)	Load lb ft (N)	ILSS psi (MPa)
Cross 1	0.165 (0.0042)	0.306 (0.0078)	1.304 (0.0331)	718 (3194)	10665 (73.5)
Cross 2	0.166 (0.0042)	0.302 (0.0077)	1.301 (0.0330)	738 (3283)	11041 (76.1)
Cross 3	0.165 (0.0042)	0.304 (0.0077)	1.298 (0.0330)	744 (3309)	11124 (76.7)
Cross 4	0.166 (0.0042)	0.253 (0.0064)	1.294 (0.0329)	620 (2758)	11072 (76.3)
Cross 5	0.161 (0.0041)	0.283 (0.0072)	1.302 (0.0331)	680 (3025)	11193 (77.2)
Cross 6	0.162 (0.0041)	0.291 (0.0074)	1.299 (0.0330)	700 (3114)	11137 (76.8)
Cross 7	0.163 (0.0041)	0.280 (0.0071)	1.297 (0.0329)	708 (3149)	11635 (80.2)
Cross 8	0.161 (0.0041)	0.244 (0.0062)	1.300 (0.0330)	580 (2580)	11073 (76.3)
Cross 9	0.159 (0.0040)	0.276 (0.0070)	1.297 (0.0329)	624 (2776)	10664 (73.5)
Cross 10	0.161 (0.0041)	0.302 (0.0077)	1.295 (0.0329)	738 (3283)	11384 (78.5)
Avg.	0.163 (0.0041)	0.284 (0.0072)	1.299 (0.0330)	685 (3047)	11099 (76.5)
Sdev.	0.002 (0.00005)	0.022 (0.0006)	0.003 (0.0001)	58 (258)	291 (2.0)

Figure 8: Test results and specimen dimensions for cross-ply laminates. [7]

The ILSS values in the Figures 6–8 are calculated according to simple beam theory equation for the max shear stress in a homogeneous beam using Equation 1, which can be found from chapter 3.1.1.

In addition to the experimental testing, Feraboli P. et al did also an analytical finite element model for each lay-up configuration. The finite element model had dimensions based on the average of the test specimens. Due to symmetry conditions, only 1/4 of the specimen was analyzed. A total of 45 plies was modelled and each ply consisted of one element. The thickness of each ply was 0.09 mm resulting in total thickness of 4.05 mm of the model. In order to investigate through thickness and across width profiles of the ILS stress, a three dimensional model was used. Different element types were tried until a type that most accurately correlated with experimental results was found. Some early models were attempted with the aid of ANSYS element type Solid Quad 8 node 82 and Shell Linear layer 99 but they did not yield reliable results. The most accurate overall result was acquired by using Solid Layered 46 element, hence it was used in further models. Solid Layered 46 element allowed the use of different fibre orientations and ply interface and shear stress profile investigation. A total of 9450 elements was used in the final model and the applied load was 2891 N, half of the tested average. The force was applied as a concentrated load.

From the finite element model, Feraboli P. et al first plotted interlaminar shear stress contours, which were similar to previous studies. However, the distribution of the shear stresses was not clear enough in the original plots, so a more accurate distribution was obtained by highlighting the central portion of the beam. The peak value occurred at about one thickness away from the support, at the symmetry axis or within a 1/4 of the thickness away, which confirmed the results obtained by experimental testing. This is suspected to be the location at which delamination originates. The values obtained with load-control approach were also confirmed by running the model in displacement-control approach, in which the model was run under a prescribed average displacement. The shear stress profile through the thickness at three different locations along the length also confirmed the results obtained by testing unidirectional specimens experimentally.

The main purpose of the study was to investigate, whether the static ILSS obtained by testing simple unidirectional laminates could be used to infer the properties of more complex stacking sequences, in particular quasi-isotropic and cross-ply. Based on the experimental and analytical test results Feraboli P. et al confirmed the validity of such investigation. They also confirmed the matrix-dominated property of the ILSS, which demonstrated in the fact that the ILSS values were independent of fiber orientation and laminate lay-up. In addition, the shear stress distributions through the thickness and across the width reported in previous studies were confirmed for other configurations by using a three-dimensional finite element model. For all the laminates the point of maximum stress was found to be in a region within one thickness away from the supporting roller. This is suspected to be the location of delamination origination, which leads to a classical interlaminar failure. [7]

3.3.2 The effect of lay-up in Jute/Glass-reinforced composites

Ahmed K. et al (2008) studied the effect of stacking sequence on tensile, flexural and interlaminar shear properties of untreated woven jute and glass fabric reinforced polyester hybrid composites. The laminates used in the testing were hand laminated and consisted of 10 plies. To obtain six different stacking sequences, the number and position of glass layers was varied. The aim of the study was to combine the cost advantages and easier processing of natural fibres and the better mechanical properties of synthetic fibres into one hybrid laminate.

The materials used in the study were woven jute fabric with a count of 22 x 12 (22 yarns in warp and 12 yarns in weft direction per inch) and plain weave glass fabric. The weight of the jute fabric was 320 g/m^2 and the glass fabric 360 g/m^2. The resin system consisted of isothalic polyester NRC 200-220, MEKP catalyst and Cobalt naphthenate accelerator.

Hybrid laminates of woven jute and glass mat were prepared by simple hand lay-up technique in a mould at laboratory temperature. PVA release agent was applied to the surfaces of the mould. Jute and glass fabrics were pre-impregnated with the matrix material consisting of isothalic polyester, accelerator and catalyst in the ratio of 1:0.015:0.015. Then the impregnated layers were placed on top of each other in the mould (30 cm x 25 cm) and pressed for 1h before removal. After 1h the

laminate was removed from the mould and cured at room temperature for 48 h. All the laminates were made with a total of 10 plies by varying the number and position of glass layers to obtain different stacking sequences. The stacking sequences are presented in Figure 9.

Symbol	Stacking sequence	Wt% of fibres		Total fibre		Thickness (mm)
		Jute	Glass	Weight fraction (%)	Volume fraction (%)	
S1	JJJJJJJJ	100	00	42.6	36	6.8
S2	GJJJJJJJG	80	20	43.0	34.7	6.6
S3	GGJJJJJGG	60	40	41.5	31.5	6.4
S4	GGGJJJJGGG	40	60	42.3	29.4	6.1
S5	JGJGJJGJGJ	60	40	41.6	31.5	6.4
S6	GJJGJJGJJG	60	40	42.0	31.5	6.4
S7	GJGJGGJGJG	40	60	41.8	29.4	6.1

J-Jute ply, G-Glass ply.

Figure 9: Laminate lay-ups.

All of the laminates were processed at total fibre weight fraction of 42%. The total fiber volume fraction was calculated using Equation 2.

$$V_f = \frac{(W_j/\rho_j) + (W_g/\rho_g)}{(W_j/\rho_j) + (W_g/\rho_g) + (W_r/\rho_r)} \tag{2}$$

In Equation 2, W_j, W_g and W_r are the weights of the jute, glass and resin, respectively, and ρ_j, ρ_g and ρ_r are the densities of jute, glass and resin, respectively. The densities for the materials are 1.1 g/m^3 for isothalic polyester, 2.55 g/m^3 for glass and 1.42 g/m^3 for jute.

Three different kinds of tests were performed to the laminates with various lay-ups: flexural testing, tension testing and interlaminar shear testing. Because of the topic of this thesis only interlaminar shear testing will be reviewed.

The interlaminar shear strength tests were conducted on a closed loop servo hydraulic MTS 810 Material Test System using data acquisition software Test Works-II in accordance with ASTM D 2344. A test sample used in the testing was a small beam of 45 mm length and square cross section i.e. its width was equal to thickness. The beam was loaded under three point bending and the loading cylinder was moving at the rate of 1.3 mm/min. A short beam was used to assure that the bending stresses were minimized and that the failure type would be interlaminar shear failure, cracking along the horizontal plane between the laminae. The interlaminar shear strength was determined by measuring the force applied at the time of failure and then calculating the stresses from Equation 1, which can be found in chapter 3.1.1. A span to depth ratio of 5:1 was selected for the test and five identical specimens were tested for each stacking sequence.

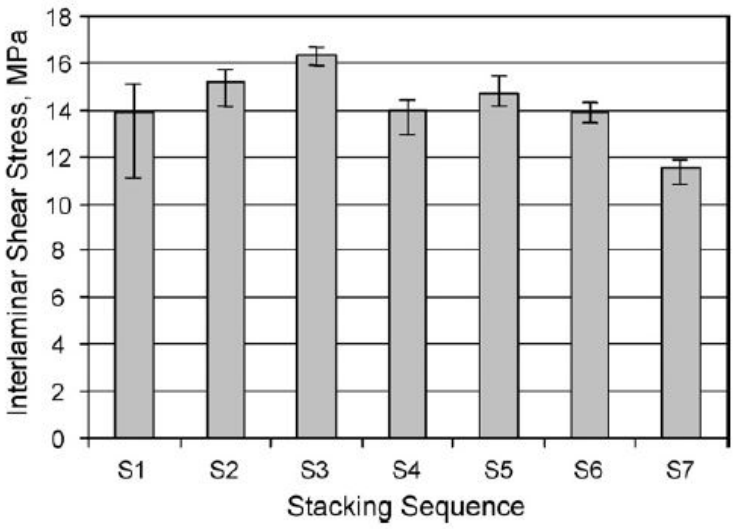

Figure 10: Determined interlaminar shear strength of the Glass/Jute/Polyester laminates.

The average values for interlaminar shear strengths for the hybrid laminates with various stacking sequences are presented in Figure 10. From Figure 10 it can be seen that the laminates that consisted of only jute plies (S1) exhibited an average interlaminar shear stress value of 13.9 MPa. Addition of glass fibre as extreme plies by 20% of the total fibre weight (S2) increased the ILSS value by 9.4% and when the weight percentage of glass fibre as extreme plies was further increased to 40% (S3) the ILSS value increased by 21.1%. Increasing the weight percentage of glass fibre to 60% (S4) resulted in decrease of ILSS. Altering the sequence of arrangement as in cases S5, S6 and S7 yielded no improvement in ILSS and the sequence S7 was found to have the lowest interlaminar shear strength of 11.56 MPa.

All the ILSS values of the hybrid composites were under 20 MPa which is significantly less than the typical values for glass fibre reinforced epoxy matrix (30-75 MPa) that had been studied in previous literature. This was probably caused by the higher tensile strength of epoxy than polyester and better adhesion of epoxy with glass fibres. [6]

4 Experiments

The main focus of this thesis was in the experimental testing of different types of composite laminates. In this chapter the various laminate types are described in detail and the test setup as well as the test methods are introduced.

4.1 Laminates and specimen preparation

The interlaminar shear strength testing was done for three main groups of laminates. The first group was aramid-fibre-reinforced laminates, the second group glass-fibre-reinforced laminates and the third group glass-fibre-reinforced filament-wound cylinder laminates.

4.1.1 Aramid-fibre-reinforced laminates

The aramid-fibre-reinforced laminates were resin-infused (vacuum bag resin injection) prior to this research. They consist of several aramid fibre layers (HexForce, twill 2/2, 20968, Hexcel) with fibre orientations of 0° and 90° in an epoxy resin (Araldite LY 5052, Aradur 5052, Huntsman). The cutting of the ILSS test specimens from the laminates was outsourced to an outside company (Muototerä Oy [25]) that used high pressure water jet to cut through the laminate.

There were six aramid-fibre-reinforced laminate plates in total and each of them differed slightly from the others. The differences are illustrated in Table 3.

Table 3: Aramid-fibre-reinforced laminates

Test series	THDR	THDC	tDR	tDC	RF	RFC
Ultrasonically cleaned reinforcement	no	yes	no	yes	no	yes
Thick diamond-like-coating	yes	yes	no	no	no	no
Thin diamond-like-coating	no	no	yes	yes	no	no

The differences between the groups were the thickness of the diamond-like-coating (prepared by Diarc Technology Ltd), and whether the fabrics had been cleaned with ultrasonic cleaning procedure before laminating. The capital T in the laminate name refers to the thick diamond-like-coating and small t to the thin diamond-like-coating. The two groups of laminates with a capital R as the first letter of their name are reference laminates, in which the fabrics were not coated with diamond-like-coating. The capital C in the laminate name refers to the laminates, which had ultrasonically cleaned fabrics. The diamond-like coating gave the laminates a distinct army green colour, whereas the laminates without diamond-like coating retained the bright yellow colour of typical aramid fibres. This is illustrated in Figure 11.

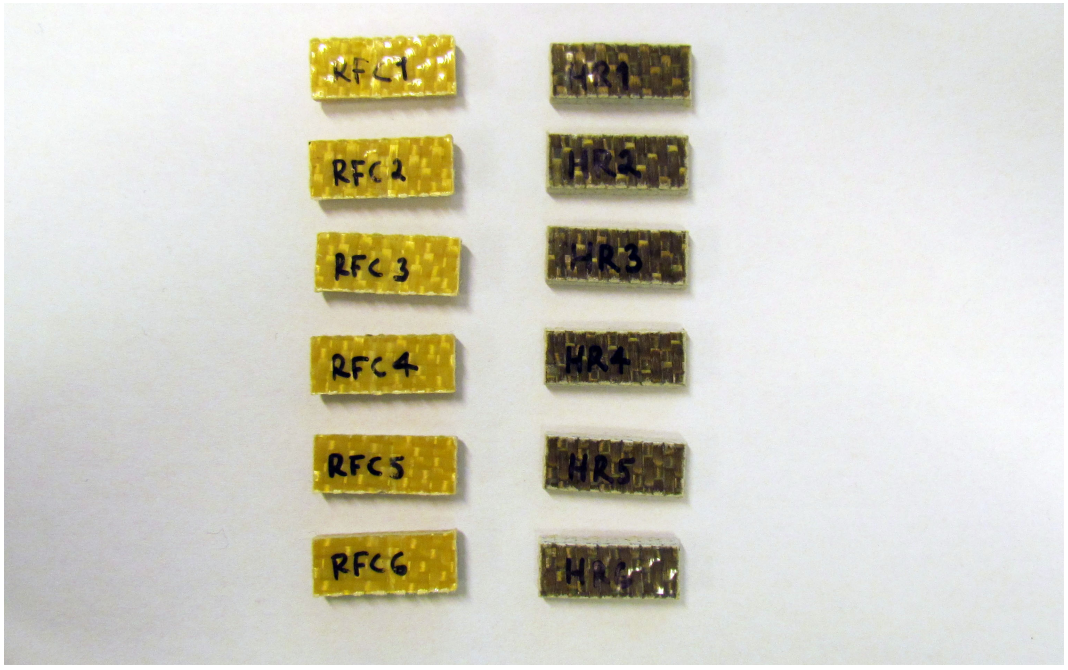

Figure 11: Aramid-fibre-reinforced specimens. The yellow reference specimens on the left and the green diamond coated specimens on the right.

The cleaning process of the fibres in laminates THDC, tDC and RFC was done in six steps. The process consisted of various cleaning steps and finally rinsing and drying the fabrics. The details of this process are presented in Table 4.

Table 4: The cleaning procedure of the aramid fabrics

1.	Immersing the aramid fabrics in tap water
2.	Ultrasonic cleaning at 50 °C for 10 minutes
3.	Replacing the tap water with ethanol
4.	Ultrasonic cleaning at 30 °C for 10 minutes
5.	Ultrasonic rinsing of the aramid fabrics with purified water (Millipore Elix 10) at 50 °C for 5 minutes
6.	Drying the aramid fabrics in a vacuum oven at 70 °C, -0.5 bar, for 14 hours.

There were two test groups of the aramid-fibre-reinforced specimens: dry and wet specimens. Before the testing started, the dry aramid-fibre-reinforced specimens were weighed on a precision scale and dried in the oven in 50 °C until the weight remained constant (see Appendix A for the drying curves). The wet specimens were conditioned in a conditioning chamber (65 °C and 95% relative humidity) in water immersion (distilled water) for a week before the ILSS testing and they were tested wet.

4.1.2 Glass-fibre-reinforced laminates

The second group of laminates that were tested for ILSS were glass-fibre-reinforced laminates. The glass-fibre-reinforced laminates were laminated and water-jet-cut [25] to the right size for testing before the beginning of this thesis project. Within the group of glass-fibre-reinforced laminates, there were two different laminate lay-ups, three different resins and different ageing conditions. The laminates were filament-wound on a rotating mandrel with a rectangular cross-section (Muovityö Hiltunen Oy / Admor Composites Oy [26,27]).

The first laminate lay-up (lay-up 1) had glass fibre layers stacked using a sequence [0°/0°/0°/0/ 90°/0°/90° / 0°/0°/0°/0°] and the second one (lay-up 2) using a sequence [0°/0°/0° / 90°/90°/90°/90° / 0°/0°/0°]. The test specimens were cut from the laminates so that the outer layers have fibres along the longitudinal axis of the specimen, in order to avoid the tensile failure of the specimen from the outer layers during ILSS testing. The two different lay-ups are illustrated in Figure 12.

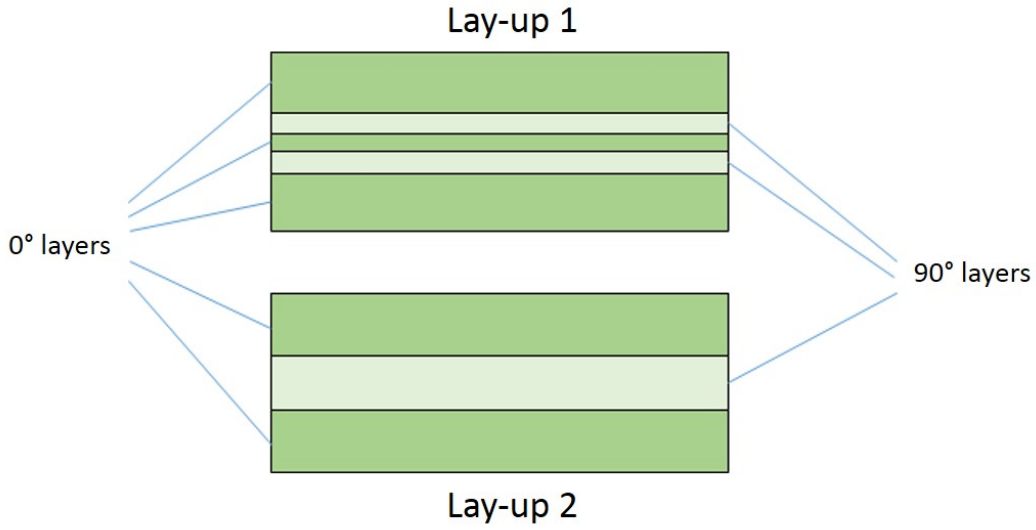

Figure 12: Two different lay-ups for the test specimens.

Three different resins were used in the glass-fibre-reinforced laminates. The test series were named Vinylester I, Vinylester II, and Polyester I specimens according to the resins used. The fibre was a glass fibre (E6CR17-2400-386, Jushi) for 0° layers and a roving (560 g/m^2, similar to Ahlstrom 9690-19-300 R12-256-T) for 90° layers.

Vinylester I was Derakane 441 (Ashland), which is a epoxy vinyl ester resin that has a lower styrene-content than ordinary epoxy vinyl esters. It also has good thermal properties as well as corrosion resistance performance. [10] It was used in the majority of the tested glass fibre-reinforced-laminates.

The second most used resin in the glass fibre reinforced test specimens was Vinylester II. It was a resin made by Swancor and it is a bisphenol-A type epoxy-based vinyl ester resin. Similar to the Vinylester I resin, Vinylester II also has a

high corrosion resistance and good mechanical properties, which is why it is often used for example in chemical storage tanks. [11]

The third used resin, Polyester I, was Aropol M300 (Ashland) resin, which is a thixotropic, pre-accelerated, orthophthalic monomer-based low styrene emission resin with long gel time. It has good hydrolysis and heat resistance and moderate mechanical properties. [12]

All the ageing in this thesis refers to a combination of elevated temperature (90 °C), pressure of ∼15 bar, and a 5% (50 g/l) water-sulphuric-acid bath (immersion).

Vinylester I specimens

The glass-fibre-reinforced laminates made with Vinylester I resin were cut into roughly 26 mm in length, 10 mm width and 3.5 mm thickness using water-jet-cutting (Muototerä Oy [25]). The loading span was selected according to standard ASTM D2344 and it was 18 mm. The accurate dimensions of each test specimen were measured before testing. Each dimension was measured in three different places of the laminate and then an average was calculated to find out the average thickness, width and length of each individual test specimen.

The test series in each condition always consisted of six individual test specimens. There were six reference specimens with lay-up 1 and lay-up 2 each and six aged specimens of both lay-ups. These were dried in an oven at 50 °C temperature until their weight remained constant on a precision scale (see Appendix A for drying curves) and then tested in room temperature. Then there were six specimens of aged laminates of lay-up 1 and lay-up 2 each that had been kept under water until testing and were tested wet in room temperature. Finally there were six specimens of aged laminates of both lay-ups that had been kept under water until testing and tested wet in 90 °C temperature. To summarize, there were a total of 24 Vinylester I specimens that were tested dry and 24 Vinylester I specimens that were tested wet. The visual appearance of Vinylester I specimens is presented in Figure 13.

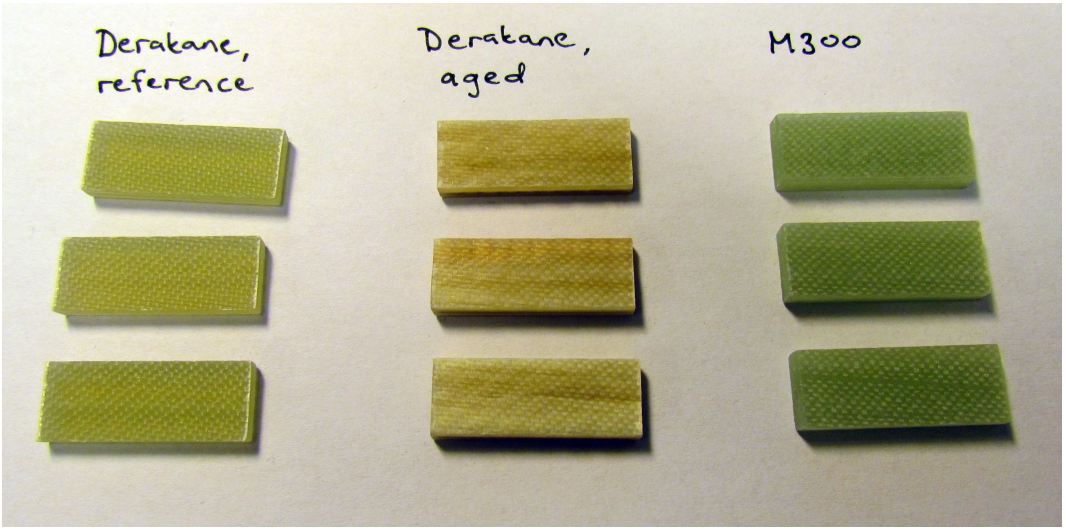

Figure 13: Vinylester I specimens and Polyester I specimens. The aged Vinylester I specimens are coloured grey.

Vinylester II specimens

There were two different sized test specimens that were made of Vinylester II resin, short and long specimens. The short test specimens were the same size with Vinylester I specimens but just much thicker. The short specimens were 26 mm long, 10 mm wide and 7 mm thick. Because of their relatively short length compared to their thickness, a loading span could not be selected according to standard ASTM D2344 but instead the same loading span that the Vinylester I specimens had (18 mm), was selected. The longer Vinylester II specimens were 43 mm long, 10 mm wide and 7 mm thick. Their length to thickness ratio was big enough to select the loading span according to standard ASTM D2344, which is why a loading span of 28 mm was selected.

Similarly to the other test specimens, a series of six test specimens were tested in each condition. Only one lay-up was used in the Vinylester II specimens but the testing temperature, specimen length and ageing varied. There were six reference specimens of both lengths and six aged specimens of both lengths. These were dried in an oven at 50 °C temperature and at a pressure of -0.5 bars until their weight stayed constant on a precision scale (see Appendix A for drying curves). Then they were tested dry in room temperature. In total there were 24 dry test specimens of Vinylester II resin. In addition to them one series of long, aged specimens was tested wet and in higher, 90 °C temperature. This was done to find out the ultimate worst ILSS value for Vinylester II laminates because it had simultaneously all the qualities that decrease ILSS value. The visual appearance of Vinylester II specimens is presented in Figure 14.

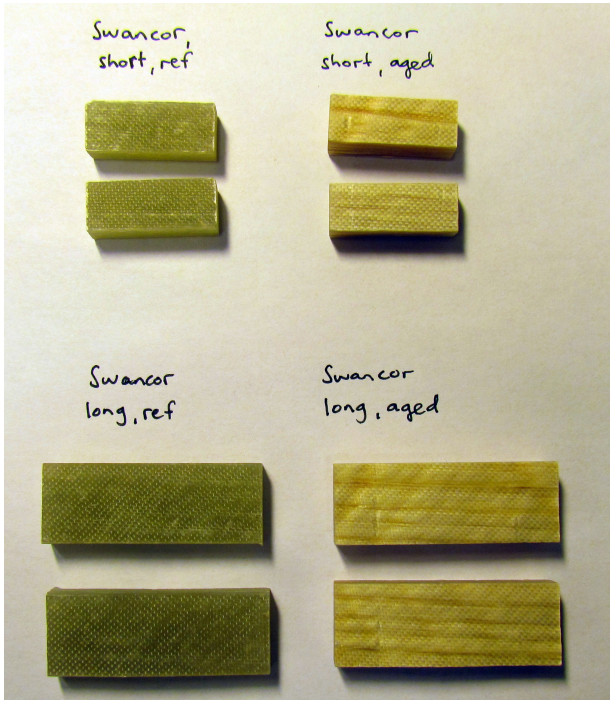

Figure 14: Vinylester II specimens. The aged specimens are coloured grey.

Polyester I specimens

Polyester I was only used in one series of test specimens without ageing in order to find out how the resin selection affects ILSS. The dimensions of the Polyester I specimens were same as the dimensions of Vinylester I specimens, so the length was 26 mm, width 10 mm and thickness 3.5 mm (again water-jet-cut [25]). The loading span was selected according to standard ASTM D2344 and was 18 mm. The Polyester I specimens were dried in an oven at 50 °C temperature and at a pressure of -0.5 bar until their weight stayed constant on a precision scale (see Appendix A for drying curves). After completely dry, they were tested for ILSS in room temperature. A picture of the Polyester I specimens is presented in Figure 13 alongside the Vinylester I specimens. The Polyester I specimens had a slightly greener colour than the yellow-green Vinylester I specimens.

4.1.3 Filament-wound specimens from a cylindrical structure

The filament-wound specimens were glass-fibre-reinforced laminates that were cut from the wall of a cylindrical structure with a radius of ~ 0.5 m. The test specimens were divided into two groups based on their exposure to an acidic liquid and pressure. The first group of specimens was a reference group, which had not been in contact with the acid medium at all and the second group had been exposed to the acid medium for two years. Both groups consisted of 16 laminate pieces, 12 of whom were finally used in the ILSS testing.

The filament-wound specimens needed a lot of manual preparation before they were ready for testing. Because of the cylindrical shape of the filament-wound structure, the unprepared filament-wound pieces (cut sections) had curved sides. This is illustrated in Figure 15 below.

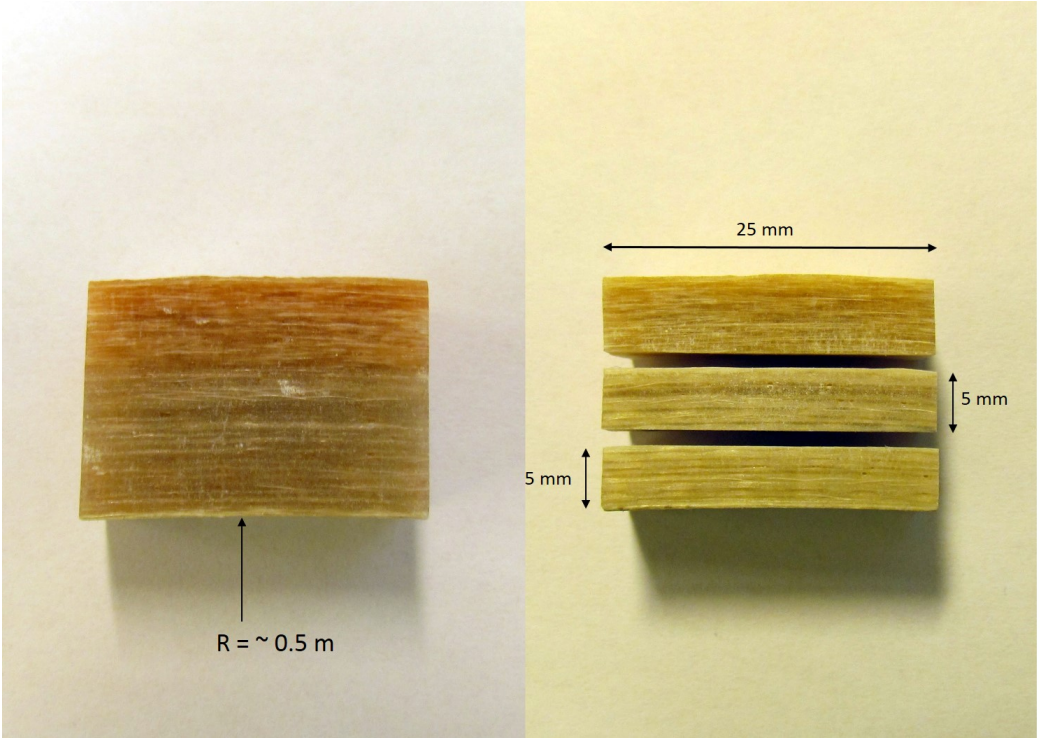

Figure 15: A filament-wound specimen as-received and cut into test specimens.

In Figure 15 it can be seen that the bottom side of the laminate has a slight curve. That is the inner wall of the cylinder, which was in direct contact with the acid medium. The thick upper layer of the specimen that has a slightly red colour is a protective outer layer and was not tested for ILSS.

The thickness of the unprepared laminates was big enough to get two test specimens out of each unprepared laminate. The laminates were cut with a circular diamond saw into a bottom layer and middle layer. These are clearly visible in Figure 15 as the two lowest layers. Both layers were roughly 5 mm thick after the cutting. To ensure the right shape and dimensions of the layers, they were further polished with a wet sand paper (ISO/FEPA grit designation P800) until their thickness was 4.5 $\pm$ 0.1 mm. This resulted in total 16 bottom and middle layer test specimens for each group of laminates with different exposure times. However, only the bottom layer test specimens were tested for ILSS and the middle layer test specimens were stored for future research.

Before the ILSS testing the test specimens were weighed on a precision scale and then put into an oven in 50 °C until the remaining moisture in them had all vaporized and their weight stayed constant (see Appendix A for drying curves).

4.2 Test setup

The experimental testing of the ILSS test specimens was done using a DARTEC M1000/RK universal straining frame. The machine was operated hydraulically and had a capability of inflicting a force in the range of ±100 kN. The actuator stroke length was 150 mm maximum, which was more than enough for the ILSS testing, since most of the test specimens experienced delamination at displacement under 2 mm. The test machine was controlled using a digital control (Multipurpose Elite, MTS) [16]

The support and loading cylinders of the DARTEC M1000/RK are presented in Figure 16. The support cylinders are the two small green circles at the figure and the loading cylinder is the bigger green circle in the middle of them. The diameter of the support cylinders was 3.2 mm and their distance to each other could be freely adjusted. The distance between them was calculated according to standard ASTM D2344 based on the test specimen dimensions. The diameter of the loading cylinder was 6.3 mm and its location was fixed. The location of the support cylinders were adjusted so that the loading cylinder would always be exactly at the middle of them.

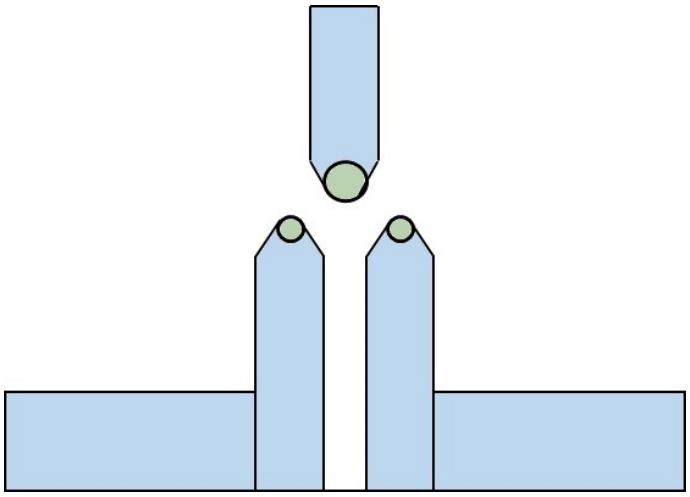

Figure 16: The support and loading cylinders.

The testing machine also had an environmental chamber which allowed for temperatures ranging from −60°C to 300°C. The environmental chamber was used at the tests that were conducted in elevated temperature. It was also easily removable from the test setup, so the tests in room temperature were possible with the same machine. [16] The DARTEC M1000/RK with the environmental chamber attached is illustrated in Figure 17.

Figure 17: DARTEC M1000/RK test machine and a conditioning chamber.

4.3 Test arrangements

The interlaminar shear strength testing was done according to standard ASTM D2344. The loading span length was set manually to 14 mm for the aramid-fibre-reinforced test specimens and to 18 mm for the glass-fibre-reinforced test specimens and to 28 mm for the long glass-fibre-reinforced specimens. The speed of testing was set at a rate of crosshead movement of 1.0 mm / min according to the standard. The computer system measured the applied force and the displacement of the loading cylinder and from the results a force-displacement graph was drawn.

To be sure that the testing conditions were accurate, a certain procedure was adopted. The dry laminates were always dehydrated in an oven at 50 °C temperature and at a vacuum pressure of 0.5 bar until their weight stayed constant on a precision scale. The typical time that the test specimens spent in the oven was around one week right before the beginning of their ILSS tests. During this one week period the test specimens were usually weighed at least two times to see that the weight did not vary much any more. The weighing logs of the test specimens are attached in Appendix A.

When the test specimens were tested in elevated, 90 °C temperature, it was necessary to determine how long it would take until the core of the laminates reaches that higher temperature. This was done via a specific test specimen that was modified so that in the core of it there was an embedded temperature sensor (thermocouple).

This sensor could then be attached to a thermometer and the core temperature measured. A picture of the specific test specimen is presented in Figure 18.

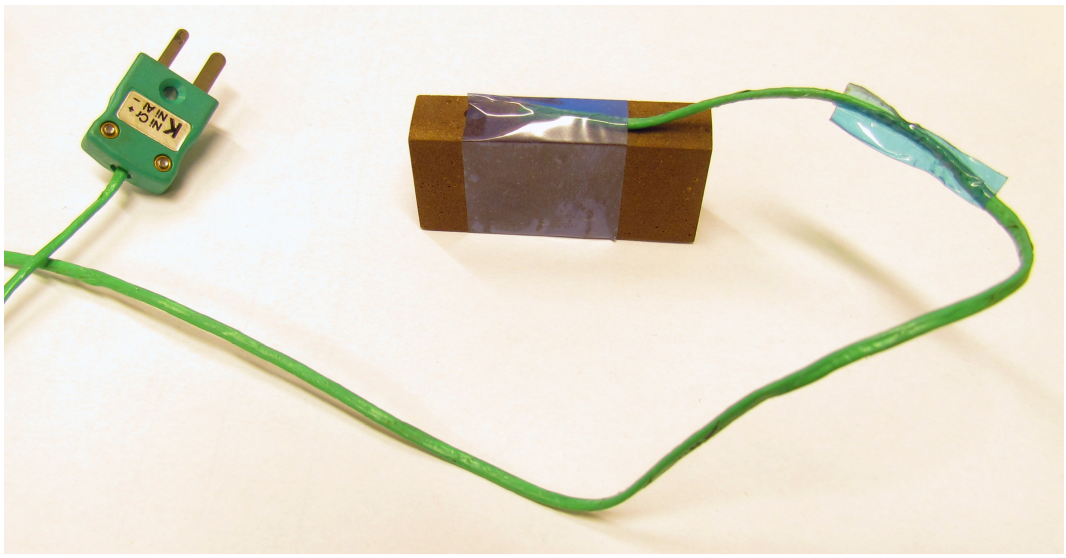

Figure 18: A specific test specimen with an embedded thermocouple that was used to determine the temperature in laminate core.

In the picture it can be seen that the temperature sensor goes into the brown specimen through the side of it. There is a hole drilled in the specimen that reaches the core of the it and the sensor is placed so that it resides in the centre of the specimen. To prevent warm air from the oven penetrating the core prematurely through the drilled hole, and to keep the wire of the sensor firmly in place, the wire was taped to the specimen. This can be seen in the picture as blue tape.

The dimensions of the temperature-measurement specimen were bigger than those of the actual test laminates. The length of it was 46 mm, the width 23 mm and the thickness 10 mm. The bigger dimensions ensured that if the actual test specimens were kept in the oven so long that the core of the temperature-measurement specimen reached the higher temperature, the core of the actual test specimens would also be in that temperature.

The test specimens that were tested wet, were kept immersed in water until just before the testing, when they were taken out of the water. They were not dried in the oven like the other specimens but only the dripping excess water was quickly wiped from their surface and then they were placed in the testing environment between the loading and support cylinders. The conditioning was performed the same way as other laminate specimens (water-acid immersion, elevated temperature and pressure). Picture of the laminates in water immersion is presented in Figure 19.

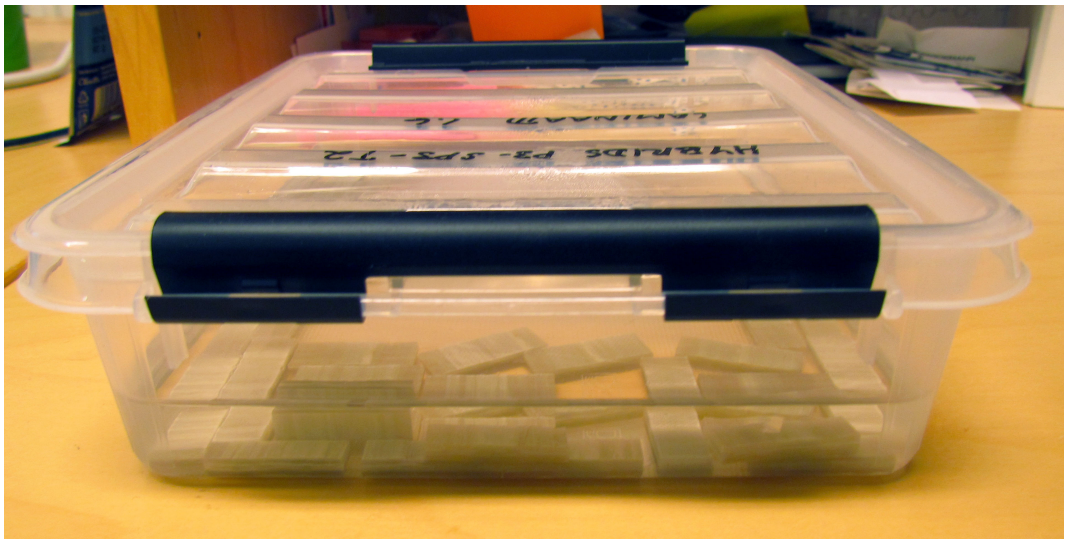

Figure 19: The aged laminates immersed in water inside a plastic container.

5 Finite element analysis

The experimental ILSS testing only gives the maximum force with which the laminate breaks. This is used to calculate the ILSS value but not much else can be concluded from that. In order to study stresses inside the laminate during testing and where the delamination could start, a finite element model of the test setup was simulated using an Abaqus-software (version 6.14-1, standard [28]).

5.1 Finite element model

Due to symmetry reasons, only half of the laminate was modelled to make the calculation process faster. The measurements for the laminate were selected to be the average dimensions of the real test specimens. The length of the model was 13 mm (half of the sample), width 10 mm and thickness 4 mm. The model of the laminate was then partitioned into eleven layers with equal thickness (0.36 mm) for lay-up 1 model and ten layers with equal thickness (0.4 mm) for lay-up 2 model to simulate the actual glass fibre reinforced layers. The partitioning also allowed for different material properties to be assigned for each individual layer. However, in this case the same glass-fibre-reinforced material was used for all of the layers, only changing the orientation of the coordinate system for the layers whose lay-up was 90 degrees to the other direction.

The material parameters were determined based on the material database of ESAComp-software [29]. At first a unidirectional ply with fibre-weight content of 60% was selected from the database. Then the material parameters were scaled so that the results of the simulations started to correlate with the actual experimental test results. This iteration process is further explained in Chapter 6.4.1.

The supporting and loading cylinders were modelled as analytical rigid surfaces. This ensured that the cylinders would not experience any elastic or plastic deformations but stay exactly the same shape during all of the simulation. The movement and rotations were also restricted in each direction for both of the cylinders, so the only object with free movement was the laminate. An exception to this was the z-direction in which the loading cylinder was allowed to move in order to inflict the loading force onto the laminate. The supporting cylinder was 3.2 mm and the loading cylinder 6.3 mm in diameter.

The modelled test setup of lay-up 2 is presented in Figure 20. The meshed laminate is in the middle, coloured light blue. The average element size was 0.4 mm and the total number of elements in the model is 12096. The Abaqus element type was linear hexahedron, type C3D8I. The two cylinders are orange, the smaller of which is the supporting cylinder and the bigger the loading cylinder (compare with Figure 16). The vertical side of the laminate directly below the loading cylinder is in the middle of the whole laminate and its movement is restricted by symmetry boundary condition.

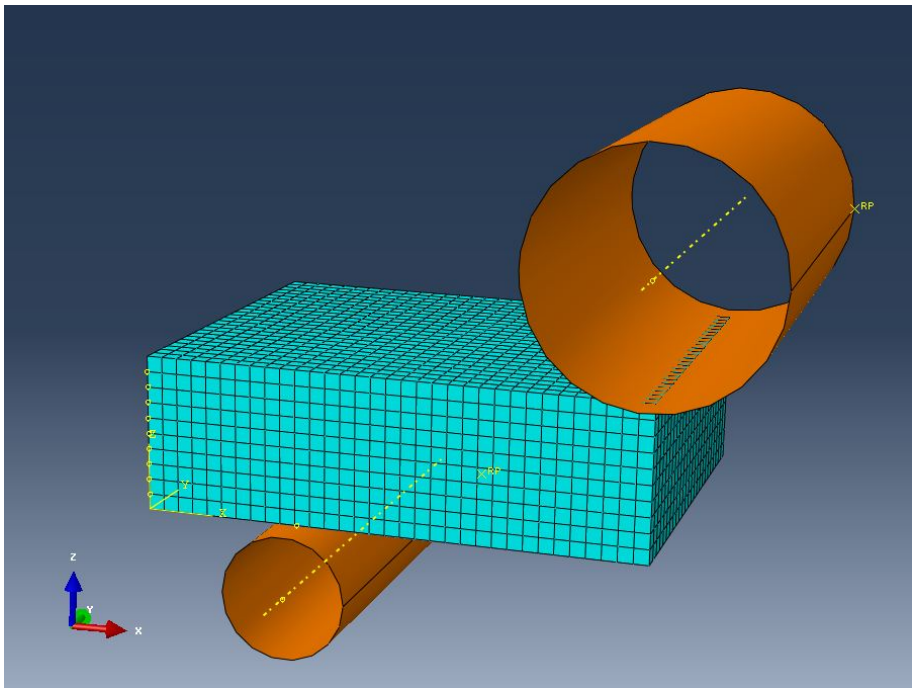

Figure 20: Finite element model of lay-up 2

Since standard stress-analysis was performed, a velocity could not be assigned for the loading cylinder. Instead of that the loading cylinder was assigned an enforced displacement. Based on the experimental test results, which showed that the load always reaches the maximum value when the displacement is around 1 mm, the simulation was set to stop when the loading cylinder had moved 2 mm downwards the z-axis. The software records the loading forces at many different displacements, so the displacement at the maximum load could easily be determined from the simulation results.

In order to see the deformations and shear stresses between each layer, element sets were created out of each interesting layer. This allowed for easy layer hiding method in the visualization module. The most interesting layers were located in the middle of the laminate where the layer directions changed from 0° to 90° or vice versa.

5.2 Boundary conditions

The boundary conditions of the model are illustrated in Figure 21. There is a force F at the right edge of the composite. That is caused by the loading cylinder, which presses the laminate at the middle. Because only half of the laminate was modelled, the right edge of the model is bound by symmetry boundary condition that restricts movement in other directions than vertical. Similarly there is a boundary condition under the laminate at the location where the supporting cylinder is. The supporting cylinder is considered a rigid body that restricts movement in vertical but allows it in horizontal direction.

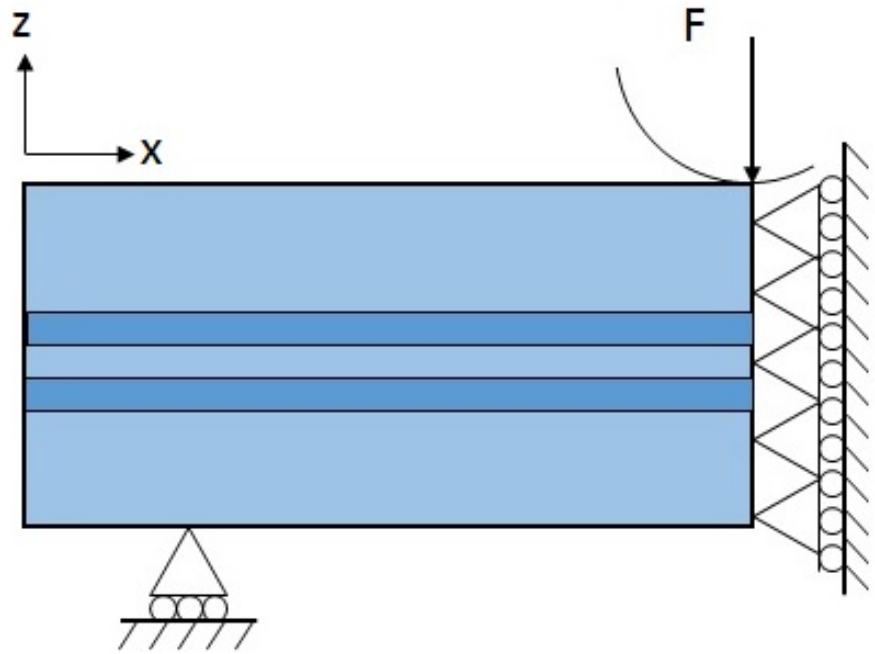

Figure 21: Boundary conditions of the finite element model

6 Results

The experimental testing of the various test specimens was divided into subgroups based on the fibre-type and testing conditions. In this chapter the results of the experimental ILSS tests are presented in the same order that the test specimens were introduced in chapter 4. After the results of the experimental test specimens, the finite element simulation results of both lay-ups are presented and finally they are compared with each other to find differences between them. Due to the sheer number of test series and specimens, the majority of force-displacement curves of the specimens are not presented here but can be found at Appendix B.

6.1 Aramid-fibre-reinforced laminates

The aramid-fibre-reinforced laminates were tested for ILSS in two different groups. In the first group the laminates had been dried in an oven until dry and in the second group the laminates were placed in water for one week before testing and tested wet. Both groups were tested in room temperature. The results show similar tendencies for both groups but the ILSS values for wet laminates seem to have generally decreased by roughly 5 MPa.

6.1.1 Dry test specimens

A total of six specimens per each dry aramid-fibre-reinforced laminate was tested for ILSS. The average ILSS and the standard deviation of the dry test specimens can be seen in Figure 22.

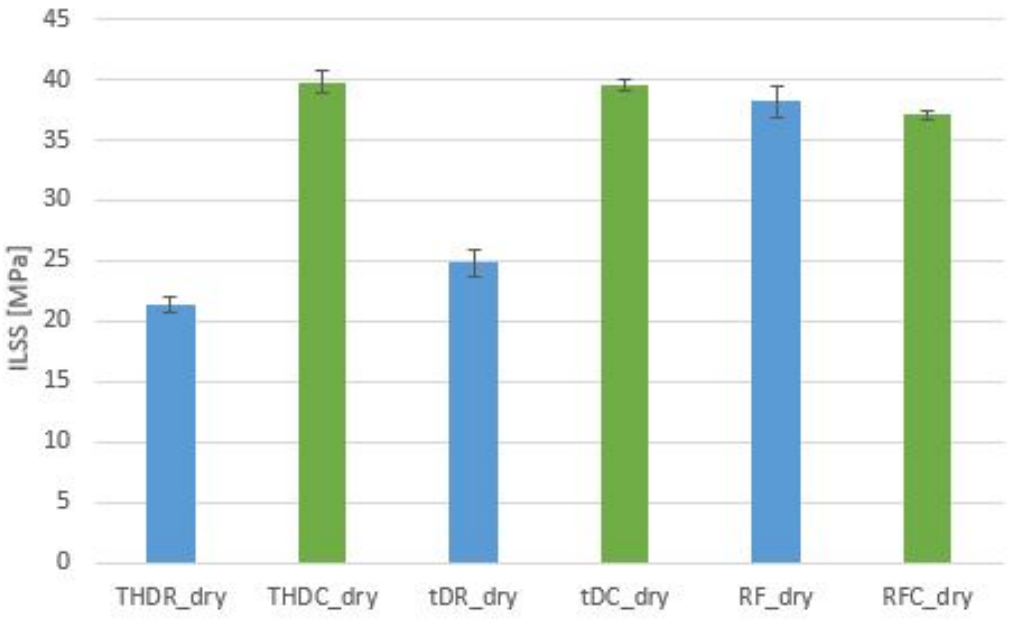

Figure 22: ILSS results for aramid-fibre-reinforced, dry laminates.

The blue bars in Figure 22 are aramid-fibre-reinforced laminates, in which the aramid fibres have not been cleaned before laminating and the green ones have been ultrasonically cleaned.

When laminates with unclean fibres (THDR, tDR and RF) are compared with each other it is clear that the laminates, in which the aramid fibres are coated with a diamond-like-coating (THDR and tDR), the ILSS value is much lower than in the reference laminate (RF). The average ILSS values for the unclean laminates are 38.2 MPa for RF, 24.8 MPa for tDR and 21.4 MPa for THDR. Compared to the reference laminate RF, the ILSS value of the laminate with thin diamond-like-coating, tDR, is 35.0% lower and the ILSS value of the laminate with thick diamond-like-coating, THDR, is 44.0% lower.

For the laminates in which the aramid fibres have been cleaned ultrasonically before laminating, THDC, tDC and RFC, the changes are not nearly as drastic. The diamond-like-coating seems to slightly increase the ILSS values but the differences between the three laminates are not very significant. The ILSS value of the reference laminate RFC is 37.1 MPa. For the laminates with thick and thin diamond-like-coating, THDC and tDC, the ILSS values are 39.8 MPa and 39.6 MPa, respectively. Compared to the reference laminate, the thick diamond-like-coating increases the ILSS value by 7.3% and the thin diamond-like-coating by 6.8%.

The biggest difference in ILSS values can be seen when same laminates with pre-cleaned fibres and unclean fibres are compared to each other. When the fibres are cleaned ultrasonically before coating them with thick diamond-like-coating, the ILSS value 21.4 MPa (THDR) increases to 39.8 MPa (THDC), which is a 86.0% increase. Similarly, pre-cleaning the fibres increases the ILSS value of the laminate with thin diamond-like-coating by 59.4% (from 24.8 MPa to 39.6 MPa). For the reference laminates without diamond-like-coating, the effect is much smaller and to the opposite direction. The ILSS value decreases by 2.9% (from 38.2 MPa to 37.1 MPa), when the fibres are cleaned before laminating.

6.1.2 Wet test specimens

A total of three specimens per each wet aramid-fibre-reinforced laminate was tested for ILSS. The average ILSS and the standard deviation of the wet test specimens can be seen in Figure 23.

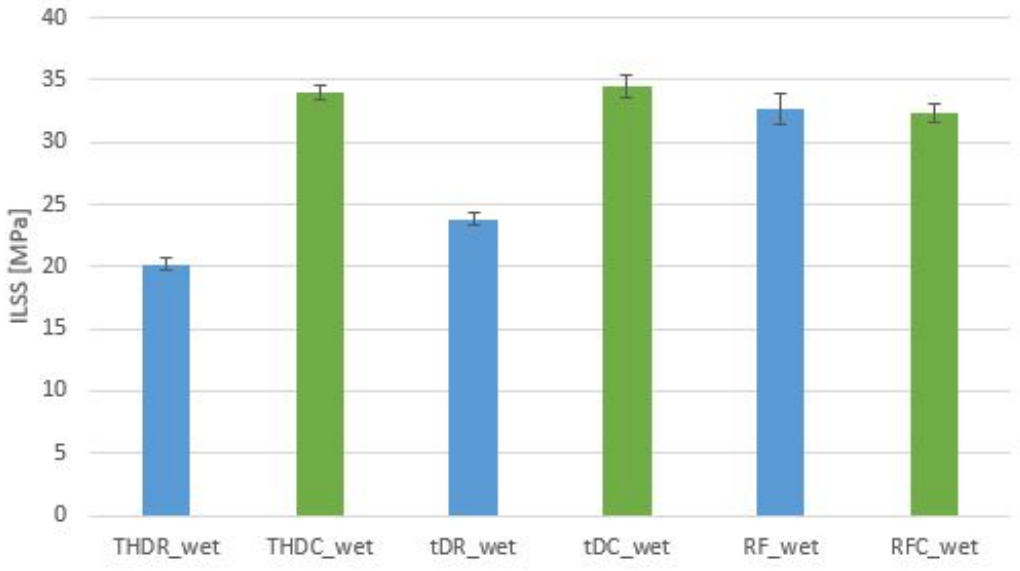

Figure 23: ILSS results for aramid-fibre-reinforced, wet laminates.

Similarly to the dry aramid-fibre-reinforced laminates, the blue bars represent test specimens with unclean aramid fibres and the green bars test specimens in which the aramid fibres were ultrasonically cleaned before laminating.

In the group of the laminates, in which the fibres are not pre-cleaned, there is again a clear drop in ILSS values between the reference laminate and laminates with diamond-like-coating. The ILSS value of the reference laminate RF is 32.6 MPa and the values for THDR and tDR are 20.2 MPa and 23.8 MPa, respectively. Percentually this means that the ILSS value for THDR is 38.1% and for tDR 27.0% lower than that of the reference laminate.

In the other group, where the fibres are ultrasonically cleaned before coating and laminating, the differences in ILSS values are not that big. Just like in dry specimens, the laminates with diamond-like-coating have a slightly higher ILSS value than the reference laminate. Whereas the ILSS value of RFC is 32.4 MPa, the ILSS for THDC and tDC are 33.9 MPa and 34.5 MPa, respectively. Proportionally this means a 6.5% increase in ILSS for tDC and a 4.7% increase for THDC.

Again the biggest differences in ILSS values are between the unclean and cleaned specimens of the otherwise identical laminates. Ultrasonically cleaning the aramid fibres before coating them with a thick diamond-like-coating increases the ILSS by 67.9% (from 20.2 MPa to 33.9 MPa) and in the case of thin coating by 44.9% (from 23.8 MPa to 34.5 MPa). In the reference laminates the cleaning does not seem to have a big effect. The ILSS decreases by 0.7% (from 32.6 MPa to 32.4 MPa) but the standard deviation is already bigger than that so the decrease is not really big enough to draw any conclusions from it.

The behaviour of the aramid-fibre-reinforced specimens in ILSS testing was not as good as hoped. They were quite flexible and did not clearly delaminate. The damage to them was more plastic and the laminate only crushed and bent under loading nose. This can be seen in Figure 24.

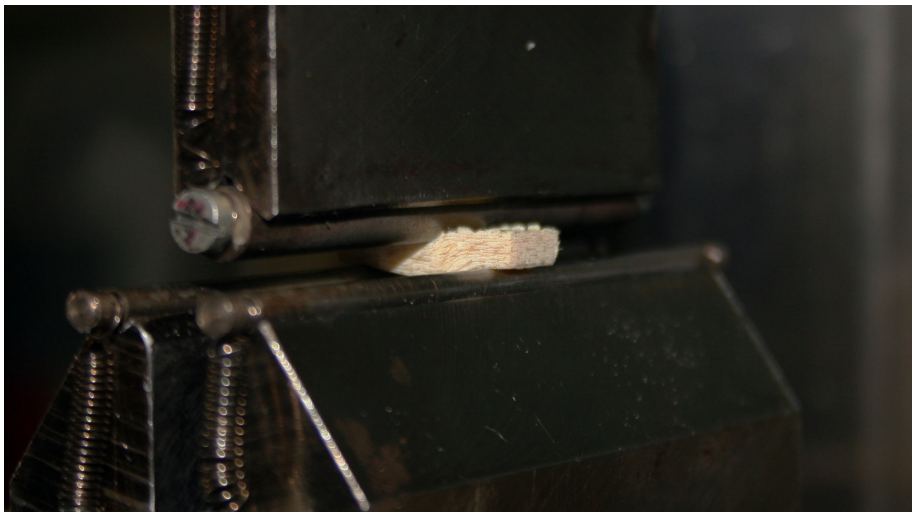

Figure 24: Aramid-fibre-reinforced test specimen in ILSS testing.

6.2 Glass-fibre-reinforced laminates

The glass-fibre-reinforced laminates consisted of four groups. There were dry and wet specimens that had been made using Derakane 441 resin (Vinylester I), specimens that had been made using Swancor resin (Vinylester II) and specimens that were made using M300 resin (Polyester I).

6.2.1 Dry Vinylester I specimens

There were two laminate series with different lay-ups that were made using Vinylester I resin. These groups were further divided to subgroups based on their ageing time and test conditions. The average ILSS values of each groups are presented in Figure 25.

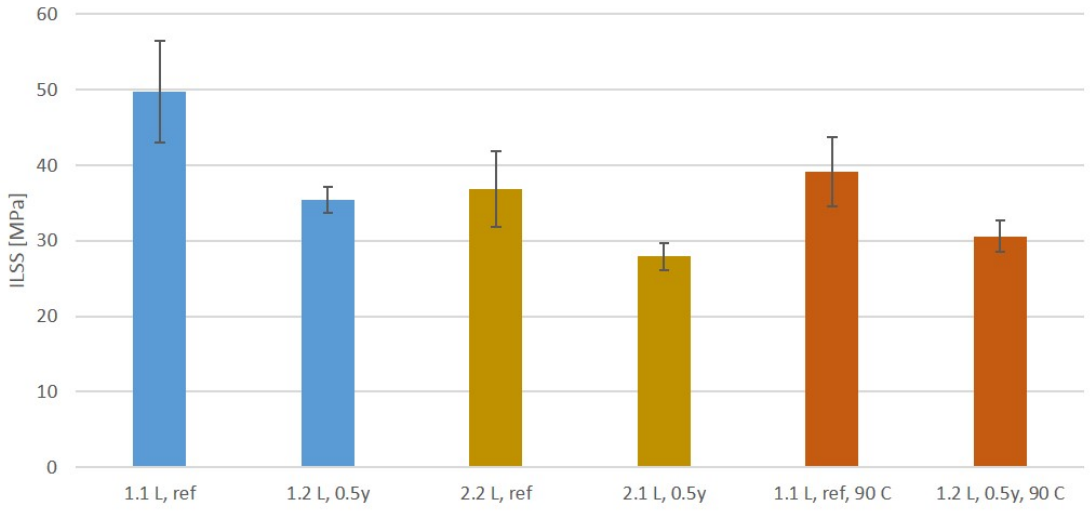

Figure 25: Dry Vinylester I specimens.

In Figure 25 each colour represents a different lay-up or test condition. The laminates with names starting with 1.x are of lay-up 1 and the ones starting with 2.x are of lay-up 2. Each colour group has two bars, the left of whom represents the reference laminate and the right the laminate that has been aged for half a year in an acidic solution.

The difference between the two lay-ups can be seen, when comparing the blue and yellow bars to each other. The ILSS of the reference laminate of lay-up 1 is 49.7 MPa and the ILSS of lay-up 2 is 36.9 MPa, which means that the ILSS of laminate of lay-up 2 is 25.9% lower than that of lay-up 1. The effect of the lay-up is similar also between the aged specimens where lay-up 2 has 21.3% lower ILSS (from 35.4 MPa to 27.9 MPa) than lay-up 1.

The ageing decreases the ILSS value for both lay-ups and also in the higher testing temperature. After half a year of ageing, the ILSS of lay-up 1 in room temperature decreases by 28.7% (from 49.7 MPa to 39.4 MPa) and in elevated, 90 °C temperature, by 21.9% (from 39.2 MPa to 30.6 MPa). For lay-up 2 the ageing decreases ILSS in room temperature by 24.3% (from 36.9 MPa to 27.9 MPa).

The higher, 90 °C, temperature has a negative effect on ILSS for both reference and aged test specimens of lay-up 1. The ILSS of the reference laminates decreases by 21.3% (from 49.7 MPa to 39.2 MPa) in 90 °C and the ILSS of the aged laminates by 13.7% (from 35.4 MPa to 30.6 MPa).

The behaviour of the dry Vinylester I test specimens in the ILSS testing was very good and the failure of the laminate typically happened suddenly accompanied with an audible, loud crack. Figure 26 below shows examples of typical force-displacement curves for dry Vinylester I specimens. The points, when the delaminations occurred are easy to spot from it, since there are sharp spikes after which the load drops drastically.

Because of the brittle behaviour of the Vinylester I test specimens, they often experienced multiple delaminations, which ultimately lead to failure. If the test was

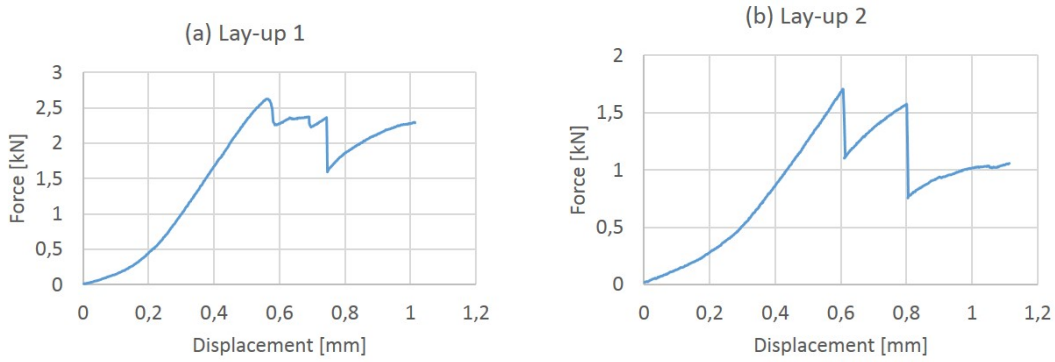

Figure 26: Typical force-displacement curves for dry Vinylester I specimens: (a) for lay-up 1 and (b) for lay-up 2

continued after the first delamination, the laminate sometimes resisted even higher load before delaminating again. A picture of a test specimen with multiple visible delaminations is presented in Figure 27.

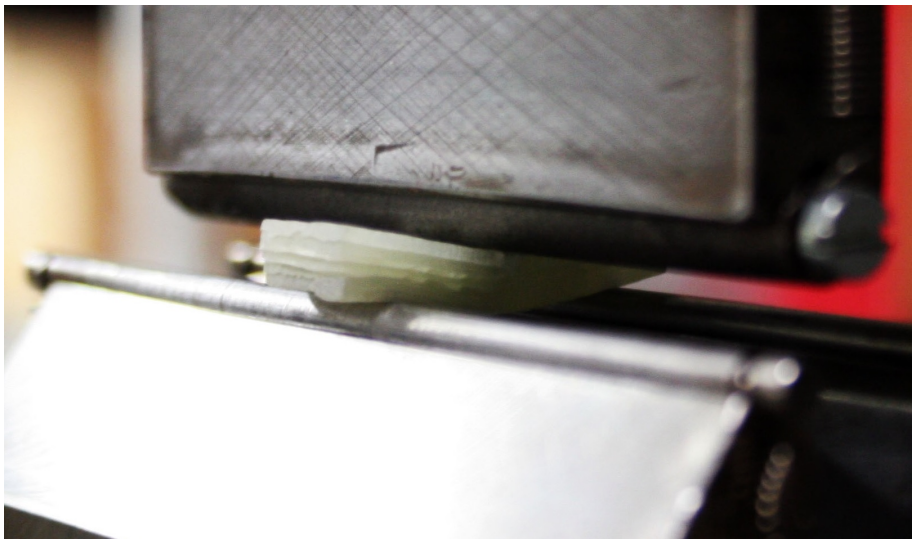

Figure 27: Multiple delaminations in dry Vinylester I specimen during ILSS testing.

6.2.2 Wet Vinylester I specimens

Some of the glass fibre reinforced laminates were aged in distilled water for half a year before testing them and they were tested wet. Both lay-ups were tested in room temperature as well as in 90 °C. The average ILSS values can be seen from Figure 28.

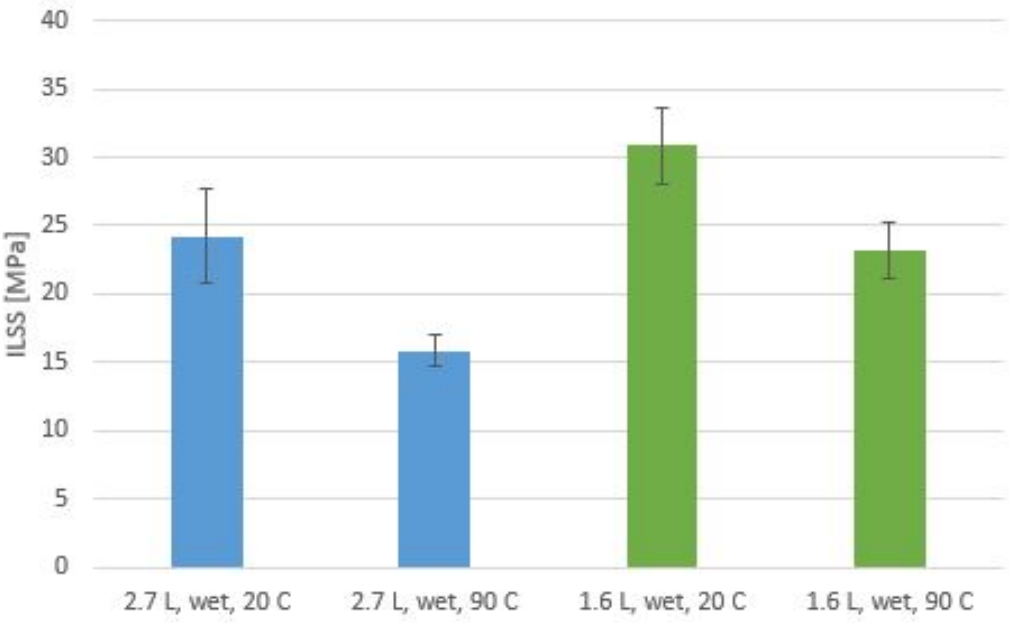

Figure 28: The average ILSS values of wet Vinylester I laminates.

Just like in the case of dry test specimens, the bars starting with 1.x are of lay-up 1 and bars starting with 2.x are of lay-up 2. The colours represent a different lay-up. Each colour has two bars, the left of whom represents the ILSS in room temperature and the right in elevated temperature.

A similar trend to the dry laminates can be seen from the graph. Once again, the laminates with lay-up 1 are showing higher ILSS values than laminates with lay-up 2. In room temperature, the test specimens of lay-up 2 have a 21.6% lower ILSS than specimens of lay-up 1 (from 30.9 MPa to 24.2 MPa). In elevated, 90 °C, temperature the ILSS drops by 31.8% (from 23.2 MPa to 15.8 MPa).

The higher temperature also has a negative effect on ILSS within the same lay-up configuration. In laminates of lay-up 1, the ILSS value decreases by 24.7% (from 30.9 MPa to 23.2 MPa) in higher temperature and in laminates of lay-up 2, it decreases by 34.5% (from 24.2 MPa to 15.8 MPa).

When tested wet, the Vinylester I specimens did not behave as well as the dry specimens. Typical force-displacement curves of both lay-ups are presented in Figure 29. The curves are quite smooth and there are not as clear spikes as in the case of dry specimens. However, sometimes there were delaminations, which can be seen from the lay-up 2 curve as the sudden drop of force at displacement of 0.95 mm.

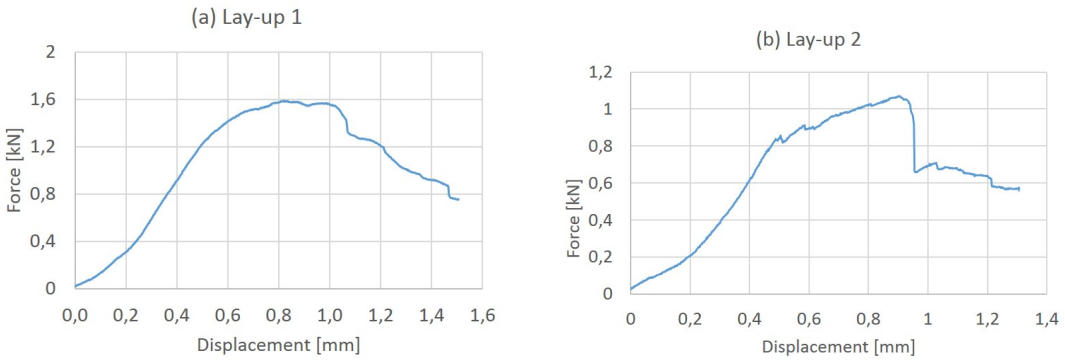

Figure 29: Typical force-displacement curves for wet Vinylester I specimens in room temperature: (a) for lay-up 1 and (b) for lay-up 2

6.2.3 Polyester I specimens

In order to test how the matrix material affects the ILSS values of the glass-fibre-reinforced laminates, one test group was made using Polyester I resin. The polyester laminates were laminated using lay-up 1 and they were tested dry, unaged and in room temperature. The average ILSS values of dry, unaged Vinylester I specimens of lay-up 1 in room temperature in comparison with Polyester I samples in exact same conditions are illustrated in Figure 30.

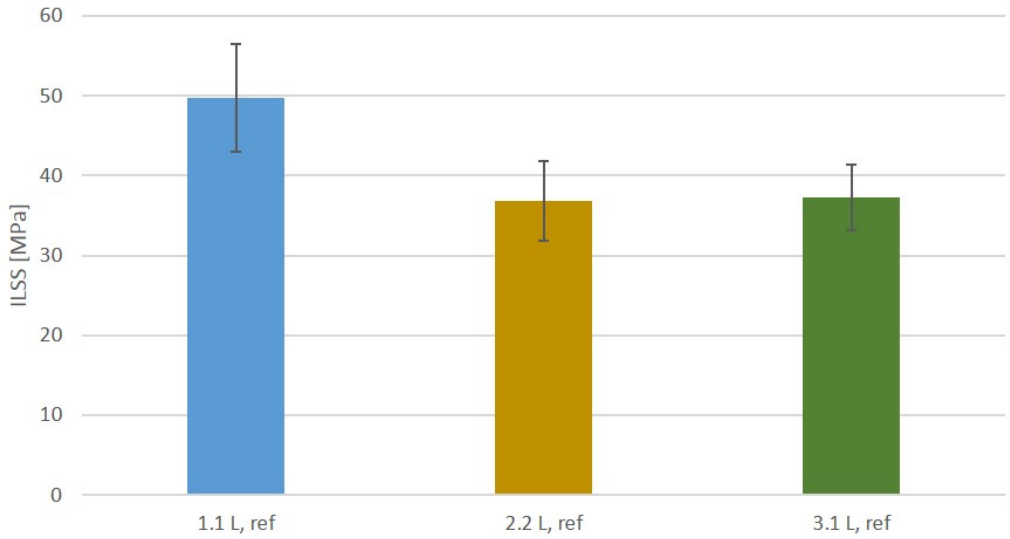

Figure 30: The average ILSS values of Polyester I laminates in comparison with Vinyester I reference laminates.

In Figure 30 the blue bar (series 1.1) represents the Vinylester I specimens of lay-up 1, yellow bar (series 2.2) the Vinylester II specimens of lay-up 2 and the green bar (series 3.1) Polyester I specimens of lay-up 1. Based on the results, it is

quite obvious that the usage of Polyester I instead of Vinylester I resin results in weaker laminates. The average ILSS value of Polyester I specimens is 37.2 MPa, which is 25.1% lower than that of Vinylester I specimens with lay-up 1. In fact, the average ILSS value of Polyester I specimens is only slightly higher (1%) than that of Vinylester I specimens of lay-up 2.

6.2.4 Vinylester II specimens

A small group of the glass fibre reinforced laminates used a different resin than the majority of them. The resin was made by Swancor (Vinylester II). Half of the Vinylester II specimens were aged in acidic solution for half a year before testing and the other half was a reference group. The average ILSS values of the Vinylester II specimens are illustrated in Figure 31.

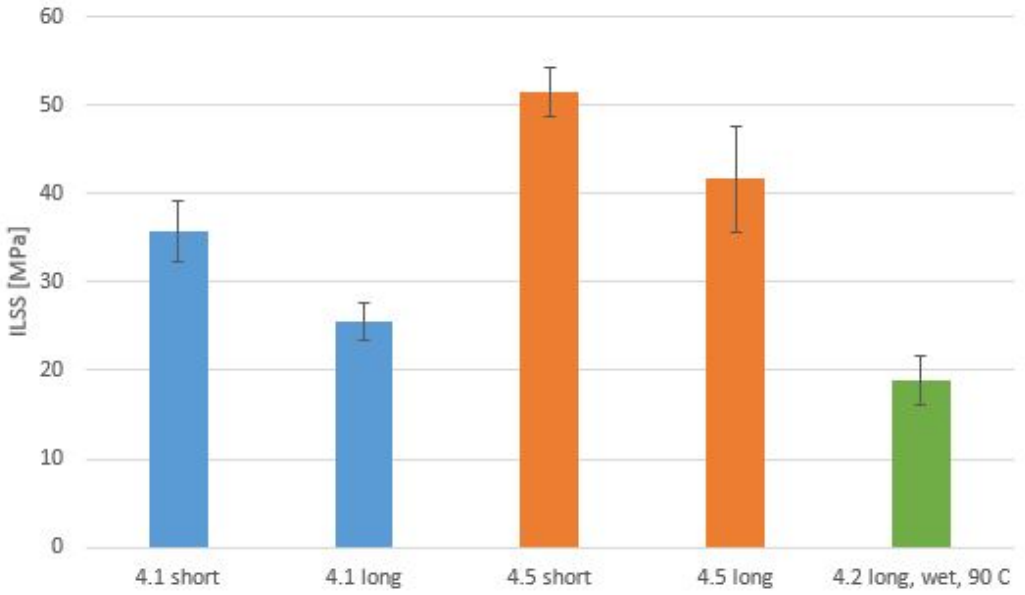

Figure 31: The average ILSS values of Vinylester II specimens.

The three colours in Figure 31 represent different ageing conditions. From each laminate there were two sizes of test specimens, long and short, which both are of the same thickness. The blue bars (series 4.1) represent the long and short laminates that were aged half a year and tested dry in room temperature. The orange bars (series 4.5) represent the long and short reference laminates that were tested dry in room temperature. The green bar (series 4.2) represents the test specimens, which were designed to give the ultimate worst ILSS value, to define the limits of the Vinylester II resin. The 4.2 series test specimens were aged in acid for half a year and immediately after that submerged in distilled water for water ageing. They were tested wet and in elevated, 90 °C temperature.

Because the short ILSS test specimens are as thick as the long ones, it was clear even before the testing that their critical force values will be higher. In the group

of reference laminates tested in room temperature, the ILSS of the long laminate is 19.1% lower than that of the short laminate (from 51.5 MPa to 41.7 MPa). For the aged test specimens, the drop is 28.5% (from 35.7 MPa to 25.5 MPa).

The ageing in acid also has a negative effect on the ILSS values. For the short laminates, the ageing decreases the ILSS by 30.6% (from 51.5 MPa to 35.7 MPa) and for the long laminates by 38.7% (from 41.7 MPa to 25.5 MPa).

The test specimens of series 4.2 showed the lowest ILSS values of all Vinylester II laminates as they were designed to. Compared to the aged, long specimens in room temperature, the test specimens of series 4.2 had a 26.2% lower ILSS value (from 25.5 MPa to 18.9 MPa) and compared to the reference specimens, the decrease was 54.8% (from 41.7 MPa to 18.85 MPa).

6.3 Filament-wound glass-fibre-reinforced specimens

A total of twelve test specimens per laminate were tested for ILSS. These were further divided in two groups of six specimens, the other of whom was tested in room temperature and the other in 90 °C. The average ILSS values of each group is presented in Figure 32.

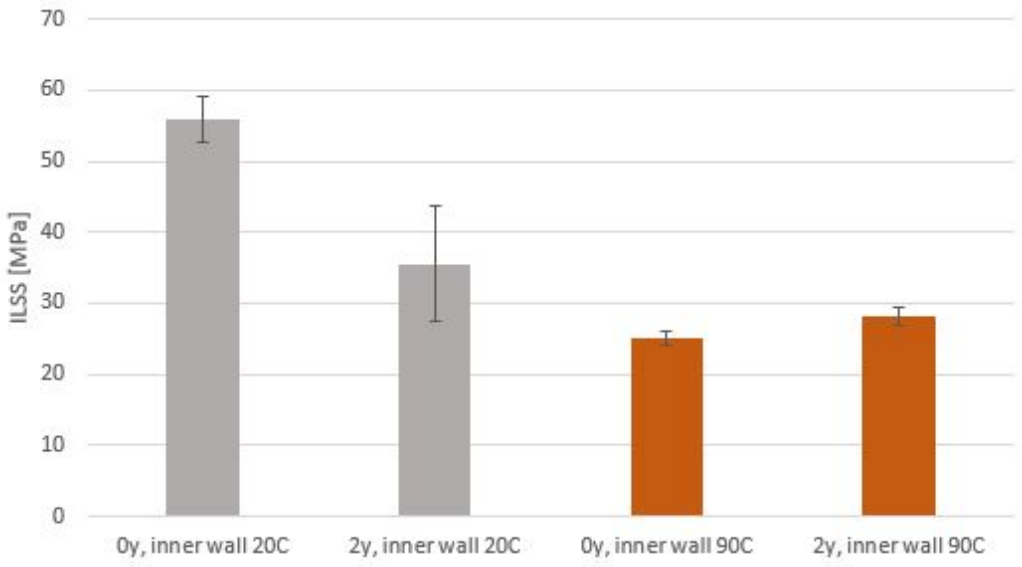

Figure 32: ILSS test specimens from the inner wall of the filament-wound cylinder.

The grey coloured bars in the graph represent the test specimens that were tested in room temperature and the red ones specimens that were tested in higher temperature. The leftmost bar of each colour represents the reference laminates that were not in contact with acid and the other bars laminates that had been aged in acidic solution for two years.

Both, higher temperature and the exposure to acid for two years, have a negative effect on ILSS. The reference specimens that have not been in contact with acid at all had the biggest drop in ILSS values in the 90 °C temperature, while the aged

test specimens also experience a drop in much smaller scale. The ILSS value of the reference laminates drops by 55.1% (from 56.0 MPa to 25.1 MPa), when the temperature is raised from 20 °C to 90 °C, whereas the ILSS of the aged test sample only drops by 20.6% (from 35.6 MPa to 28.3 MPa). However, it should be noted that the standard deviation of the aged test specimens in room temperature is quite high, so some of the specimens actually exhibit similar ILSS values as the aged specimens that are tested in 90 °C.

When only the ageing effect is taken into consideration, the results are a bit surprising. In room temperature the ILSS value decreases by 36.4% (from 56.0 MPa to 35.6 MPa) but in 90 °C temperature the ILSS actually slightly increases, by 12.5% (from 25.1 MPa to 28.3 MPa).

The behaviour of the filament-wound specimens in ILSS testing depended quite much on testing temperature. In room temperature the laminates were brittle and the failure mode was predominantly delamination. In some cases the delaminations were visible to plain eye. Example of a test specimen with visible delamination is presented in Figure 33. The sample in the picture is one of the acid aged specimens that was tested in room temperature.

Figure 33: Filament-wound specimen with visible delamination.

The laminates that were tested in elevated 90 °C temperature were much more flexible. The deformations were plastic and in some cases the laminates remained in the bent form after testing. This is illustrated in Figure 34 where two differently aged laminates are tested in elevated, 90 °C temperature. The upper laminate in the picture is the reference laminate and the lower one an aged laminate. The temperature seemed to have a greater effect on the reference laminate, which can be seen in the picture where the reference laminate is visibly more bent that the aged laminate. This can be a result of embrittlement that has happened during the ageing in high temperature acid, which has made the aged laminate more brittle.

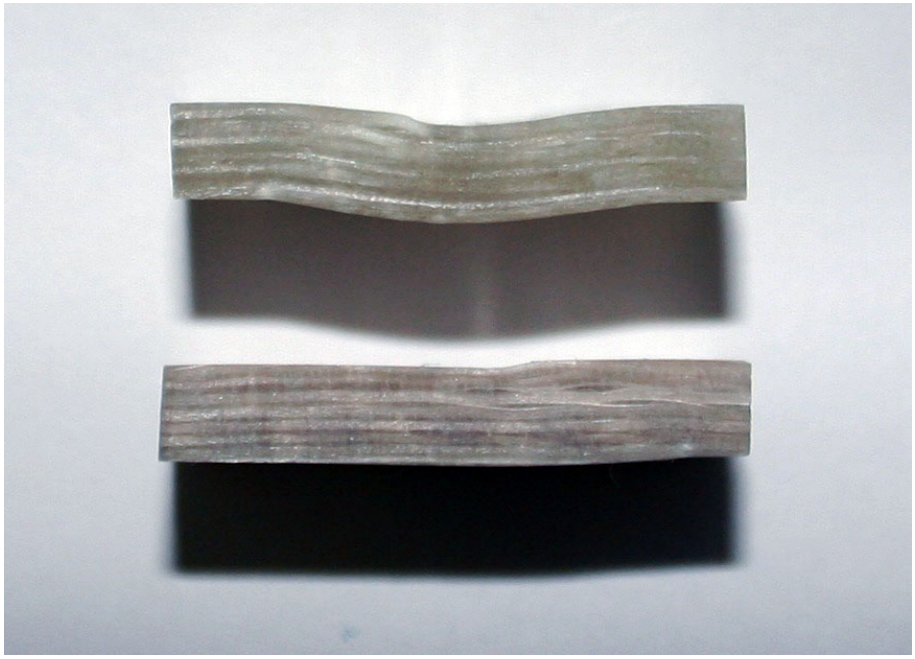

Figure 34: Filament-wound specimens tested in elevated temperature. The upper one is a reference laminate and the lower one a laminate that has been aged for two years.

6.4 Finite element simulation results

A finite element simulation was run for the tests of both lay-ups, so that the differences between the lay-ups could be compared to each other. The simulation results in this subchapter are presented so that the results of the model with lay-up 1 are first, followed by the results of the model with lay-up 2.

6.4.1 Adjusting the simulation parameters

In order to find an accurate material model with which the simulation would correlate with the experimental test results, the simulation was run with three different material models. First, the simulation was run with a unidirectionally reinforced ply consisting of E-glass and epoxy with a fibre weight percentage of 60% as the material. The mechanical properties of it were $E_1 = 45$ GPa, $E_2 = E_3 = 10$ GPa, $G_{12} = G_{13} = 5$ GPa, $G_{23} = 3.85$ GPa and $\nu_1 = \nu_2 = \nu_3 = 0.3$. Then the simulation was run with two different fibre weight percentages by scaling the values of the material with 60% fibre weight content. Specifically, the Young's moduli (E_1, E_2 and E_3) and the shear moduli (G_{12}, G_{13} and G_{23}) were scaled and the Poisson values left untouched. The scaling was done simply with Equation 3

$$A_{new} = \frac{A_{old}}{60} x \tag{3}$$

where A_{new} refers to the E or G value of the scaled material model, A_{old} to

the original E or G value of the 60% material model, and x to the desired fibre percentage of the new material model (e.g. 55% or 70%).

At first, a material model with 55% fibre weight content was simulated and then a material with 70%. After the simulations were complete, XY-data of the reference point of the loading cylinder was printed into a text file. This was done for each of the simulations with different material models. The XY-data consisted of force and displacement of the reference point of the loading cylinder in z-direction. Then force-displacement curves for each different fibre-weight percentage simulation was plotted in a single graph to compare the effect of different material models. To see, which material model correlated most accurately with actual test results, the six force-displacement curves of experimental test specimens were plotted in the same graph. Specifically the six test specimens were dry Vinylester I laminates that were unaged and tested in room temperature. The simulation results with different material models for both lay-ups are presented in Figures 35 and 36.

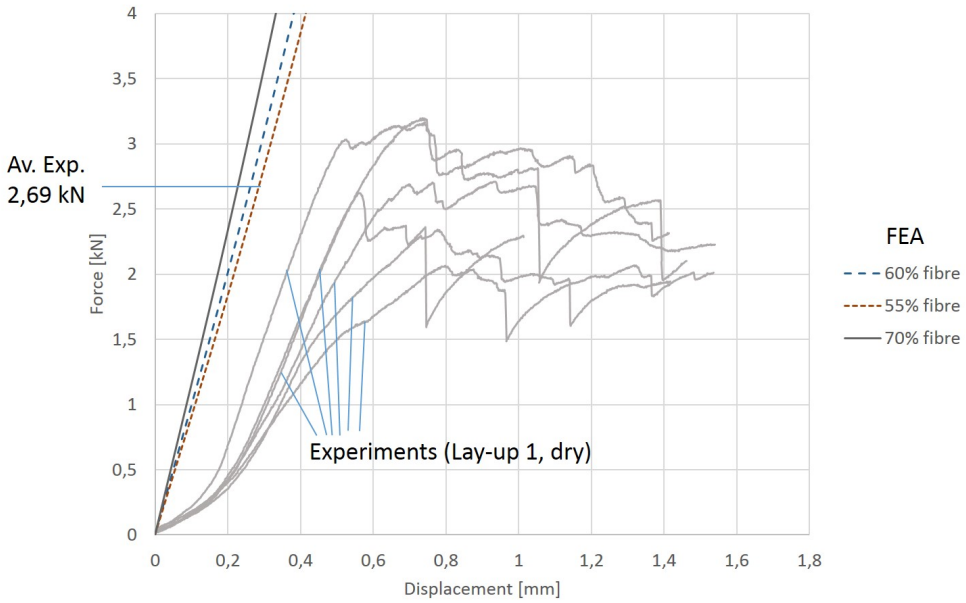

Figure 35: The force-displacement curves of lay-up 1 with different fibre-weight percentages.

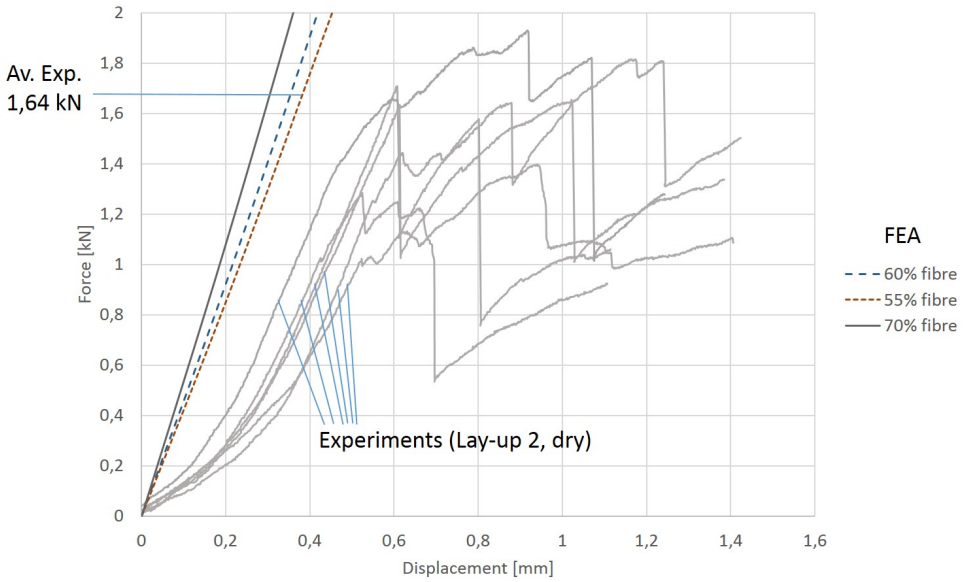

Figure 36: The force-displacement curves of lay-up 2 with different fibre-weight percentages.

In Figures 35 and 36 the grey force-displacement curves represent the experimental test specimens. The brown, blue and black curves represent the simulation results with material models with 55%, 60% and 70% fibre-weight ratio, respectively. For both lay-ups, the material model with fibre-weight ratio of 55% is a too soft material, which results in slightly lower slope than the simulation should give. The simulation model with 60% fibre-weight ratio has a slightly steeper slope than the model with 55% ratio but still not enough. That is why a 65% was not even tested but the next simulation was done with 70% fibre-weight ratio. Indeed, the simulation results with the 70% ratio seem to correlate with the actual test results better than the smaller fibre-weight ratios. This is why finally the material model with 70% fibre weight ratio was selected for both lay-ups in the simulations.

6.4.2 Lay-up 1

The finite element model of the laminate with lay-up 1 was partitioned so that in z-direction each element represents one unidirectionally reinforced ply. This allowed for different material orientations to be assigned for the layers that had a different fibre orientation. Because lay-up 1 consisted of 11 plies, the ply in the middle of the laminate was split into two elements so that the shear stresses in the neutral plane of the laminate could be observed. Although the simulation was run until the displacement of the loading cylinder was 2 mm in z-direction, the results presented in the following figures are taken at a displacement of 0.7 mm, which more closely represents the displacement, where the first delamination happened for the experimental test specimens. A side view of the shear stress distribution of the laminate with lay-up 1 is presented in Figure 37.

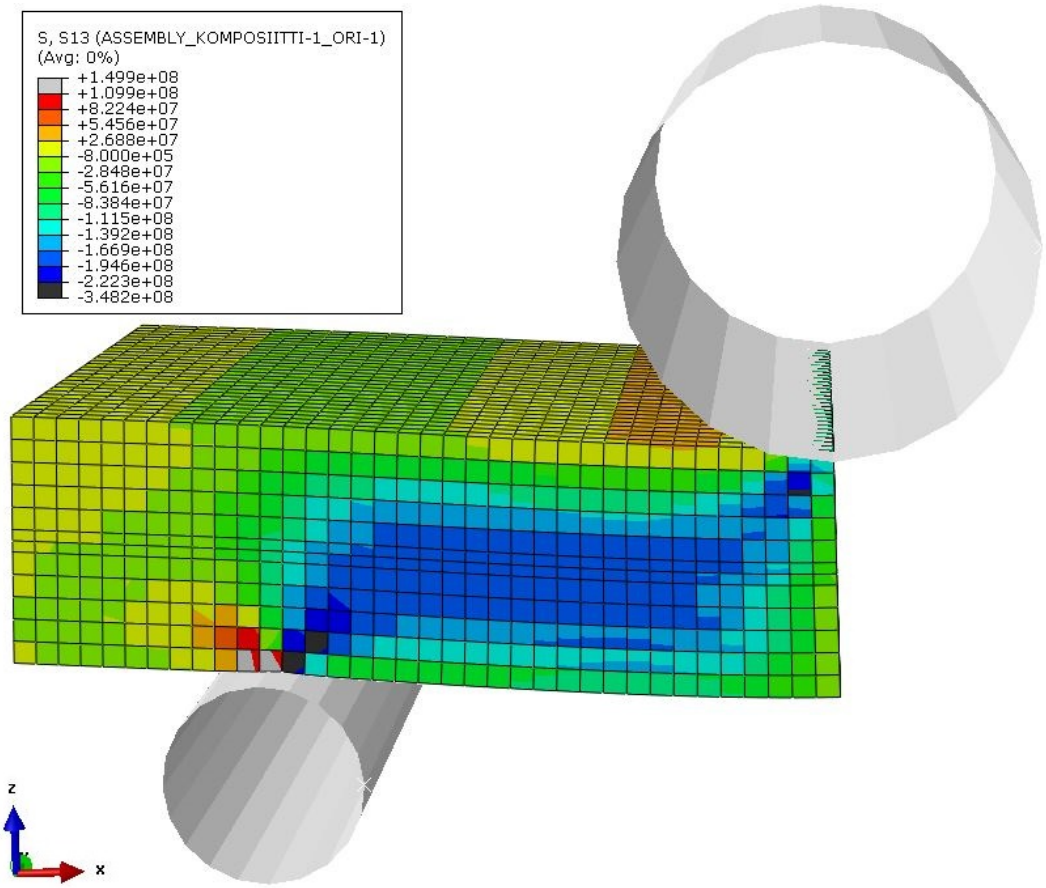

Figure 37: The shear stress distribution at the side of the laminate with lay-up 1.

The shape of the shear stress contour in Figure 37 resembles closely the ones obtained by Feraboli et al in 2003 [7] and Xie M in 1995 [5]. Both of the previous studies had a similar contour as the blue area in Figure 37. The shape of the contour is a parallelogram with slightly extended corners near the loading and supporting cylinders. The units in the legend are standard SI-units for shear stress, Pascals, and are ranging from 150 MPa to -350 MPa to visualize the shear stress contour clearly. Some single elements directly in touch with the support cylinder experience shear stresses higher than the values in the legend, which is why they are coloured grey. The experimental test specimens experienced some plastic deformations at those areas but delamination does not originate there, which is why these stresses are not very interesting and could be left outside the legend values.

A more accurate understanding of the shear stress distribution inside the laminate is acquired when some of the plies are removed from the results. The simulation was still run with all layers in place but only in the visualization some of the layers were removed to see between them. Three different cross-sections of the simulation model with lay-up 1 in x-y plane are illustrated in Figures 38– 40. Each figure has a small picture of the laminate cross-section from the side with an arrow pointing to the interface where the cross-section is taken.

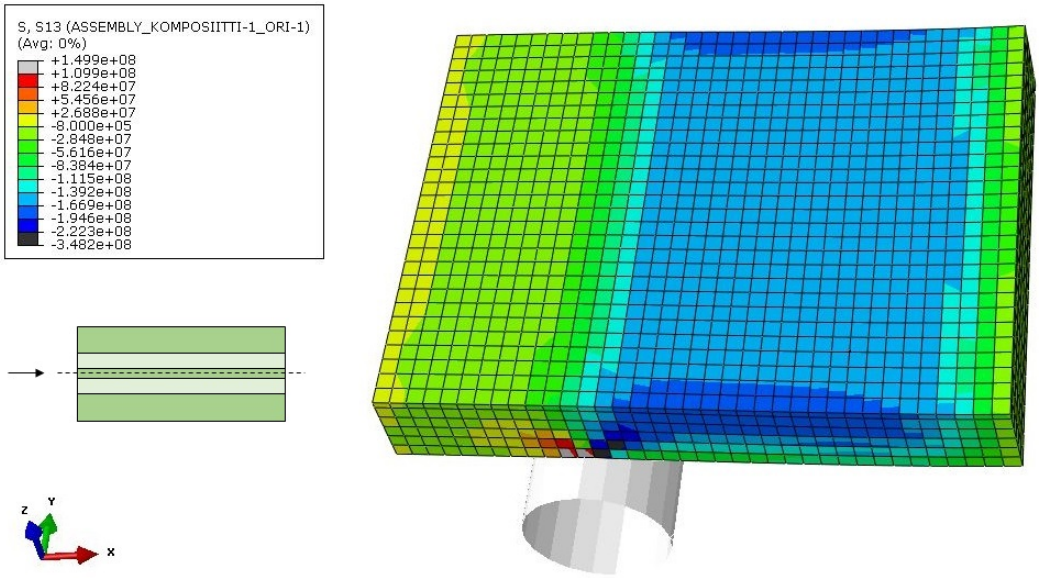

Figure 38: The shear stress distribution at the neutral plane of the laminate with lay-up 1.

The shear stress distribution in the middle of the laminate with lay-up 1 is illustrated in Figure 38. This is also know as the neutral plane. Based on the colour chart in the legend, it is easy to see that the highest shear stresses in neutral plane are located near the edges of the laminate in the area between the loading and support cylinder. These areas with highest shear stresses are coloured dark blue in the picture. The area between the loading and supporting cylinder also generally seems to have higher stresses than the area outside of it. This is visible in the picture as the blue area that crosses the whole laminate from one edge to other. In the part of the laminate between the supporting cylinder and the free edge, the shear stresses quickly reduce close to zero. These reducing stresses can be seen in the colour change from dark green into lighter green and finally into yellow at the free edge of the laminate. The risk area where the delamination most probably starts in the neutral plane is between the cylinders at the edges of the laminate.

The next two figures, Figure 39 and 40, provide an interesting view to the areas where the delamination was suspected and often observed to originate from in the experimental testing. These areas are the interfaces, where the fibre orientation changes 90° to another direction in the x-y -plane. Figure 39 shows the shear stress distribution for lay-up 1 laminate in the upper interface, where 0° fibres change to 90° fibres.

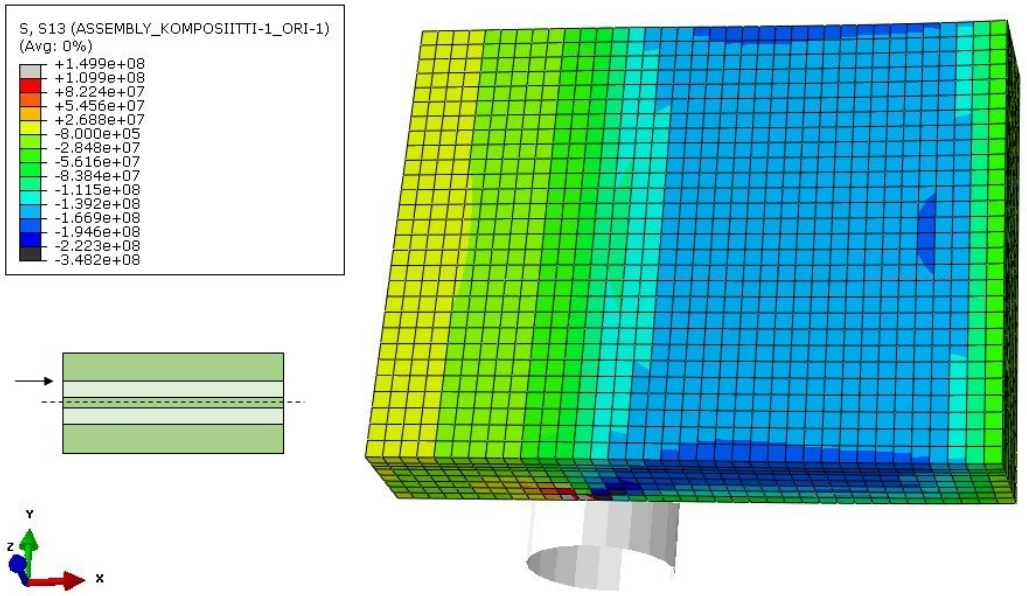

Figure 39: The shear stress distribution at the upper interface of the laminate with lay-up 1.

The upper interface of laminate with lay-up 1 presented in Figure 39 shows very similar trends to the picture of the neutral plane of the same lay-up. Again, the highest shear stress areas are located at the edges of the laminate in the area between the loading and supporting cylinder. However this time, probably because the upper interface is farther away from the supporting cylinder in z-direction than the neutral plane, the high stress areas are smaller and closer to the loading cylinder in x-direction. Interestingly there is also a new high stress area that was not present in the neutral plane. This area is in the middle of the laminate in y-direction and close to the loading cylinder in x-direction. In the left side of the laminate at the area that starts from the support cylinder and continues until the free edge of the laminate, the stresses gradually fade away from dark to light green and then to yellow. This time however, the yellow area is much larger than in the neutral plane. This happens because of the greater distance from the loading cylinder in z-direction. The high risk areas for delamination in the upper interface of lay-up 1 are located between the cylinders at the edges of the laminates and in the middle of the laminate close to the loading cylinder.

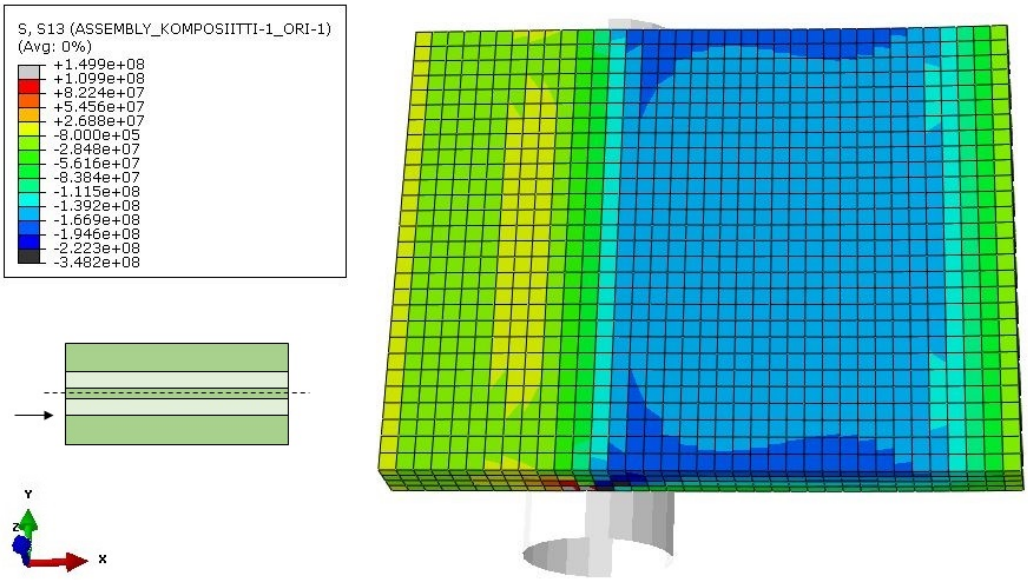

Figure 40: The shear stress distribution at the lower interface of the laminate with lay-up 1.

The shear stresses at the lower interface of laminate with lay-up 1 are illustrated in Figure 40. At this interface the orientation of the fibres changes from 90° to 0°. Not unlike in the pictures of neutral plane and upper interface, the lower interface also shows the highest shear stresses in the area between the two cylinders, near the edges of the laminate. The short distance in z-direction between the supporting cylinder and the lower interface of the laminate seems to result in high stresses that reach farther inside the laminate than in upper interface and neutral plane. This is seen in Figure 40 as the two dark blue spikes pointing towards the middle of the laminate above the supporting cylinder. Interestingly in the lower interface the stresses do not linearly fade to zero at the area between the supporting cylinder and the free edge of the laminate but there is an area with lower stresses surrounded by higher stress areas. This appears in Figure 40 as the isle of yellow elements surrounded by green elements slightly to the left of the supporting cylinder.

Based on the visuals of the three cutting planes of lay-up 1 model, it seems probable that the delamination starts at the lower interface of the laminate, where the high-stress areas are the largest. In all of the cutting planes, the high stress areas are located at the long edge of the laminate between the cylinders. This indicates that the delamination starts at the edge of the laminate and then continues to propagate deeper between the layers until the crack reaches from edge to edge.

6.4.3 Lay-up 2

The finite element model of the laminate with lay-up 2 was partitioned into ten layers so that in z-direction each element represents one unidirectionally reinforced ply. Each partition was given an orientation depending on the fibre orientation

and then one material model was assigned for each partition. Because of the even number of the fibre reinforced plies in the lay-up 2, none of the plies needed to be split in order to visualize the neutral plane of the laminate. The simulation was run until the displacement of the loading cylinder was 2 mm along z-axis but the results presented in figures below were taken at a frame where the displacement was 0.7 mm in order to get results that more accurately represent those of the experimental test specimens. A side view of the shear stress distribution of the laminate with lay-up 2 is presented in Figure 41.

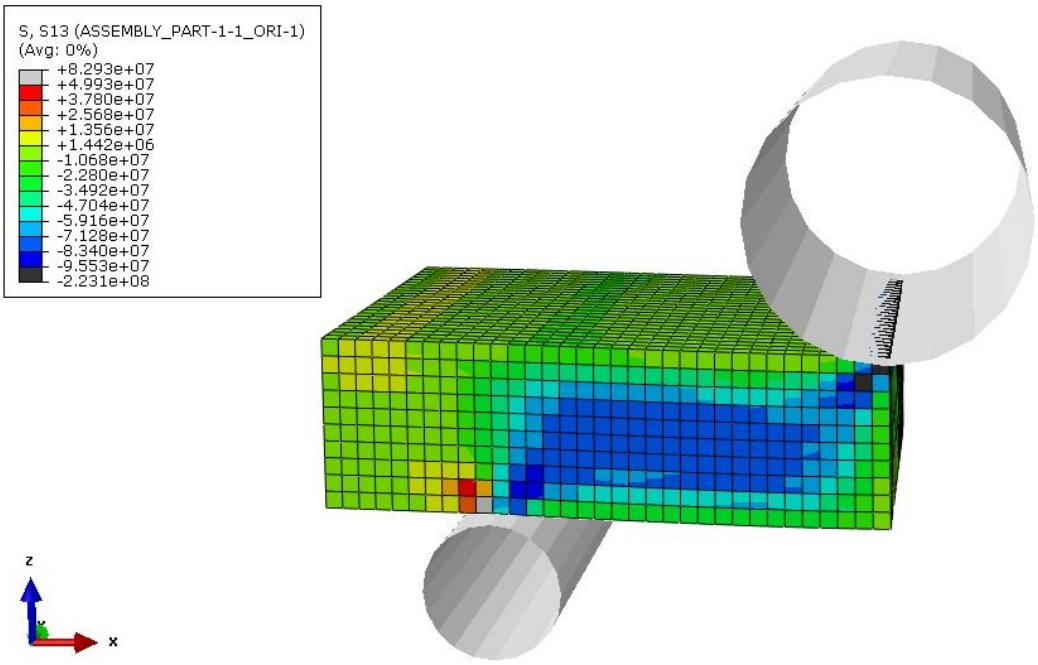

Figure 41: The shear stress distribution at the side of the laminate with lay-up 2.

Similarly to lay-up 1 results, the shape of the shear stress contour in Figure 41 takes the form of a parallelogram with slightly extended corners near the loading and supporting cylinders, which closely resembles the shape obtained in literature [5,7]. The shear stress values in the legend in the upper left corner are ranging from 83 MPa to -223 MPa, which is significantly less than the shear stress values obtained from lay-up 1 simulations. In order to visualize the shear stress contour at the side of the laminate more clearly, the scale of the legend was adjusted so that the stresses in some single elements directly under the loading cylinder and above the supporting cylinder are off the scale. This is why there are some grey and black elements visible in the figure.

Again, a more accurate analysis of the shear stresses in the laminate can be achieved, when layers are removed from the simulation results. This allows for visuals in the most interesting cross-sections of the lay-up: neutral plane, upper interface and lower interface. These cross-sections are illustrated in Figures 42– 44.

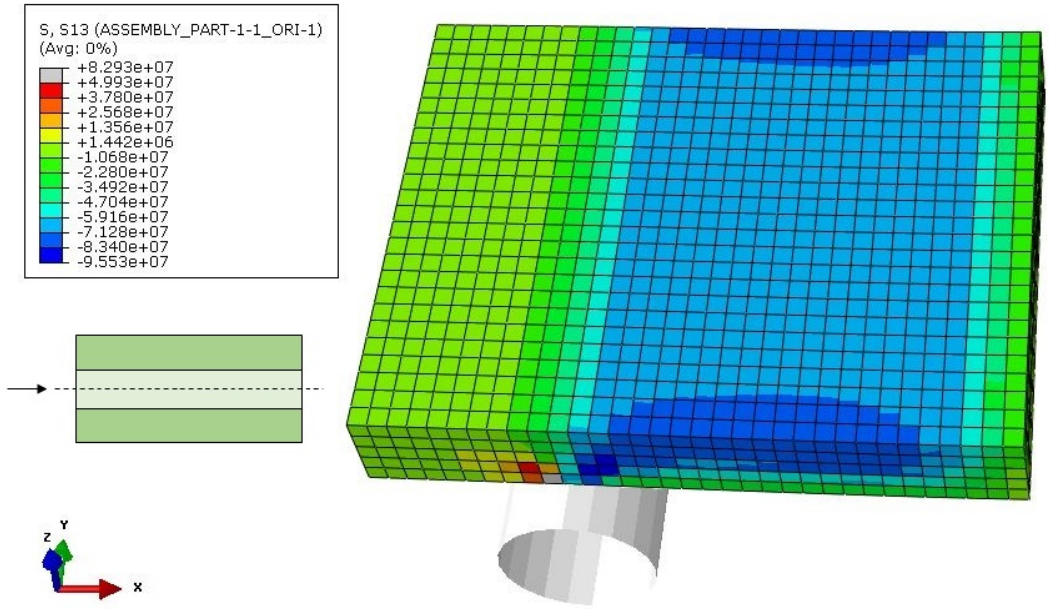

Figure 42: The shear stress distribution at the neutral plane of the laminate with lay-up 2.

Figure 42 shows the shear stress distribution at the neutral plane of the laminate with lay-up 2. The highest stresses are located in the area between the loading and supporting cylinders. The area is coloured blue in the picture. The stresses peak at the edges of the laminate, where two clearly visible dark blue half-oval-shaped regions can be seen. In the area between the supporting cylinder and the free edge of the laminate, the shear stresses quickly diminish, which can be seen as the sudden colour change from blue to light blue and finally to green. The risk areas, where the delaminations probably start in this plane, are the edges of the laminate between the loading and supporting cylinders.

More interesting cross-sections are presented in Figures 43 and 44, which show the shear stress contours in the planes, where the fibre directions change. In experimental testing these interfaces were found to be the problem areas, where the delamination very often started. Many times the delamination reached through the whole specimen and was located at the interface of plies that had different fibre orientations. Figure 43 shows the shear stress contour in the upper interface of the laminate with lay-up 1, where the fibre orientation changes from 0° to 90°, when moving downwards along the z-axis.

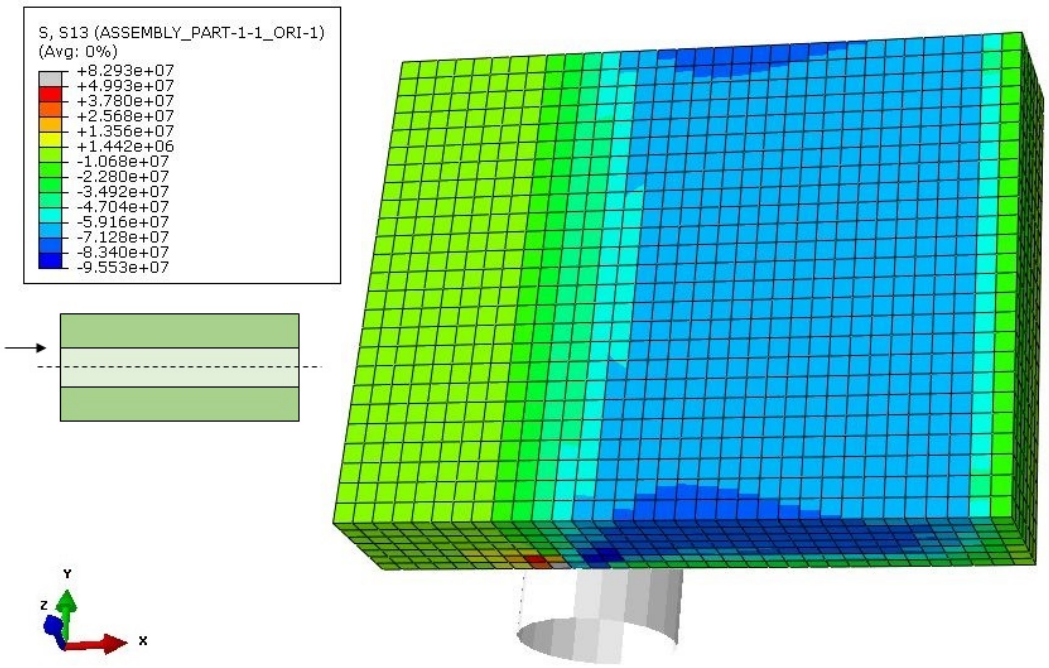

Figure 43: The shear stress distribution at the upper interface of the laminate with lay-up 2.

The shear stress distribution at the upper interface of lay-up 2 illustrated in Figure 43 shows similar trends to the upper interface of lay-up 1. The stresses are distributed quite evenly in the area between the loading and supporting cylinder. There are two small areas with high stresses at the edges of the laminate, which are visible in the picture as the two dark blue areas but they are significantly smaller in size those at the neutral plane of the same laminate. The high stress areas are also closer to the supporting cylinder than the loading cylinder. Outside the area between the cylinders, the stresses gradually return close to zero, which is seen as the green areas at the left end of the laminate. The critical area for delaminations is the blue area between the two cylinders, especially at the edges of the laminate.

The lower interface where the ply fibre orientation changes back from 90° to 0° is presented in Figure 44.

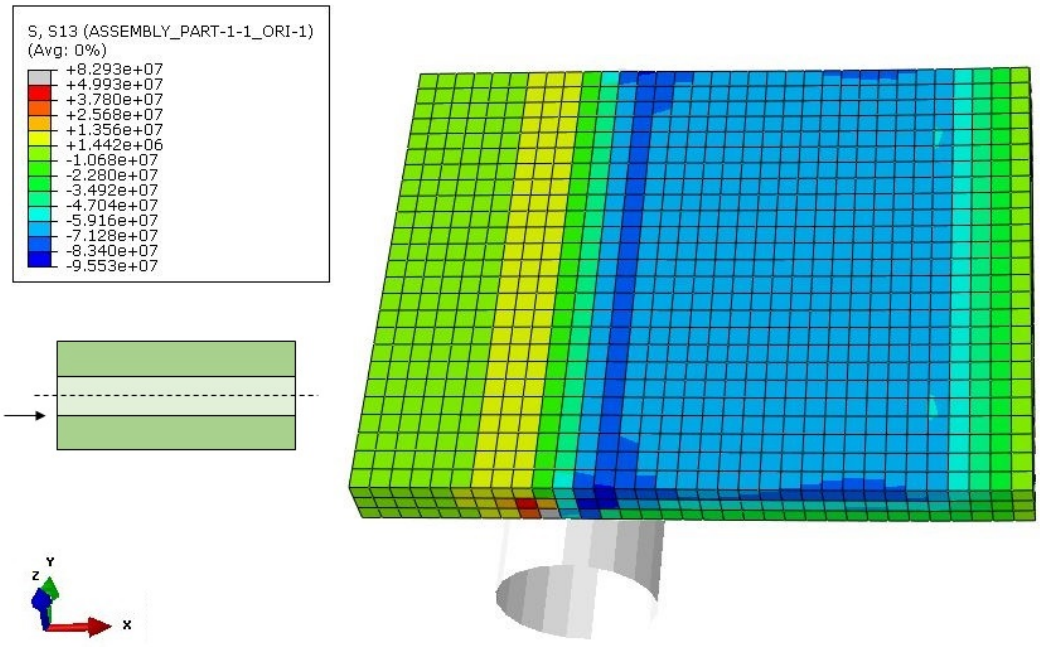

Figure 44: The shear stress distribution at the lower interface of the laminate with lay-up 2.

The lower interface of the model with lay-up 2 presented in Figure 44 shows some interesting characteristics that differ from the previous shear stress distributions of lay-up 2 and lay-up 1. Generally, the blue high stress location is at the usual place between the two cylinders but now the areas with highest stresses starting from the edges of the laminate reach through the laminate from one edge to the other above the supporting cylinder. This is probably due to the close distance in z-direction from the lower interface to the supporting cylinder. In the area between the supporting cylinder and the free edge of the laminate the stresses reduce greatly. The smallest shear stresses in the cross-section are located just slightly to the left of the supporting cylinder, which demonstrates as the yellow area between two green areas. Apart from that the stresses follow the trend shown in the previous cross-sections, where both ends of the laminates have elements coloured green.

Based on the visuals of the simulation results of lay-up 2 it seems likely that the delaminations start at the area between the two cylinders and from the edges of the laminate. The highest risk for delamination seems to be at the lower interface, where the high stress areas reach through the laminate width from one edge to the other. This could cause a delamination through the laminate, which correlates well with the experimental test specimens, where the delamination often extended through the laminate visibly separating two layers from each other.

6.5 Comparison of Lay-up 1 and Lay-up 2

In order to get a better understanding of the differences between the shear stress distribution between both lay-ups, shear stress curves were drawn along the edge of the laminate that is parallel to x-axis. The values for the graphs were taken from Abaqus using the "probe values" tool and then saved to a text file and further processed in Excel. The shear stress values as a function of distance in x-direction are presented in Figures 45– 48. The shear stress values presented in the following figures for both lay-ups are taken at a loading cylinder displacement of 0.7 mm, which closely represents the displacement when the linear part of the force-displacement curves ended and failure happened for the experimental test specimens (see Appendix B for force-displacement curves). Each shear stress curve also has a callout of the force that was inflicted to the loading cylinder in the simulation, when the displacement was 0.7 mm. It is interesting to note that with the same displacement of the loading cylinder, the force inflicted to it in the simulation of lay-up 1 (9.0 kN) is over twice as strong as the force in the simulation of lay-up 2 (4.0 kN). This indicates clearly that the laminate with lay-up 1 is more rigid and does not bend as easily as the laminate with lay-up 2.

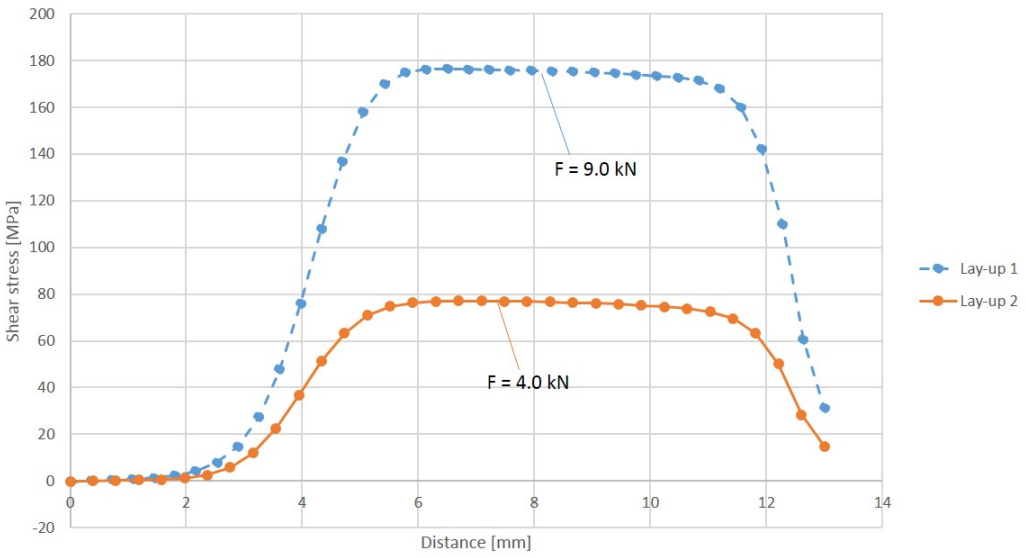

Figure 45: The shear stresses along the x-axis in the neutral plane for both lay-ups, at a displacement of 0.7 mm.

Figure 45 shows the shear stress curves in the neutral plane of both lay-ups. At first glance, the stresses seem to be much higher in the laminate with lay-up 1 but it is important to notice that the neutral plane of lay-up 1 is at a layer, where the fibre direction is 0°, i.e. along the x-axis and the neutral plane of lay-up 2 is at a layer with fibre direction of 90°, which is perpendicular to the x-axis. Hence, it is only natural that the stresses in the neutral plane of lay-up 1 are higher, since it has the load carrying fibres in the direction the force applies to. The shear stress values

that the simulation gives for lay-up 1 are ranging from 0 to 180 MPa and for lay-up 2 from 0 to 80 MPa. For both lay-ups the peak values are located between 5 and 12 mm along the x-axis and do not have any single peaks but seem to plateau at the highest value and stay there. The peak values of lay-up 2 (68 MPa) are 61.7% lower than the peak values of lay-up 1 (178 MPa). The area between 5–12 mm is the same that is visible in Figures 38 and 42 as the blue area between the loading and supporting cylinders. The visual images of the finite element model did not have clear peaks apart from the dark blue area at the edges of the laminate and the same is true for the graphs showing the shear stress distribution at the neutral plane.

Because the fibre direction is different in the neutral plane for the two lay-ups, the simulated shear stresses were also scaled with the ultimate compressive stresses, which were found from the ESAComp material database [29] for both directions of the glass-fibre-reinforced ply with 60% fibre-content. The ultimate compressive stress in fibre direction was 675 MPa and perpendicular to fibre direction 120 MPa. Because the neutral plane of lay-up 1 has fibres in x-direction, the shear stress values for lay-up 1 were divided by 675 MPa and similarly the shear stress values of lay-up 2 were divided by 120 MPa to get scaled versions of the stresses that could be compared to each other. The scaled shear stress distributions for both lay-ups are presented in Figure 46.

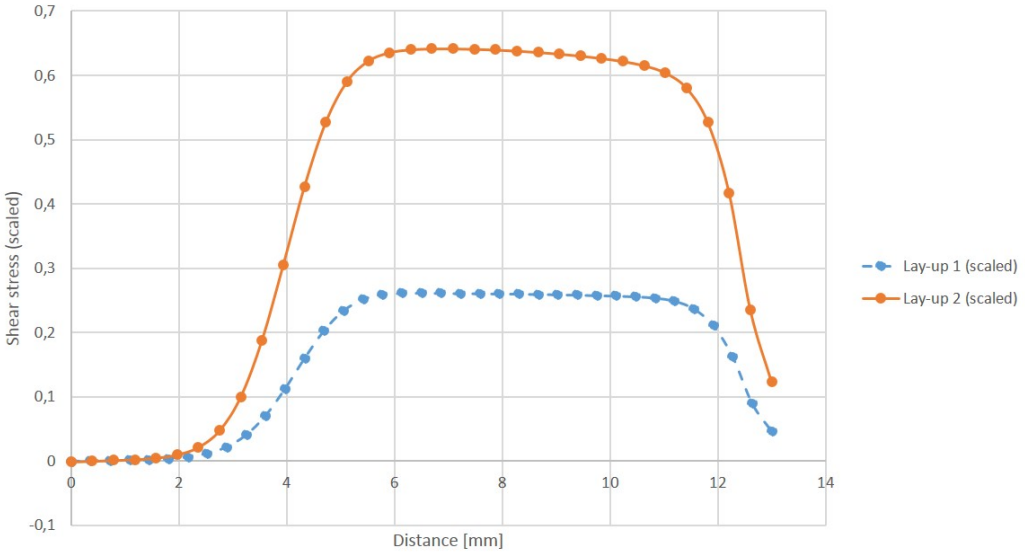

Figure 46: The shear stresses along the x-axis in the neutral plane for both lay-ups, scaled with ultimate compressive stresses in fibre direction, at a dispacement of 0.7 mm.

In Figure 46 the vertical axis has scaled values of the shear stresses (the actual values divided by 675 MPa or 120 MPa), so they do not have a unit like MPa, but should be considered as relative values, with which the stresses between the lay-ups can be compared to each other. When the shear stresses are scaled, the curves

change so that the values of lay-up 2 are now higher than the values of lay-up 1. The peak values of lay-up 1 (0.27) are 57.8% lower than the peak values of lay-up 2 (0.64). This indicates that the neutral plane of lay-up 2 is also quite highly stressed. However, it has to be noted that the scaling with ultimate compressive stresses might not accurately correlate with ultimate shear stress values and the true relation of the curves could be slightly different. Ultimate compressive stresses were used for scaling because other data was not available in the ESAComp database.

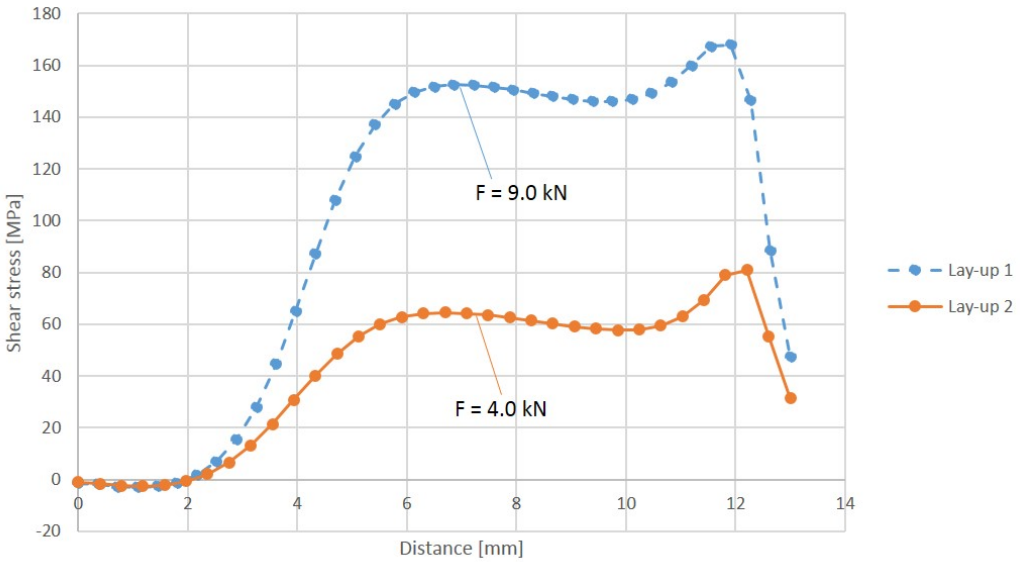

Figure 47: The shear stresses along the x-axis in the upper interface for both lay-ups, at a displacement of 0.7 mm.

Figure 47 illustrates the shear stress curves in the upper interface of both lay-ups. Because of the sudden change in the fibre direction from 0° to 90 ° in the upper interface, the simulation gives two different stress values in the same interface depending on the layer selected. To get results from lay-up 1 and 2 that are comparable to each other, only the stresses taken from the 0° layer are presented in the graph. There is much more variation in these graphs compared to the neutral plane curves presented in previous figures. Generally the shear stresses for lay-up 1 are much higher than those of lay-up 2 but it is also important to note that the upper interface of lay-up 1 is closer to the centre of the laminate in z-direction than the upper interface of lay-up 2. In the area between the free edge of the laminate and the supporting cylinder (from 0 to 4 mm), the shear stress at first gets slightly negative values, after which it starts to rapidly increase for both lay-ups reaching the first peak at the distance of 6 mm along the x-axis. Then the stresses again have a slight decrease between 6 and 10 mm distance. Both lay-ups reach the peak shear stress value at 12 mm. For lay-up 1 the peak value is around 170 MPa and for lay-up 2 around 80 MPa. The peak value of lay-up 2 is 52.9% lower than the peak value of lay-up 1. When these graphs are compared to the cross-sections of the

upper interfaces of both lay-ups, once again the graphs show the highest values at the blue area that is located between the loading and supporting cylinder. However, the peak values that in the graphs are located at 12 mm, are not as clearly visible in Figures 39 and 43. This is probably due to the colour scaling of the picture that is not accurate enough to visualize different shades of dark blue at the edge of the laminate. The cross-section of laminate with lay-up 1 does have some slight indications of the highs stresses at 12 mm distance along the x-axis, which is visible as the single dark blue isle of elements in the middle of the laminate. If the delamination starts at the upper interface, the graphs and the visualization of the cross-sections suggest that the most critical stresses are at the 12 mm distance, which is only 1 mm away from the loading cylinder and that the delamination probably originates at that area.

The shear stresses in the lower interface of both lay-ups are presented in Figure 48. Similarly to the upper interface curves, to make the curves of both lay-ups comparable to each other in the interface where the material direction changes from 90° to 0° in relation to the x-axis, the values were taken from the elements whose fibre direction was 0° because that is the direction in which the fibres carry loads.

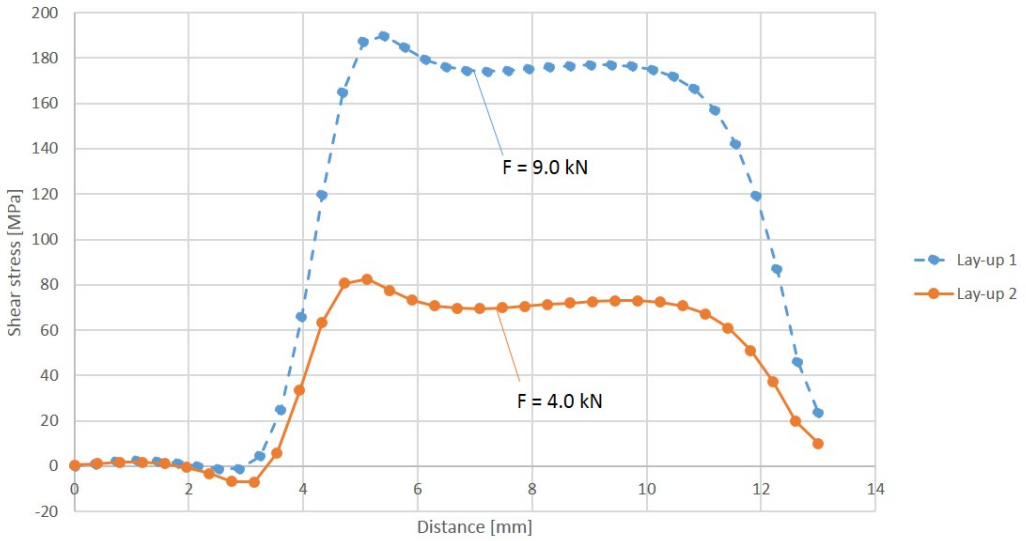

Figure 48: The shear stresses along the x-axis in the lower interface for both lay-ups, at a displacement of 0.7 mm.

For the lower interfaces, the shear stress values start from positive and then get slightly negative values at the area before the supporting cylinder (from 2 mm to 4 mm). After the supporting cylinder, the stresses start to increase rapidly and reach their peak value at a distance of around 5 mm along the x-axis. Then the values decrease in the order of 10 MPa and plateau until 10 mm, after which they start to decrease close to zero under the loading cylinder. For lay-up 1 the peak value in the shear stress is at the area of 190 MPa and for lay-up 2 around 85 MPa. The peak value of lay-up 2 is 55.3% lower than the peak value of lay-up 1. At the plateau

the stresses for lay-up 1 stay around 180 MPa and for lay-up 2 around 70 MPa. In comparison to the cross-sections presented in Figures 40 and 44, the area between 5 and 11 mm where the stresses are the highest, correlates well with the area of blue elements between the supporting and loading cylinder. For both lay-ups, the peak values appear quite clearly in the pictures of the cross-sections. In the cross-section of lay-up 1, the dark blue area at the distance of 5 mm along the x-axis reaches farther into the centre of the laminate than anywhere else along the edge of the laminate. From the picture of lay-up 2 lower plane cross-section this peak value is visible even more clearly than in the picture of lay-up 1. In the cross-section of lay-up 2 the dark blue area at the lower plane of the laminate reaches from edge to edge through the laminate. The slightly negative values between 2 and 4 mm are also visible in the cross-sections as the yellow area. The visualizations of the cross-sections and the stress curves both indicate that the most critical areas for delamination for lower interface are located in the distance of 5 mm from the free end of the laminate, about 1 mm after the supporting cylinder. Since the area with high stresses reaches through the whole laminate, the delamination starting here can easily crack the whole laminate open into two pieces. This was also documented for the experimental test specimens that sometimes had very clear delaminations through the laminate that were visible to the naked eye. The reason for the location of the high-stress-area is probably in the size of the supporting cylinder, which is quite small in diameter compared to the loading cylinder and therefore causes higher pressure at the area around it. This can be clearly seen in Figure 37, where the elements directly over and slightly to the right of the supporting cylinder have much higher stresses than the elements around them. Similarly, the loading cylinder inflicts a pressure to the laminate, which causes higher stresses around it, which can be seen as the peak stress in Figure 47.

Even though the graphs that are presented in Figures 45–48 are good for comparing different lay-ups to each other, they can not accurately be compared to the ILSS values of the experimental test specimens, because the forces (9 kN and 4 kN) are much higher than those of the experiments. In addition to that, the shear stress values taken at the free edge of the simulated laminate tend to be higher than the values in the middle of the laminate because of so called free-edge-effect [22,23]. This can easily be seen in Figures 37–44 as the dark blue areas near the edges of the laminate. In order to get simulated shear stress values that can be compared to the values of the experimental tests, shear stress distribution curves were drawn along the y-axis in the lower interface of both lay-ups, at the x-distance of 5 mm, which was identified as the peak stress area in Figure 48. The shear stress curves in y-direction for both lay-ups are presented in Figure 49.

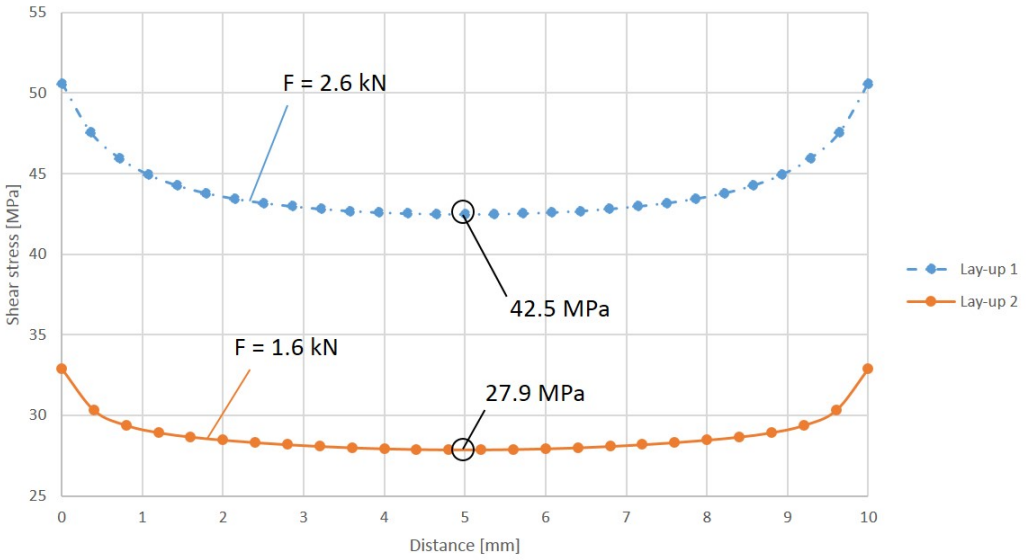

Figure 49: The shear stresses along the y-axis in the lower interface for both lay-ups.

Instead of the constant displacement of 0.7 mm, which results in much higher forces than the experimental ultimate forces, the values in Figure 49 are taken at frames, where the simulation force was similar to the experimentally measured ultimate force. The values for the curve of lay-up 1 are taken at a frame, in which the force inflicted to the loading cylinder was 2.6 kN (compare with Figure 35) and the values for the curve of lay-up 2 at a frame, in which the force was 1.6 kN (compare with Figure 36).

The simulated shear stresses in the middle of the laminate at the critical area (x = 5 mm, y = 5 mm) presented in Figure 49 are 42.5 MPa for lay-up 1 and 27.9 MPa for lay-up 2. This means, the simulated shear stress of lay-up 2 is 34.4% lower than that of lay-up 1. The simulated difference between the two lay-ups is higher than that of the experiments, which was 25.9% (see Figure 25). Interestingly the simulated ILSS values for both lay-ups are slightly lower than the experimentally tested values. The experimental ILSS value of lay-up 1 specimens was 49.7 MPa and the simulated value 42.5 MPa, which is 14.5% lower than the experimental value. Similarly the experimental ILSS value of lay-up 2 was 36.9 MPa and the simulated value 27.9 MPa, which is 24.4% lower than the experimental value.

7 Discussion

Ideally, an ILSS test using the short beam shear method should result in a clear delamination at the neutral plane of the laminate, where the normal stresses change from compression to tension. Typically laminates that are tested for ILSS are unidirectionally reinforced. This ensures that the mechanical properties of the laminate do not change through the laminate thickness and cause sudden changes in shear stresses. In this thesis the focus point was in two different laminate lay-ups to study how the changes in lay-ups affect the ILSS behaviour of the laminates and whether good ILSS results can be achieved when using multidirectionally reinforced laminates.

Based on the experimental test results, the ILSS values of the specimens with lay-up 1 were generally higher than those of lay-up 2. With the test specimens of the same geometry, the reference specimens of lay-up 1 had about 26% higher ILSS values than the laminate with lay-up 2. Similar behaviour was observed within the aged test specimens, which showed a 21% difference in the ILSS values between the two lay-ups. However, the ILSS value is not the only quality that tells about the ILSS behaviour of the laminates.

The visual study of the experimental test specimens after ILSS testing revealed that the critical delaminations that reached through the laminate from one side to the other happened almost predominantly at the lower interface of the test specimens, where the fibre direction changes by 90°. This behaviour was observed for the test specimens of both lay-ups. In addition, the test specimens of lay-up 1 had more often visible delaminations also between several other layers, whereas the specimens of lay-up 2 more often delaminated visibly only at the lower interface. This difference in behaviour is probably caused by the order of the fibre-reinforced-layers in lay-up 1, which results in four interfaces in which the fibre direction changes, compared to lay-up 2, which only has two such interfaces. The visual study indicates that the most critical areas for the multidirectionally reinforced laminates of this study in shear are located at the interfaces, where the fibre direction changes suddenly, which causes high gradients in the shear stresses.

The effect of temperature was detrimental to the ILSS behaviour of the test specimens of both lay-ups. The elevated temperature decreased the average ILSS values of the laminates but in addition to that, it affected the type of failure the specimens experienced during shear. This is visually easy to see when studying the force-displacement graphs of different test series presented in Appendix B. Where the force-displacement curves of the reference specimens tested in room temperature had an almost constant slope until a delamination, which dropped the force significantly, the specimens tested in higher temperature had much smoother and rounder force-displacement curves. The specimens tested dry in room temperature are brittle and fail predominantly by delamination but the specimens tested in higher temperature are less brittle and more ductile, which is why the sharp drops in the force-displacement curves are almost nonexistent. Instead of delamination, the failure at an elevated temperature is probably more due to the softening of the resin, which causes plastic deformation.

The moisture absorbed in the specimens had a similar effect, but not as drastic as the higher temperature. The specimens tested wet showed some drops in force-displacement curves but the delaminations were not as clear as with the dry specimens tested in room temperature. When the force-displacement curves of lay-up 1 specimens tested in room temperature are compared to the wet specimens of lay-up 2, it seems that the specimens of lay-up 2 have slightly better ILSS behaviour. Even though the moisture absorbed in the specimens makes the force-displacement curves somewhat rounder before delamination, the curves of lay-up 2 have sharper drops in forces than the curves of lay-up 1. In the worst test conditions, when both the temperature is elevated and the specimens tested wet, the force-displacement curves of both laminates are round and no delaminations can be detected. This indicates that the resin-fibre-combination of the test specimens used in this study is not very well suited for standard ILSS testing at a high temperature or wet conditions.

The ageing in water-suphuric-acid bath negatively affected the average ILSS values of the test specimens. For the specimens of lay-up 1, the ageing decreased the ILSS values by 28.7% and for lay-up 2 by 24.3%. Theoretically, the ageing should have the same effect regardless of the lay-up. The fact that the drop of the ageing is higher for lay-up 1 specimens than for lay-up 2 specimens, indicates that lay-up 1 is more suitable for the studying of the effect of ageing, since the effects of ageing are more clearly visible in the ILSS values of lay-up 1.

The study of the force-displacement curves shows that the aged specimens of lay-up 2 have sharp drops in ILSS values, which indicates that the main failure mode for lay-up 2 specimens is still delamination when aged. For the specimens of lay-up 1, the results are not as clear. The force-displacement curves of the aged lay-up 1 specimens tend to be round at the top and have only minor drops in forces, which indicates that the failure mode of the aged specimens of lay-up 1 is a mixture of plastic deformations and delaminations. Overall, the results show that the standard ILSS testing is a suitable method for studying the effects of ageing, as long as the test specimens are tested dry and in room temperature.

The finite element analysis of the two lay-ups confirmed the results that were already observed by visually studying the experimental test specimens: the critical area for delamination seems to be the lower interface, where the fibre direction changes by 90°. The slopes of the simulation curves in Figures 35 and 36 resemble closely the linear region of the force-displacement curves of the experimental test specimens. However, the fact that the simulation curves start to rise straight from the origin of the graph and the curves of the experimental test samples at a displacement of around 0.2 mm result in quite large differences in forces at the same displacement between the experiments and simulations.

In order to get simulated shear stress values that are comparable to the experimental results, the shear stress values of the simulations were taken at a frame, in which the force inflicted on the loading cylinder was roughly the same as the average ultimate force in the experimental tests. The absolute shear stress values of the finite element simulations were 42.5 MPa for lay-up 1 and 27.9 MPa for lay-up 2, which are 14.5% and 24.4% lower than the absolute values of the experimental specimens, respectively. However, in the simulations the difference between the shear stresses

of lay-up 1 and lay-up 2 was 34.4%. That is slightly higher than the difference of the experimental specimens, which was 25.9%. The difference between the absolute shear stress values of the simulations and the experiments is probably a result of the material-model used in the simulation, the values of which were approximated by scaling the values of the material model with 60% fibre content.

An important issue to notice about the simulations is that since the stresses were taken from the free edge of the composite specimen model, some uncertainty in the results is expected. The free-edge effect is well documented in the literature [22], [23] and results in higher stresses at the free edges of the laminate, where there is a stress discontinuity. Moreover, the results of the finite element simulation are affected by the element mesh (fineness) of the finite element model. When the average element size in the mesh is increased or decreased changing the total number of the elements, the simulation results may change as well [24]. In this thesis a mesh-dependency analysis of the simulation results was not conducted.

8 Conclusions

Interlaminar shear strength, ILSS, is an important value when comparing different composite systems to each other. ILSS value tells how well a composite can resist shear stresses that cause delamination between the fibre-reinforced-plies of the laminate. ILSS is typically measured experimentally and the test methods have been standardised in order to achieve comparable results between laminates of different composition.

ILSS tests are typically conducted to composites that are reinforced unidirectionally. The primary focus point of this thesis was to determine the ILSS values and behaviour of multidirectionally reinforced glass-fibre laminates. The secondary goal was to see how the ageing of the laminates in water or in acidic liquid affect the ILSS. Test specimens of different lay-ups were tested in order to find out how the ILSS changes, when the order and direction of the glass-fibre-reinforced plies change. In addition to that, finite element simulation models were created of both lay-ups to study, where in the laminate do the high stress areas form during the testing.

The ILSS testing of the filament-wound test specimens revealed that very often the delaminations occurred at the area, where the fibre direction changes by 90°. The same behaviour was observed, when the finite element simulations of the tests were studied. Based on the simulation results, the peak shear stresses formed close to the supporting cylinder at the lower interface of the laminate. The difference in the ILSS values between the two lay-ups was 34.4% in the simulations but 25.9% in the experiments.

Conducting the ILSS tests at an elevated temperature and/or in wet conditions changed the ILSS behaviour of both lay-ups for the worse. Especially at the elevated temperature, the laminates did not show clear delaminations but rather experienced plastic deformations, probably due to the softening of the resin. The ageing of the test specimens before testing did not affect the ILSS behaviour but decreased the ultimate force, with which the failure occurred.

The difference between finite element analysis and experimental results suggest different failure modes for true laminate specimens, when the lay-up is changed. In order to fully understand the phenomenon, further studies in the field of ILSS testing of multidirectionally reinforced glass-fibre-composites are needed. This would require even more experimental testing with many different lay-ups accompanied by finite element simulations and could be beneficial to industries, where multidirectionally reinforced composites are widely used.

References

[1] D 2344/D 2344M. Standard Test Method for Short-Beam Strength of Polymer Matrix Composite Materials and Their Laminates. 2010.

[2] BS EN ISO 14130. Fibre-reinforced plastic composites - Determination of apparent interlaminar shear strength by short-beam method. 1998.

[3] BS 2782: Part 3: Method 341A. Determination of apparent interlaminar shear strength of reinforced plastics. 1977.

[4] EN 2563. Aerospace series - Carbone fibre reinforced plastics - Unidirectional laminates - Determination of the apparent interlaminar shear strength. 1997.

[5] Xie M, Adams D. 1995. Study of three- and four-point shear testing of unidirectional composite materials. Composites 1995;26:9.

[6] Ahmed, K. S., Vijayarangan, S. 2008. Tensile, flexural and interlaminar shear properties of woven jute and jute-glass fabric reinforced polyester composites. Journal of materials processing technology, 207(1), 330-335.

[7] Feraboli P., Kedward K.T. 2003. Four-point bend interlaminar shear testing of uni- and multi-directional carbon/epoxy composite systems. Composites: Part A 34 (2003) 1265-1271. doi: 10.1016/S1359-835X(03)00204-5.

[8] Saarela Olli, Airasmaa Ilkka, Kokko Juha, Skrifvars Mikael, Komppa Veikko. 2007. Komposiittirakenteet. Helsinki. Muoviyhdistys ry. 494 s. ISBN: 978-951-9271-28-6

[9] [Internet source]. 2015. [Cited: 19.3.2016]. Available at: http://oliviakaiafauel.tumblr.com/post/115017352710/weaving-is-a-technique-in-which-the-yarns-are

[10] Ashland. 2015. [Internet source]. [Cited: 2.3.2016]. Available at: http://www.ashland.com/Ashland/Static/Documents/APM/DERAKANE%20441%20400%20TDS.pdf

[11] Swancor. 2009. [Internet source]. [Cited: 2.3.2016]. Available at: http://www.technipolymers.com/TDS/901-PT-VE-30.pdf

[12] Ashland. 2010. [Internet source]. [Cited: 2.3.2016]. Available at: http://gel-top.dk/cgi-files/mdmgfx/file-599-319125-14720.pdf

[13] Pavlidou, S., & Papaspyrides, C. D. 2003. The effect of hygrothermal history on water sorption and interlaminar shear strength of glass/polyester composites with different interfacial strength. Composites Part A: applied science and manufacturing, 34(11), 1117-1124.

[14] AZOnetwork. 2001. [Internet source]. [Cited: 10.3.2016]. Available at: http://www.azom.com/article.aspx?ArticleID=743

[15] Rod Martin. 2008. Ageing of composites. Woodhead Publishing Series in composites science and engineering. ISBN:1845694937, 9781845694937.

[16] DARTEC M1000/RK operating manual. 1991.

[17] Holmes Mark. 2014. Global carbon fibre market remains on upward trend. Reinforced Plastics, 58(6), 38-45. doi:10.1016/S0034-3617(14)70247-4

[18] Gardiner Ginger. 2009. The making of glass fiber. Composites World. [Online magazine]. [Cited 22.3.2016]

[19] Thomason James. 2015. Glass Fibre Sizing. Blurb, Incorporated. ISBN: 9781320678391.

[20] Teijin. 2012. Annual Report. [Internet source]. [Cited: 22.3.2016]. Available at: http://www.teijin.com/ir/library/annual_report/pdf/ar_10_06.pdf

[21] Hebei Maple Fiberglass Industry Co.,Limited. 2016. [Internet source]. [Cited:26.3.2016]. Available at: http://www.frpmachining.com/faqs/frpgrp-pipe-filament-winding-machine

[22] Whitcomb, J. D., Raju, I. S., and Goree, J. G. 1982. Reliability of the finite element method for calculating free edge stresses in composite laminates. Computers & Structures, 15(1), 23-37.

[23] Schellekens, J. C. J., & De Borst, R. 1993. A non-linear finite element approach for the analysis of mode-I free edge delamination in composites. International Journal of Solids and Structures, 30(9), 1239-1253.

[24] Sigmund, O., & Petersson, J. 1998. Numerical instabilities in topology optimization: a survey on procedures dealing with checkerboards, mesh-dependencies and local minima. Structural optimization, 16(1), 68-75.

[25] Muototerä Oy. 2016. [Internet source]. [Cited: 5.4.2016]. Available at: http://muototera.fi/

[26] Muovityö Hiltunen Oy. 2016. [Internet source]. [Cited: 5.4.2016]. Available at: http://www.muovityo.com/

[27] Admor Composites Oy. 2016. [Internet source]. [Cited: 5.4.2016]. Available at: http://www.admorcomposites.fi/

[28] Dassault Systemes. 2016. Abaqus unified FEA. [Internet source]. [Cited: 5.4.2016]. Available at: http://www.3ds.com/products-services/simulia/products/abaqus/

[29] Componeering Inc. 2016. ESAComp software. [Internet source]. [Cited: 5.4.2016]. Available at: http://www.esacomp.com/

A Specimen drying curves

Before testing, some specimens were dried in an oven at 50 °C until their weight remained constant. In this appendix all the drying curves of different test series are presented. Every graph consists of several curves of different colour, each of which represent one test specimen. All the test specimens were weighed three times: once before putting them in the oven, and then twice before testing them for ILSS.

Aramid-fibre-reinforced specimens

Below, all the drying curves of aramid-fibre reinforced specimens are presented. For further explanation for the name of each graph, see Table 3 on page 21 of this thesis.

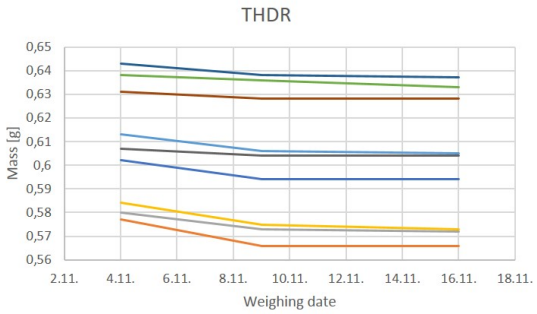

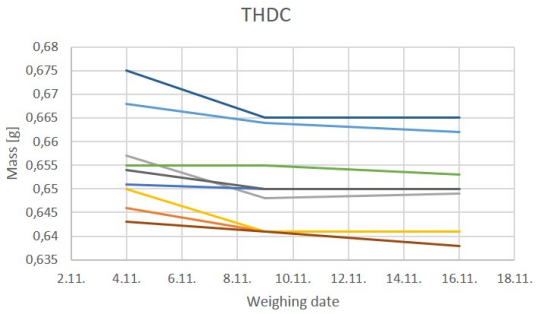

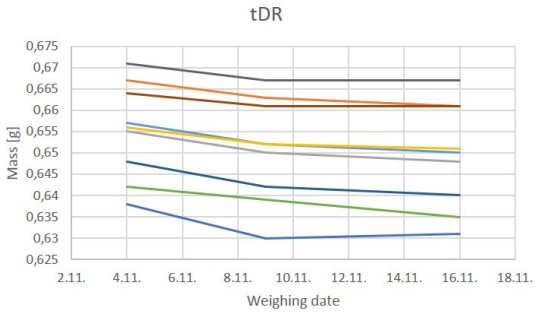

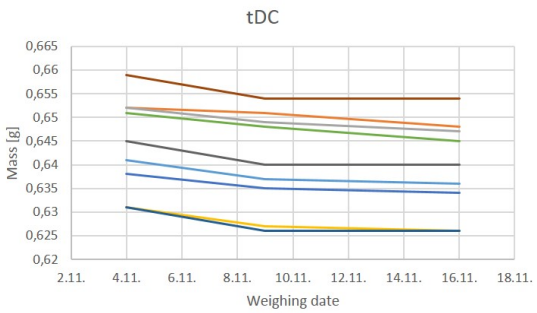

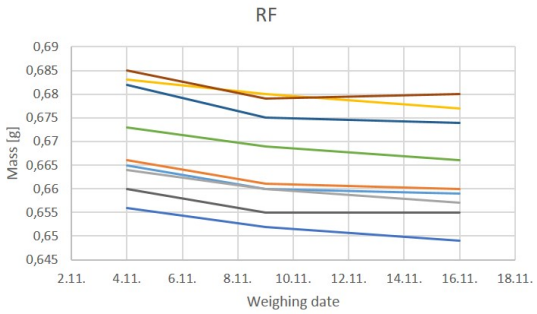

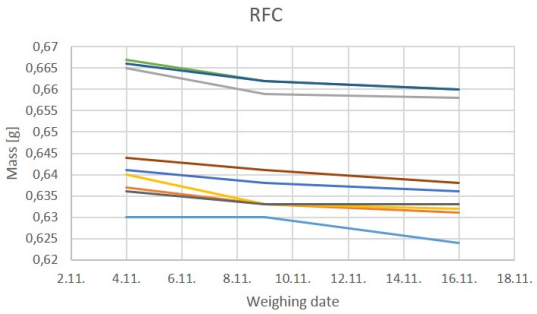

Vinylester I specimens

The test specimens that were made using Vinylester I resin were laminated half a year prior the beginning of the ILSS testing. Because of this, almost all of the moisture absorbed in the laminates had already vaporized when the laminates were put into the oven to dry. During different weighings of the laminates, the changes in their mass were only in the order of 0.001 g. This is why the drying curves of Vinylester I specimens seem to be very straight.

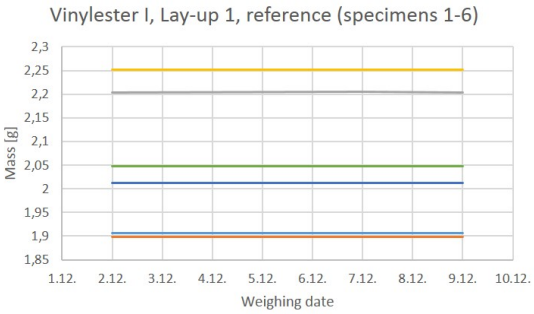

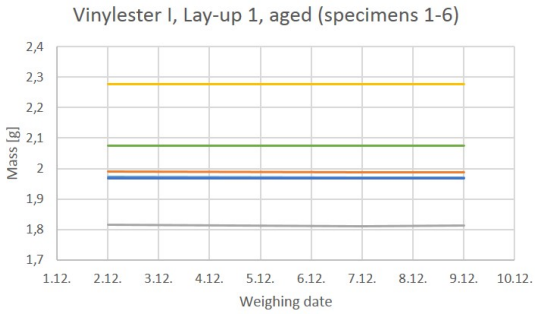

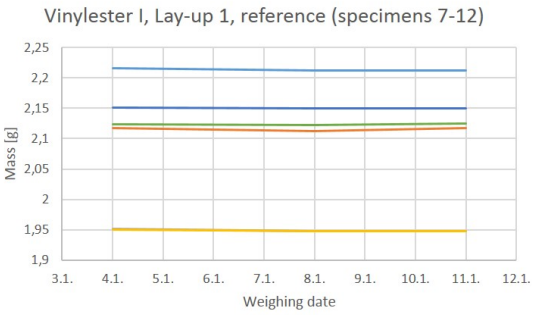

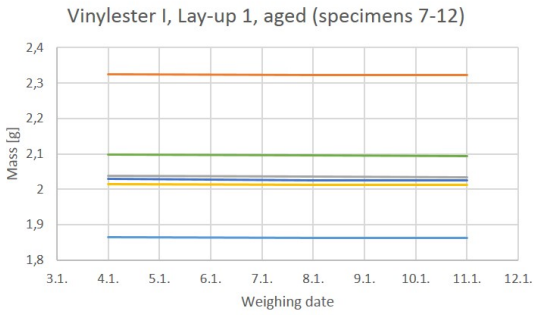

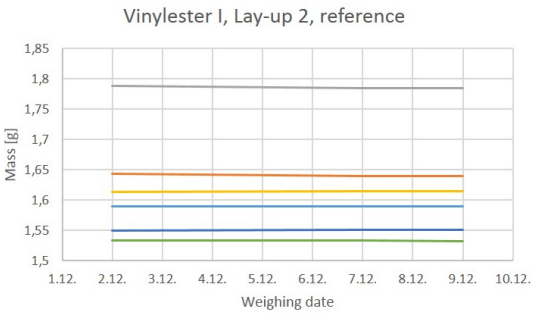

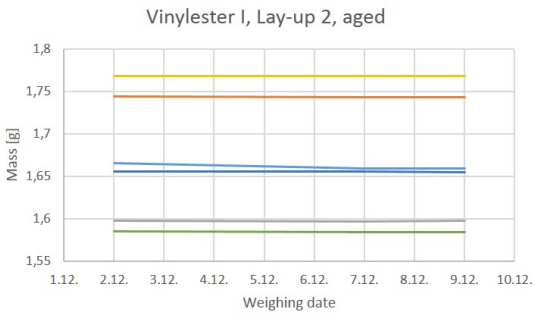

Vinylester II specimens

The test specimens that were made using Vinylester II resin were laminated half a year prior the beginning of the ILSS testing. Because of this, almost all of the moisture absorbed in the laminates had already vaporized when the laminates were put into the oven to dry. During different weighings of the laminates, the changes in their mass were only in the order of 0.001 g. This is why the drying curves of Vinylester II specimens seem to be very straight.

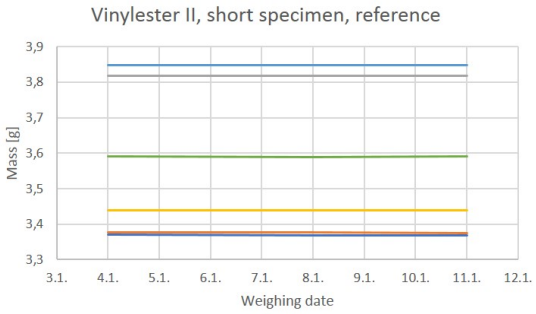

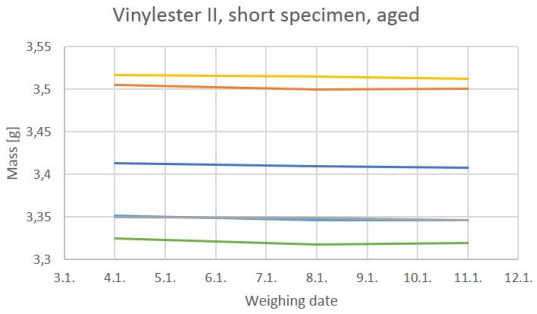

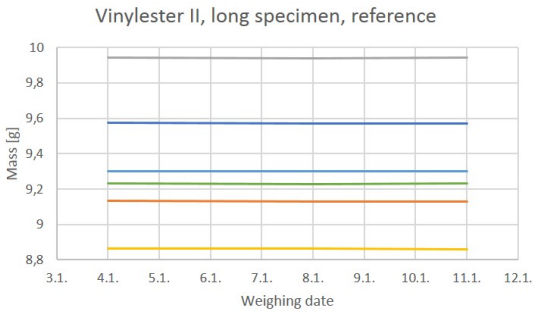

Filament wound specimens

The filament wound test specimens were laminated two years prior the beginning of the ILSS testing. Because of this, almost all of the moisture absorbed in the dry reference laminates had already vaporized when the laminates were put into the oven to dry. However, the aged test specimens that had been exposed to acid had absorbed some moisture, which is why their drying curves show a visible change in slope.

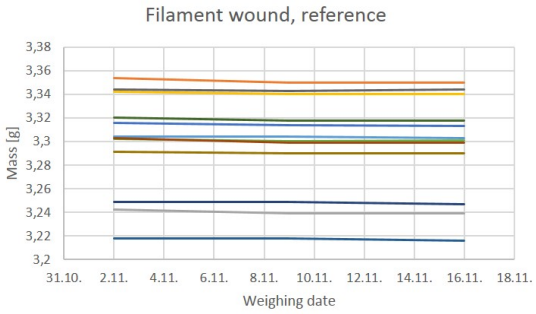

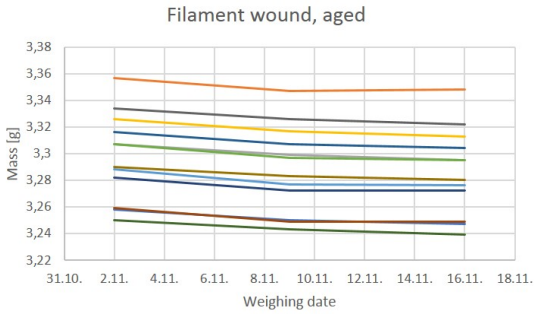

Polyester I specimens

Similarly to Vinylester I and II specimens, the Polyester I specimens were laminated half a year prior the beginning of the ILSS testing. Their weight virtually did not change at all during the drying in the oven, which is why their drying curves are very straight.

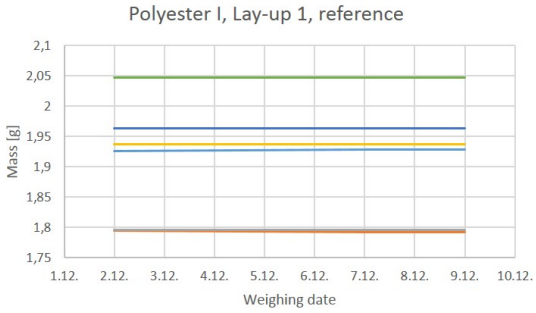

B Force-displacement curves

During the ILSS testing, two defining variables were measured: the displacement of the loading cylinder and the force inflicted to the loading cylinder. The test was continued until the maximum force was achieved and a failure in the laminate happened. In this appendix, all the force-displacement curves of the test specimens are presented. Each graph presents every force-displacement curve of one test series. Different test specimens have curves of different colour.

Dry aramid-fibre-reinforced specimens

Below, all the force-displacement curves of dry aramid-fibre reinforced specimens are presented. For further explanation for the name of each graph, see Table 3 on page 21 of this thesis.

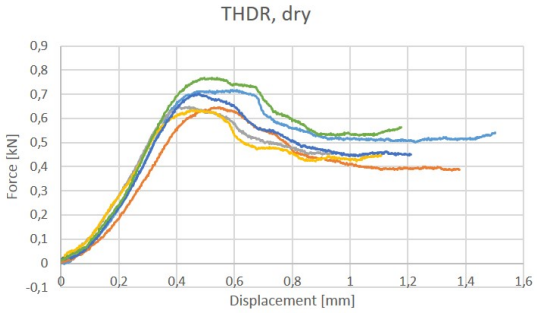

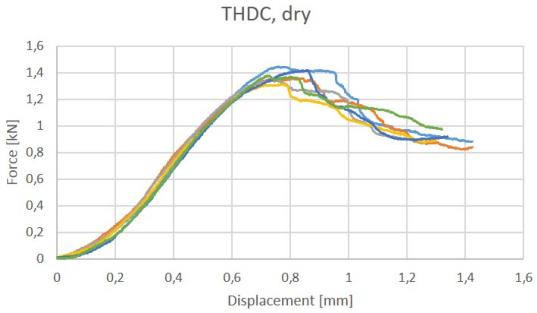

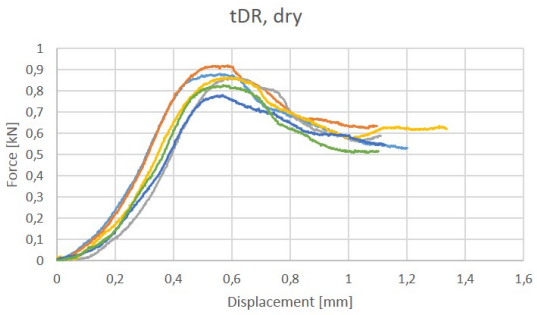

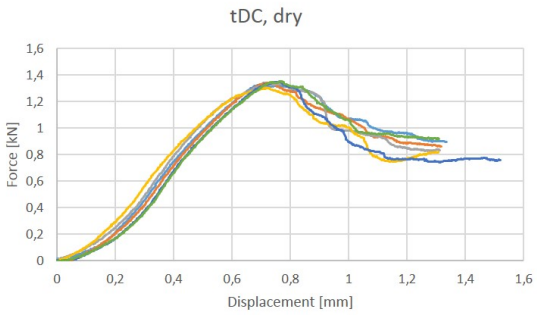

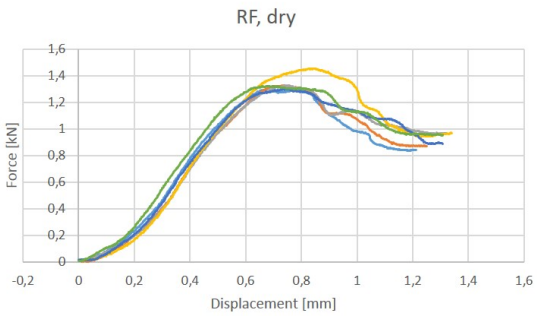

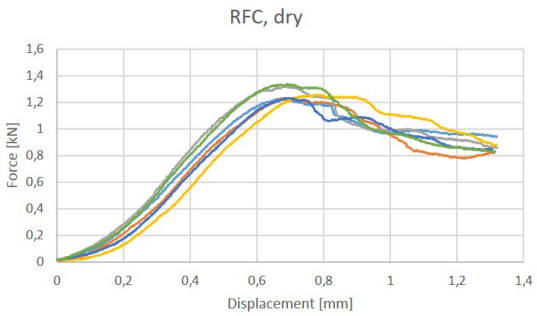

Wet aramid-fibre-reinforced specimens

Below, all the force-displacement curves of wet aramid-fibre reinforced specimens are presented. For further explanation for the name of each graph, see Table 3 on page 21 of this thesis. When wet, the aramid-fibre-reinforced specimens did not delaminate clearly during the testing, which is why their force-displacement curves are very round and smooth.

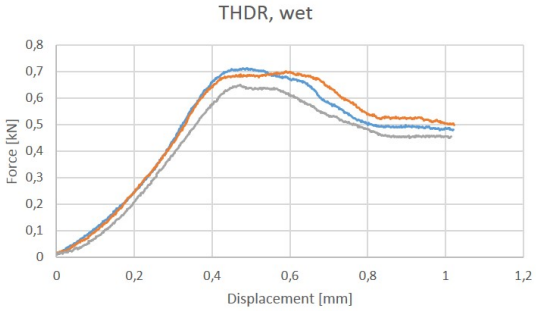

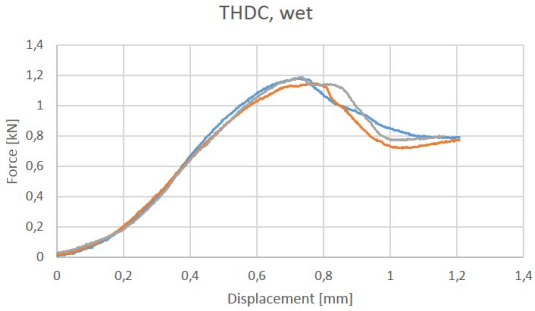

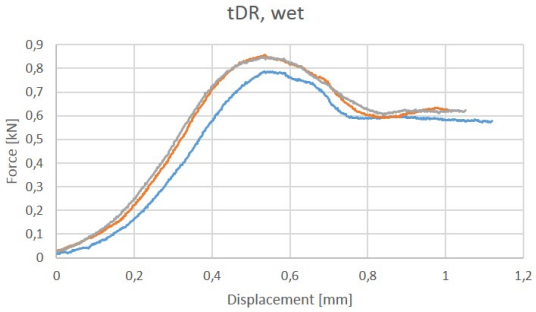

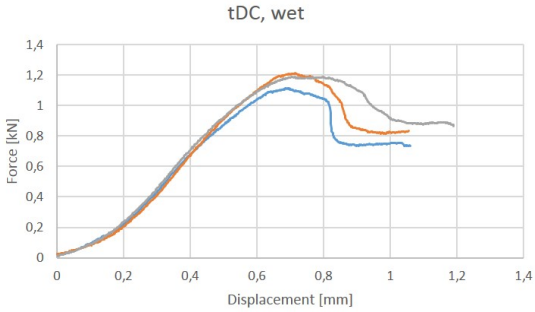

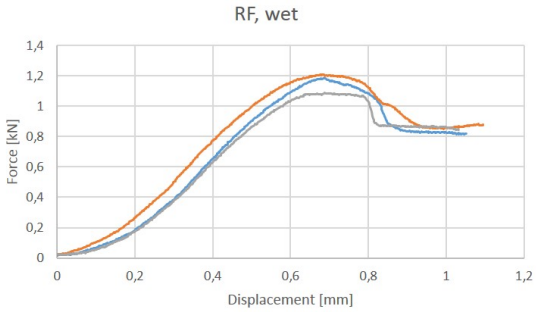

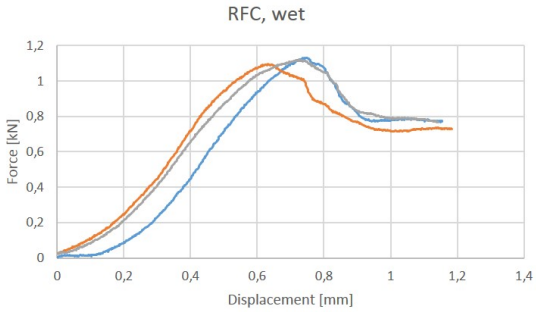

Dry Vinylester I specimens

In this section all the force-displacement curves of dry Vinylester I specimens are presented. The reference specimens that were not aged are on the left side and the aged specimens on the right. The specimens tested in room temperature have much clearer delaminations than the ones tested in elevated temperature. This can be seen as the sharp spikes in the curves of specimens that were tested in room temperature.

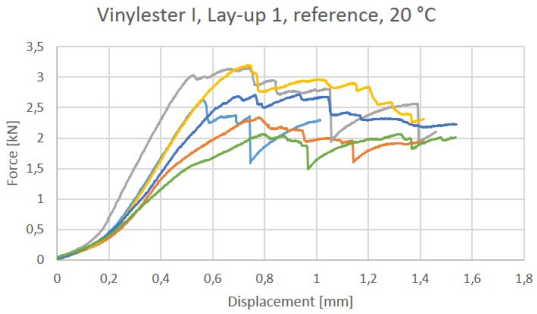

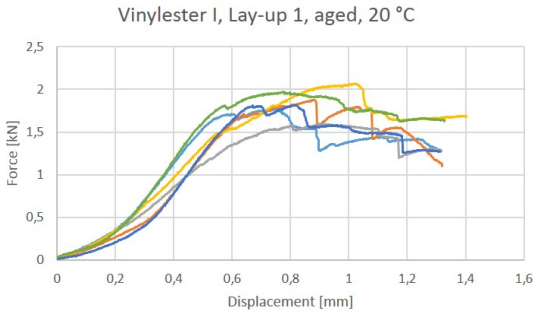

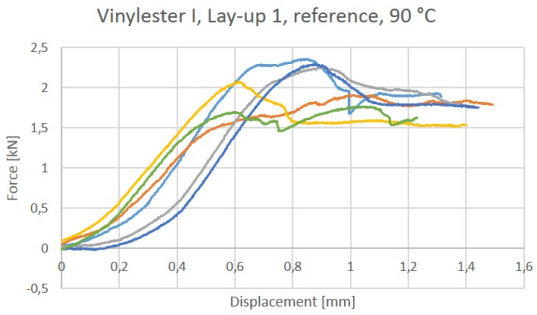

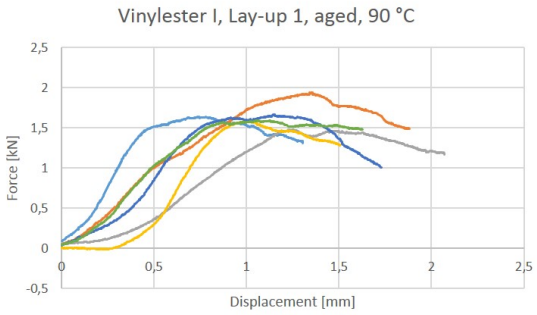

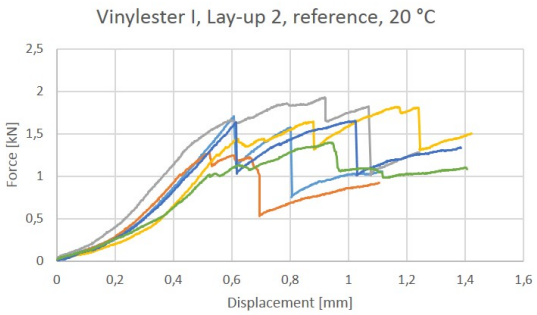

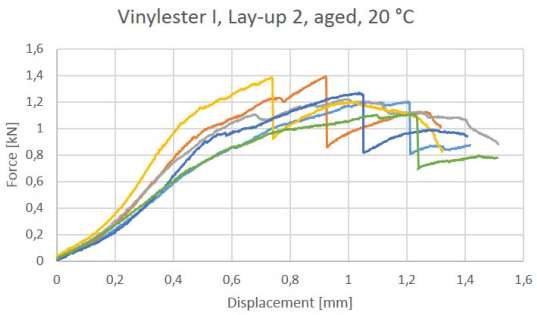

Wet Vinylester I specimens

In this section the force-displacement curves of wet Vinylester I specimens are presented. The curves of the specimens that were tested in room temperature are on the left and the curves of the specimens tested in higher temperature are on the right. Because of the absorbed moisture, these curves are much more round and smooth than the curves of the specimens that were tested dry.

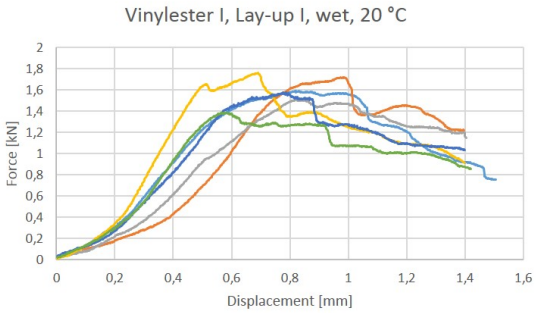

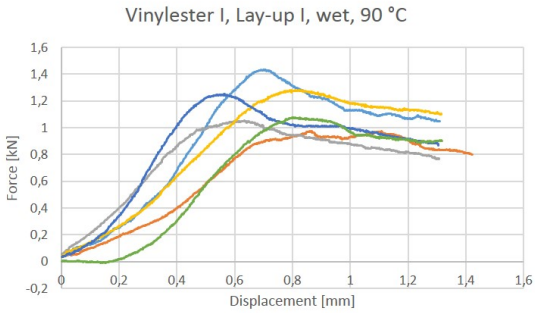

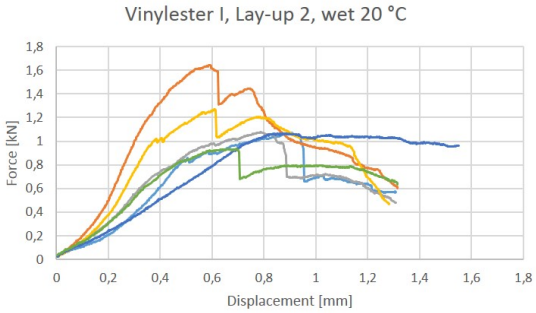

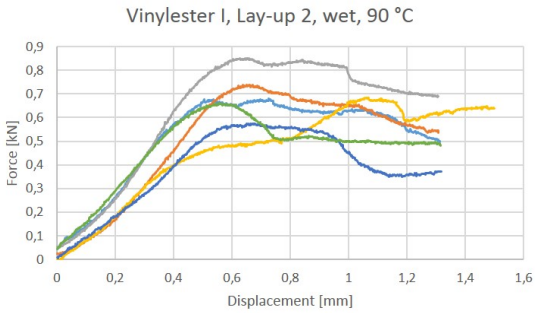

Polyester I specimens

Below, the force-displacement curves of Polyester I specimens are presented. There were only one test series with Polyester I resin, which is why there is only one graph.

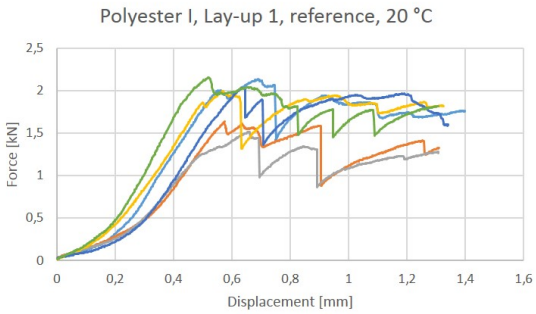

Vinylester II specimens

In this section, the force-displacement curves of all the Vinylester II specimens are presented. The reference specimens that were not aged are on the left and the aged specimens on the right. The lowest graph shows the specimens that were tested in the worst conditions for ILSS: aged, wet and in elevated temperature.

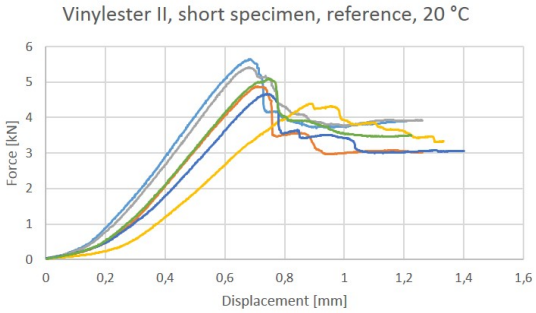

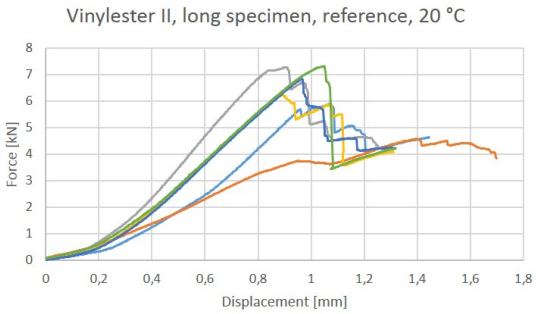

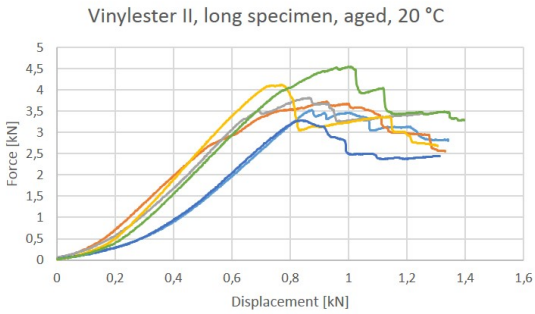

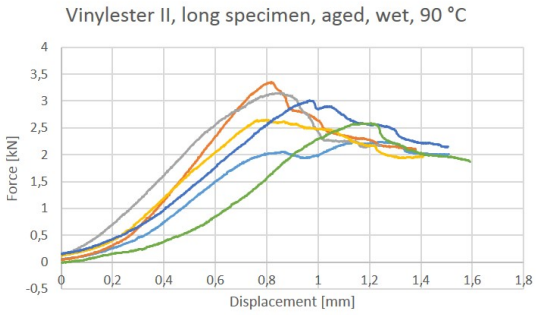

Filament-wound specimens

Below, all the force-displacement curves of the filament-wound specimens are presented. The reference specimens that were not aged are on the left and the aged specimens on the right. The specimens tested in higher temperature have much smoother and rounder ILSS curves, because they did not delaminate but experienced plastic deformations.